



**Università degli Studi di Napoli “Federico II”
Facoltà di Ingegneria**

Dipartimento di Ingegneria dei Materiali e della Produzione

**Research Doctoral Thesis in
Ingegneria Chimica, dei Materiali e della Produzione
XVIII Cycle (2002-2005)**

**MAGNETO-ELASTIC CHARACTERIZATION AND
THERMAL STABILITY OF THE COMPOSITE
MATERIALS MADE OF MAGNETIC AND
NON-MAGNETIC CONSTITUENTS**

Coordinator: Prof. Nino Grizzuti

Supervisor: Prof. Paolo Netti

Student: Cornelia Lorelai Hison

Advisor: Prof. Luciano Lanotte

ACKNOWLEDGEMENTS

Without the support of the following people, the work presented in this dissertation would not have been possible.

Most importantly, I would like to express my sincere gratitude to my advisor, Luciano Lanotte, outstanding educator, for his encouragement and care at all levels, and for his expert guidance and mentorship in my professional development. He had a decisive influence over my life and my future, giving me the opportunity to work in his research group. Thank you, Professor Lanotte!

I would like to thank Prof. Paolo Netti, who accepted to be my supervisor.

A special thank to my colleagues Giovanni Ausanio and Vincenzo Iannotti for their substantial help and pertinent observations and discussions throughout the experimental work and data analysis. I am also grateful to Cesare Luponio for his generous assistance during the experiments and for the useful discussions on polymers. Thanks are extended also to Antonio Maggio and Stefano Marrazzo for technical assistance.

I would like to express my special thanks and gratitude to my parents in law, Desdemona and Giacomo Germano for their love, spiritual and material support, and for the wonderful moments we spent together in the last four years since I am here, providing me a warm and familiar environment.

Finally, I would like to thank my husband, Roberto Germano, for his love, patience and understanding, and for helping me keep perspective on the important things in life.

PREMISE

The research activity performed in the frame of this PhD thesis **has been developed based on the common interest** in the field of the elastomagnetic composite materials **and** on the **extensive scientific background in composite materials and elastomagnetism** from the Physical Sciences Department and Materials Engineering and Production Department from Engineering Faculty of “Federico II” University of Naples, respectively.

The research activity is basically focused on the development, elastomagnetic characterization and performance investigation (in view of application as core material for sensors and actuators) **of the elastomagnetic composites made of magnetic micro-particles uniformly dispersed inside a non-magnetic, elastomeric matrix.** This kind of materials are not exactly new, but new is the idea to take advantage from the pinning mechanism of the magnetic moments of the filling particles on their own body and from the coupling between the magnetic and elastic reaction mechanical moments. **These composites, exhibiting elastomagnetic effects different from the classical magnetoelastic ones** (i.e. Joule and magnetomechanical effects), **are expected to be the precursors of an important class of multifunctional materials** due to their peculiar, specific elastomagnetic performances and **unique ability to detect and actuate deformations at the same time.**

The thesis is structured in eight chapters and general conclusions.

At the beginning (Chapter I) of the thesis, **the most recent and relevant state of the art in composite materials** consisting of magnetic particles dispersed in a non-magnetic, elastic matrix **are reviewed.** There **are pointed out** their strengths, as well as **their weaknesses which give the premises for the development of the elastomagnetic composites.** For the benefit of the reader, and with the aim to have the theoretical frame for the forthcoming considerations, the concepts of magnetostriction and magnetoresistance, which are between the most important effects in these composites, are briefly introduced.

In Chapter II are presented the developed elastomagnetic composites, describing thoroughly their preparation process, and pointing out their key required characteristics: the magnetic micro-particles (soft ferromagnetic or small permanent magnets) must exhibit a strong coupling between the magnetic moment and their body; the composite matrix must have a good elastic behavior up to relative deformations of about 15%.

The thesis is continuing with the introduction of the **elastomagnetic effects** (Chapter III), followed by the presentation of **their theoretical model** (Chapter IV). The **experimental verification of the direct and inverse elastomagnetic effects** is presented in **Chapters V and VI, respectively**. The obtained experimental results are consistent with the theoretical predictions, proving definitively the self-consistency of the developed elastomagnetic model.

Based on the predictions of the experimentally validated theoretical model of the elastomagnetic effect, **deformation and vibration detection sensor and actuator prototypes with elastomagnetic core materials were developed**. In Chapters VII and VIII are presented in detail the **sensing/actuating core material preparation, the developed sensor and actuator prototypes, the functioning models and their experimental verification and validity limits, the used experimental set-ups and investigation techniques** of the core performances, concluding with the presentation of the **optimum production parameters required to obtain the best sensing/actuating performances and their competitiveness with the standard materials actually used for similar target sensors and actuators**.

The last chapter is focused on the investigation of the developed elastomagnetic composites stability under dynamic mechanical solicitation and with the temperature, considering that the assessment of the **thermal stability and mechanical ageing** is a matter of strong interest for the engineering process of these composites as core material for sensors and actuators.

In the Conclusion, a critical analysis of the obtained results is performed, emphasizing the original contribution brought by the researches developed in the frame of this thesis to the incremental improvement of the state of the art in the field of composite materials made of magnetic particles inside a non-magnetic, elastic matrix. Finally, **there are also discussed the future trends**, giving an insight into the future development of the elastomagnetic composites as core materials for intelligent devices.

1. COMPOSITE MATERIALS MADE OF MAGNETIC PARTICLES INSIDE A NON-MAGNETIC, ELASTIC MATRIX

1.1. Introduction

A particular group of magnetic materials, for which the interest have been regained in the last few years are the composites consisting of magnetic particles dispersed in a non-magnetic, elastomeric matrix during the cross-linking process. The renewed interest for these materials is justified by their fundamental physics potential for the thorough understanding of the micromagnetic interactions between the filling particles inside the elastic matrix and by the wide range of application possibilities in the modern technology for the development of new, competitive devices which must meet current and anticipated market requirements.

Terminologies such as magnetostrictive, magnetorheological and magneto active/sensitive materials (elastomers) have been used as synonyms in various literatures to describe these composites made of magnetic particles inside a non-magnetic, elastic matrix (such as silicone, vinyl alcohol or other elastomers), exhibiting elastic properties which can be changed by the action of an external magnetizing field.

The magnetic particles (which may be aligned during the composite production by means of an external magnetizing field) within the non-magnetic, elastic matrix exhibit unique properties, which are not characteristic of the monolithic magnetic materials, such as strong dependence of the magnetic permeability on stress, together with good mechanical characteristics [1,2]. Due to the above mentioned magnetoelastic characteristics, as well as due to their ability to be: manufactured into complex shapes (using for example the mold injection methods) and easily machined, these composites have already found many applications as sensors, high strain actuators, converters, controlled vibration dampers, variable stiffness components, etc [3-5].

The fundamental premises of the research efforts accomplished for the development of this kind of composites are given by the following limitations of the

already known magnetic materials:

► In many applications, the magnetic and mechanical performances of the magnetic materials must meet simultaneously certain specifications. For example, the magnetic materials used for sensors and actuators must be elastic, susceptible to deformation and strong. The great majority of magnetic materials, such as ferromagnetic metals, metal alloys and ceramics show small susceptibility to deformation, being frequently brittle. At the same time, the improvement of the mechanical properties in the case of ferromagnetic materials, by changing the chemical composition and/or by additional annealing, is possible on limited scale.

► Various applications of the magnetic materials, such as ultrasonics generators, electromechanical transducers, stress sensors, etc., are based on the magnetostriction phenomenon, requiring sufficiently high values of magnetostriction. Unfortunately, the magnetostriction is quite small for most typical ferromagnetic materials (such as iron, nickel and cobalt): their relative change in length at saturation magnetization, called saturation magnetostriction, $\lambda_s = \Delta l / l_0$ (where Δl =change in length and l_0 =initial length), is of the order of 10^{-5} - 10^{-6} [6]. That is why, sustained research efforts have been conducted for many years for the development of new magnetostrictive materials. A much greater saturation magnetostriction, of the order of 10^{-3} , called giant magnetostriction, is displayed at room temperature by some compounds of rare-earth elements such as monolithic Terfenol-D alloys ($Tb_{0.27-0.30}Dy_{0.73-0.70}Fe_{1.90-1.95}$) [7]. Unfortunately, these materials have their limitations related to the eddy current losses, mechanical brittleness and difficulty in manufacturing.

Considering the above mentioned, many research investigations on the production, characterization and application of composite materials, made of magnetic particles inside an elastomer matrix, have been developed and, in the following, some of these studies are presented in order to give the picture of the actual state-of-the-art in the field.

Before summarizing some of the most recent researches developed in the field of composite materials made of magnetic particles inside a non-magnetic, elastic matrix, the concepts of magnetostriction and magnetoresistance, which are between the most important effects in these composites, will be briefly introduced with the aim to have the theoretical frame for the forthcoming considerations.

1.1.1. Magnetostriction

The magnetostriction is a phenomenon which characterizes the magnetoelastic materials. The direct magnetostrictive effect, or Joule effect (from the English physicist James Prescott Joule who was the first to discover it in 1842, in an iron rod [8]) represents the change in the physical dimensions of a ferromagnetic material, when subjected to a magnetic field [7, 9, 10]. The inverse magnetostrictive effect, or Villari effect (from E. Villari who described first this effect in 1865 [11]) is the change in the magnetization state of a ferromagnetic material, in response to a mechanical stress [7, 9, 10]. The magnetostrictive effects are inherent, and have no detrimental effects on the material, being in first approximation repeatable (will not degrade with time) and instantaneous. The magnetostrictive performances of a material can be optimized by tailoring the magnetic domains structure, through the control of the alloy composition, sample shape, thermal annealing, etc. [7].

Magnetostriction arises from the reorientation of the atomic magnetic moments in the presence of an external magnetic field or stress. The ferromagnetic materials are a collection of tiny permanent magnets or, more exactly, magnetic domains consisting of many atoms, within which all the magnetic moments are oriented in the same direction. When the magnetic moments in all the domains are completely aligned along the magnetizing field axis, occurs saturation, further increment of the applied magnetic field determining no further increase of the material macroscopic magnetization and consequently of the magnetostrictive

deformation. The magnetostriction varies with the temperature and vanishes at Curie temperature.

For a bulk isotropic material (bar shaped, with the length l and thickness w) in isotropic demagnetized state, the longitudinal magnetostriction, due to the action of a magnetic field applied along the main axis of the sample, is the relative deformation measured along the direction of the applied field, $\lambda_{||}=(\Delta l/l_0)_{||}$, while the transversal magnetostriction is the relative deformation observed in the plane perpendicular to the direction of the applied field, $\lambda_{\perp}=(\Delta w/w_0)_{\perp}$. Considering negligible the volume magnetostriction, one can write: $\lambda_{||}+2\lambda_{\perp}=0 \Rightarrow \lambda_{\perp}=-\lambda_{||}/2$. In practical cases, $-\lambda_{||}/2\lambda_{\perp}$ is usually smaller than unity, this indicating an anisotropy of the demagnetized state. Taking into account that $\lambda_{||}$ and λ_{\perp} depends on the applied magnetic field, at saturation one has: $\lambda_{||}=\lambda_s$ and $\lambda_{\perp}=-\lambda_s/2$. This is true only for an isotropic demagnetized state, otherwise λ_s obtained from $\lambda_{||}=\lambda_s$ and λ_s obtained from $\lambda_{\perp}=-\lambda_s/2$ are different. In this case, λ_s must be measured using the equation: $\lambda_s=(2/3)(\lambda_{||}-\lambda_{\perp})=(2/3)\lambda^{\gamma,2}$ (where $\lambda^{\gamma,2} = -b^{\gamma,2}f(H)/c^{\gamma}$, where $b^{\gamma,2}$ is the magnetoelastic coupling coefficient, c^{γ} is the relevant elastic coefficient and $f(H)$ is a function of the applied magnetic field which depends on the initial state of the sample, on the magnetic anisotropy of the material, etc. [12]; at saturation $f(H)=1$ and $\lambda^{\gamma,2} = -b^{\gamma,2}/c^{\gamma}$), which is independent on the demagnetized state [7].

λ_s is an important intrinsic material parameter, whose value depends on the chemical composition and temperature.

Magnetostriction can be positive or negative, the sample undertaking an elongation or a contraction in the direction of the applied magnetic field. From this point of view, the magnetostrictive materials can be classified in zero magnetostrictive ($\lambda_s \leq 10^{-9}$), low magnetostrictive ($\lambda_s = 10^{-6} \div 10^{-4}$), and giant magnetostrictive ($\lambda_s \geq 10^{-3}$) [13, 14].

In Figure 1 is presented a comparison between the saturation magnetostriction of some classical ferromagnetic materials already used in many applications and of some crystalline and amorphous alloys and multilayers recently produced, indicating the difference in sign and range of magnitude [14]. This figure is conceived to give a good picture of the situation, placing in the upper position of the diagram, materials with maximum positive saturation magnetostriction, while in the bottom part of the diagram are placed the materials with maximum negative magnetostriction. The materials with the smallest saturation magnetostriction are placed in the middle region of the diagram. From the left to the right of the diagram, the materials exhibit an increasing magnetization energy.

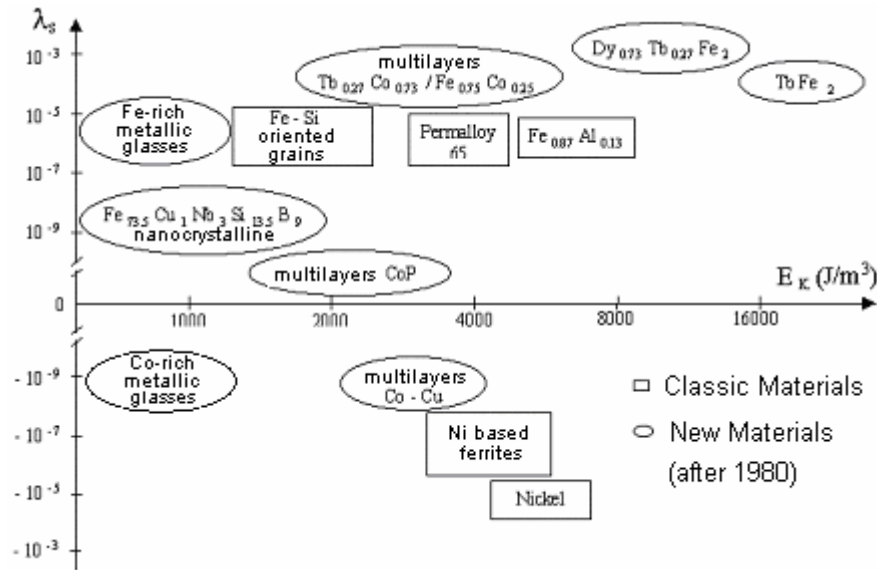


Figure 1. Saturation magnetostriction coefficient, λ_s , of classical and new ferromagnetic materials as function of the magnetization energy.

It can be observed that the material based on Fe and rare-earth elements, $Tb_{0.3}Dy_{0.7}Fe_{1.9-2}$ (Terfenol-D, which comes from terbium (TER), iron (FE), Naval Ordnance Labs (NOL), and Dysprosium (D)) has the highest magnetostriction among the ferromagnetic materials. Terfenol-D was developed during the 1970's in the Naval Ordnance Laboratory in Washington, by A.E. Clark and collaborators [13] with the aim to improve of the sonar technology. Since that time, Terfenol-D has become the preeminent magnetostrictive material, although research continues into new materials constantly. The very high magnetostriction

value of this material is determined by the strong spin-orbit interactions (due to the presence of Tb and Dy, two elements with oppositely signed magnetocrystalline anisotropies, which decrease the material magnetocrystalline anisotropy at room temperature) and by the anisotropic charge distribution of the 4f electrons of the rare earth atoms [7]. At room temperature, Terfenol-D presents the best compromise between large magnetostriction (static strains up to 2×10^{-3} and dynamic strains of 3.5×10^{-3} [15]) and relatively low magnetizing field (50-200 kA/m) [13, 16]. Technologies of all kinds are incorporating Terfenol-D into a variety of products such as sensors, actuators, ultrasound devices, high power ultrasonic motors for diverse industries such as automotive, aerospace, etc, capitalizing on its force, displacement, and frequency capabilities.

Practically, the magnetostrictive materials to be used for actuators must produce relatively large deformations in as small as possible magnetic field. A remarkable improvement in what concern lower magnetization fields is obtained for ferromagnetic multilayers (e.g. $\text{Tb}_{0.27}\text{Co}_{0.73}/\text{Fe}_{0.75}\text{Co}_{0.25}$, $\text{Tb}_{40}\text{Fe}_{60}/\text{Fe}_{50}\text{Co}_{50}$ [17]) and materials produced by new, innovative techniques (e.g. powders metallurgy). The giant magnetostrictive thin films/multilayers have predominantly been used as various microactuators in microelectromechanical systems (MEMS) [17].

The materials with almost zero magnetostriction ($\lambda_s=10^{-6}$ - 10^{-9}) are the amorphous alloys based on Co (e.g. $\text{Co}_{74}\text{Fe}_6\text{B}_{20}$, $(\text{Fe}_{0.06}\text{Co}_{0.94})_{72.5}\text{Si}_{12.5}\text{B}_{15}$, etc), the nanocrystalline $\text{Fe}_{73.5}\text{Cu}_1\text{Nb}_3\text{Si}_{13.5}\text{B}_9$ (FINEMET) and Fe-M-B, M: Hf, Zr, Nb, etc (NANOPERM) ribbons and the Co-Cu and Co-P multilayers (in which the deformation effect during magnetization is attenuated by the non magnetic layers) [18-20]. In the case of the soft magnetic nanocrystalline alloys (such as FINEMET, NANOPERM, etc), the reduced magnetostriction determines a general improvement of the soft magnetic characteristics and the possibility to be used in power transformers and magnetic heads. Undoubtedly, the interest for the soft magnetic Fe based amorphous materials (placed in the extreme left in Figure 1) is very high

due to their particular characteristics, such as very high permeability, high saturation induction (about 1 T), together with low coercivity, which guaranty very good strain and field sensitivity for sensors applications [21]. These alloys, with typical compositions $\text{Fe}_{86}\text{B}_{14}$, $\text{Fe}_{81}\text{B}_{13}\text{Si}_2\text{C}_4$, $\text{Fe}_{80}\text{B}_5\text{Si}_{15}$, etc, are obtained by rapid quenching from the melt [22].

The classical materials made by pure metals (e.g. Ni), the alloys such as Permalloy-65 and Ferrites exhibit magnetostrictive characteristics already exceeded by the new developed materials. Among them, the most interesting ones are the Fe-Si based alloys with oriented grains, widely used for transformer cores [23].

1.1.2. Magnetoresistance

The magnetoresistance is the property of some magnetic materials to change their electrical resistance when subjected to an external magnetic field. The relative change in electrical resistance, m , defined as $m = \Delta\rho/\rho_0$ (where $\Delta\rho$ is the change of resistivity under the action of the magnetic field and ρ_0 is the resistivity at zero field) is called magnetoresistance. The magnetoresistance effect (MR) was first discovered by William Thomson (also known as Lord Kelvin) in 1857, but at that time he was unable to lower the electrical resistance of any material by more than 5%. Nowadays, there are known materials with large magnetoresistance and, depending on the MR magnitude, they are called Giant magnetoresistant (GMR), Colossal magnetoresistant (CMR) or Tunnel magneto-resistant (TMR) [24, 25].

The first broad class of applications of the magnetoresistive materials concerns the magnetic field sensors. These materials allow a change in magnetic field to be detected as a change in electrical resistivity. The MR materials are used in magnetoresistive read heads for high density magnetic recording, for linear and angular position sensors in the automobile industry, for ticketing applications, etc [26].

Generally, the m value for monolithic samples of ferromagnetic materials is quite small 1-3% [27]. A much higher magnetoresistance, GMR, was discovered in ferromagnet/paramagnet multilayer structures such as cobalt or permalloy thin layers separated by non-ferromagnetic metallic layers (generally copper), for which m averages 65% [28]. Practically, the Giant Magnetoresistance was discovered in Fe/Cr multilayers, in 1988, independently by Baibich, A. Fert and collaborators from the University of Paris-Sud [29] and Binasch and collaborators from Jülich Research Center in Germany [30]. In these multilayers, for certain thickness of the Cr interlayer, the magnetizations of the adjacent Fe layers are oriented anti-parallel by an antiferromagnetic interlayer exchange coupling [31]. Under the action of a magnetic field, the multilayer resistance decreases drastically, when the magnetization of the two layers progressively aligns in the field direction. The antiparallel configuration can be also obtained in multilayers for which the consecutive magnetic layers have different coercivities [32] or by combining hard and soft magnetic layers. The best known structure to obtain an antiparallel arrangement is the spin valve structure [33].

The GMR effect is usually seen in a large number of multilayered systems combining ferromagnetic transition metals or alloys, with non-magnetic metals, where the two thin ferromagnetic layers are generally separated by a thin paramagnetic spacer layer [34]. The GMR was also discovered in alloys with nanocrystalline structure [35-37].

The GMR phenomenon has been generated a great interest from physicists and engineers, considering there have been both new physics to be investigated and huge technological application potential for magnetic recording, data storage (the introduction of GMR read heads is the origin of the considerable increase in the information storage density on hard drives; moreover, this discovery launched a new research area in physics: that of spin electronics, or spintronics), robotics, sensors, telecommunications etc. [38-39].

1.2. State-of-the-art

1.2.1. Composite materials based on Terfenol-D

In the research efforts for the development of new, cost-effective materials, with simultaneously improved magnetostrictive and mechanical characteristics, starting from the traditional Terfenol-D alloy [40-43], whose brittleness in tension and development of high eddy current losses are limiting factors for applications, alternative production routes such as sintering [44, 45] and polymer-bonding [46, 47] were developed. Among them, the polymer-bonding method is considered to have distinct advantages over the others in being simple and cost-effective. The composite material made of Terfenol-D powder inside a polymer matrix exhibits, apart comparable magnetostrictive strain, many improved performances with respect to the bulk Terfenol-D alloy [46, 48, 49]:

- ▶ an increased resistivity and much lower eddy current losses (e.g., sixfold reduction in the total energy loss at high frequencies [50]), due to the insulating role of the non-metallic matrix, which assure the broadening of the application range to high-frequency (up to 100 kHz and beyond);
- ▶ about four times higher tensile strength; the composite matrix can better accommodate tensile and shear loading states.

The polymer-bonded Terfenol-D composites were first reported by Sandlund and collaborators (1994) [46], and later by Ruiz de Angulo and collaborators [47] (1996). Sandlund, from Feredyn Europe, Uppsala, Sweden, produced two types of rod-shaped (0.9 cm diam. × 4.33 cm) composites: one in which the Terfenol-D particles are randomly oriented inside the elastic matrix (isotropic composite), and the other one in which the Terfenol-D particles are magnetically oriented (anisotropic composite). The measured magnetostriction at 160 kA/m reached about 0.8×10^{-3} for the anisotropic composite and about 0.5×10^{-3} for the randomly oriented composite. (Note that the single-crystal saturation magnetostriction for the

Terfenol-D alloy is $(3/2)\lambda_{111} \cong 2.4 \times 10^{-3}$. Some physical, electrical and magnetic characteristics of the traditional and composite Terfenol-D are comparatively presented in Table 1 [46], while in Table 2 are given some piezomagnetic properties of the developed Terfenol-D composites.

Table 1. Physical (δ -density), electrical (ρ -resistivity) and magnetic characteristics (T_C -Curie temperature, M_s -saturation magnetization and λ -magnetostriction) of nickel, Terfenol-D composites (isotropic and anisotropic) and traditional Terfenol-D. Reproduced from [46].

	$\delta \times 10^{-3}$ (kg/m ³)	$\rho \times 10^8$ (Ω m)	T_C (°C)	M_s (T)	$\lambda \times 10^6$ at 120 kA/m
Nickel	8.8	7.8	358	0.61	50
Isotropic composite	7.5	30000	380	0.80	400
Anisotropic composite	6.8	60000	380	0.71	620
Terfenol-D	9.2	60	380	1.0	1100-1400 ^a

^a Depending on composition.

Table 2. Piezomagnetic characteristics (H: magnetic field, μ_{rel} : relative permeability, d: piezomagnetic constant ($d = \delta\lambda/\delta H$), Y^H : Young's modulus at fixed magnetic field, H , k_{33} : material coupling factor ($k_{33}^2 = \left(\frac{d^2}{\mu^\sigma}\right) Y^H$ with μ^σ - permeability at fixed stress σ)), of the isotropic and anisotropic Terfenol-D composites.

	H(kA/m)	μ_{rel}	d (nm/A)	Y^H (Gpa)	k_{33}
Isotropic composite	40	4.1	3.8	20.2	0.24
	80	2.8	3.7	19.7	0.28
	120	2.2	3.1	19.2	0.26
Anisotropic composite	40	4.0	5.8	19.5	0.36
	80	2.9	5.9	17.0	0.40
	120	2.2	4.8	17.0	0.38

As can be seen from these tables, the anisotropic composites exhibit higher magnetostriction, as well as double resistivity and therefore, they are preferable for most purposes. The magnetomechanical properties and the high resistivity make the Terfenol-D composite very attractive for high-frequency applications.

Ruiz de Angulo and collaborators (1996), from the Birmingham University, prepared composites made of $Tb_{0.27}Dy_{0.73}Fe_{1.93}$ powder particles (with the size $< 25 \mu m$) inside an epoxy resin matrix, in the shape of rod (4 cm in length and 0.6 cm in diameter). The obtained value of the magnetomechanical factor was comparable with those of the Terfenol-D cast rods. During the measurements of the magnetomechanical factor, two phenomena were observed: the existence of a threshold value of the applied magnetic field required to produce a measurable magnetomechanical factor, and an abnormal behavior of the characteristic frequencies with the applied field, with respect to the traditional Terfenol-D rods [47].

Further research in the field of Terfenol-D particles inside a non-metallic binder were developed by Duenas and collaborators (1996), and Kim and collaborators (1998), who focused their researches on the maximization of the magnetostrictive response as function of the constituents characteristics (such as particle size and binder properties) [51, 52]. Other investigations have been accomplished by measuring properties such as magnetomechanical coupling factor [46, 53], elastic moduli [53], magnetoelastic field gradient coefficient [54], and compressive strength as function of processing parameters [54]. In the works of Sandlund and Ruiz de Angulo the main emphasis is given to the characterization of the Terfenol-D composites and little is reported on the optimization of the fabrication parameters. This aspect was thoroughly investigated in the works of Lim and collaborators, from Korea Institute of Science and Technology, between 1998 and 1999 [51, 54]. In the effort to fabricate Terfenol-D composites with good magnetic (including magnetostrictive) and mechanical characteristics, these properties were investigated as function of particle size, binder content, compaction pressure, and particles alignment during the compaction process. It was found

that the magnetostrictive properties tend to improve with the particle size increase, while a high compression strength is obtained for low particle size. The optimum size of the Terfenol-D particles for which reasonably good magnetostrictive properties are combined with a large compressive strength was estimated to be 112.5 μm [54]. The optimum binder content was determined to be in the range 3-4 wt%, but it was difficult to determine the optimum compaction pressure since its increase deteriorates the magnetostrictive properties, while improving the mechanical strength [54]. At that time, Lim stated that the properties of the polymer-bonded Terfenol-D composites can be improved further by the refinement of the fabrication parameters.

In 2000, Duenas and collaborators from Mechanical and Aerospace Engineering Department, University of California, Los Angeles, reported new results on the magnetostrictive response of Terfenol-D resin composite [49]. Samples made of Terfenol-D powder dispersed inside a low viscosity (to permit sufficient particles wetting and reduced number of voids for the improvement of the magnetostriction response), non-metallic binder were prepared in the bar shape (12.7 mm \times 12.7 mm \times 25.4 mm) [49]. The Terfenol-D particles (with the size $< 300 \mu\text{m}$) were magnetically oriented along the main sample axis. A magnetostrictive strain response comparable to that of bulk Terfenol-D was obtained for an optimum volume fraction of Terfenol-D particles inside the epoxy resin of 20%. The study of the mechanical loads effect on the magnetomechanical response showed that the preload increasing induces an increase of the magnetostriction saturation, as well as of the required field for saturation. The rule-of-mixtures model was used to explain the obtained experimental results [49].

1.2.2. Composite materials made of silicon steel(+graphite)/iron(+graphite) particles inside a silicone matrix

Trying to obtain a new material, with a substantial increase in susceptibility to deformation under normal conditions, Bednarek (1997), from Physics Department, University of Lodz, Poland, prepared a composite material, consisting of silicon steel particles (with an almost spherical shape, $\Phi=0.15-0.20$ mm) dispersed into a silicone (commonly used for gluing and sealing) matrix called ferroelast (Figure 2) [55, 56]. As starting material for the magnetic particles, he used a plate of silicon steel containing 4% Si (utilized for the production of transformers plates), which was first cut into small pieces and then grounded in a special electric mill. The obtained particles were annealed for 3 h at 500°C, in neutral atmosphere [56]. The ferroelast composite was prepared by mixing uniformly the magnetic particles with the unpolymerized silicone, which has the consistency of a paste. In contact with the atmosphere, the silicone is subjected to polymerization, becoming an elastic solid body.

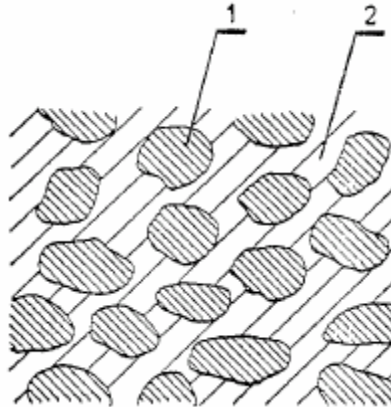


Figure 2. Ferroelast structure: 1-ferromagnetic particles, 2-polymer matrix.

Samples in the shape of rods (20 mm in diameter and 30-60 mm in length) were prepared by the extrusion method. The Young's modulus, E_m , of the polymerized silicone is 0.25×10^6 Pa and the Young's modulus of the silicon steel is 2.3×10^{11} Pa [55]. The high susceptibility to deformation, large extensibility limits, high tensile and fatigue strength, soft magnetic characteristics, together with a minimum density of energy lost during excess re-

magnetization can be optimized by tailoring the content of silicon steel particles in the composite (expressed by the filling factor, p_f , defined as the ratio of the total volume of the silicon steel particles to the composite total volume) and the preparation parameters [56].

Bednarek introduced an equivalent model of the ferroelast structure and derived a formula describing the dependence of λ , characterizing the susceptibility of the material to deformations caused by a heterogenous magnetic field, on the filling factor p_f [56]. This dependence was experimentally verified for various contents of silicon steel particles in the ferroelast, p_f ranging from 0.05 to 0.95. It was found that the susceptibility to deformation caused by a heterogenous magnetic field increases for small values of p_f , while for larger p_f values, the limit of ferroelast extensibility due to the increasing content of non-deformable ferromagnetic particles is decisive, causing a reduction in the susceptibility to deformation [56].

Very interesting results were obtained by Bednarek for the magnetostriction and magnetoresistance of these materials on which there were developed simultaneous measurements [57]. The structure of the investigated composites consisted of silicon steel particles (with an almost spherical shape, $\Phi=0.15-0.20$ mm) and graphite particles (with the size < 0.5 μm), uniformly dispersed inside an elastic matrix of commercial silicone. The graphite particles were used to decrease the matrix resistivity. The contents of silicon steel and graphite particles in the composite matrix are described by the filling factors $p_f=V_f/V_z$ and $p_g=V_g/V_z$, respectively (where V_f and V_g are the total volume of silicon steel and graphite particles, respectively, and V_z is the total volume of the composite material).

It was found that the length of all investigated samples (rod shape, 20 mm in diameter and 60 mm in length) was increasing under the action of an external magnetic field. This means that the material displays a positive magnetostriction, which is the result of the ferromagnetic particles - magnetic field interaction and of the mutual interaction between the magnetized particles [57]. During the magnetostriction measurements, the magnetic induction

was changed uniformly in the range 0-8 T [57]. Under the influence of the magnetic field, the silicon steel particles tend to set their easy magnetization direction along the field axis, and magnetic poles are induced in them such that the unlike poles appear near the boundaries of neighboring particles. The interaction (through attraction forces) between these poles, mediated by the silicone matrix, causes the particles displacement and alignment in chains, and then columns, directed along the magnetic field lines. The particles rotation and displacement distort the elastic matrix, determining the composite elongation, manifested as magnetostriction. Considering that the silicone content in the composite samples is limited to 20-40% by the presence of the silicon steel and graphite particles, thin walls of silicone exist between the filling particles. The elongation of the composite sample is practically possible due to the elongation of these walls (the breaking strain of the pure silicone reaches 500% [55, 57]), because both kinds of filling particles are not susceptible to elongation. Both the rate of increase in magnetostriction and its maximum value in 8T magnetic field depend strongly on p_f and p_g : the samples with higher value of p_f exhibit a faster magnetostriction increase and the maximum value at $B=8T$ is also higher. The maximum value of magnetostriction is ranging from 0.14×10^{-2} (for the samples with $p_f=0.2$ and $p_g=0.6$) to 0.80×10^{-2} (for the samples with $p_f=0.4$ and $p_g=0.2$) [57]. When p_f is kept constant, the maximum magnetostriction value is decreasing with p_g increasing. These results were explained in the following way. The increase in p_f results in a stronger interaction between the composite material and the magnetic field; simultaneously, the p_f and p_g increase causes an increase of the effective Young's modulus of the sample, which becomes less susceptible to strain. As a result of these two competitive processes, the samples with higher values of p_f and p_g exhibit lower magnetostriction. In any case, the maximum magnetostriction values found for the studied samples are remarkably higher than: for the typical ferromagnetic materials such as Ni and Fe (which are of the order of magnitude of 10^{-5} , at room temperature [58]), and for the silicon steel used for the particles production (which are of the order of 10^{-6} [59]). When the

induction of the applied magnetic field decreases, the magnetostriction decreases in a similar way as during the field increasing, and the characteristic curve segments are repeating in the reversed order. However, the decrease of magnetostriction however occurs much slowly than its increase and, as a result, when the field is completely switched off, the magnetostriction is not reaching the initial value and the samples exhibit magnetostriction hysteresis. The measured value of the magnetostriction hysteresis is ranging from 0.03×10^{-2} (for the samples with $p_f=0.2$ and $p_g=0.4$) to 0.13×10^{-2} (for the samples with $p_f=0.4$ and $p_g=0.4$) [57]. The possible reason for the magnetostriction hysteresis is the disruption of some weak connections between the silicon steel particles and the elastic matrix. The magnetostriction hysteresis is disadvantageous in the case of practical application and the material must be improved.

In what concern the magnetoresistivity measurements, the effective resistivity of all investigated composites, ρ_z , decreases with the magnetic field increase. This means that the composite displays a negative magnetoresistance [60]. The silicon steel resistivity is 5.6×10^{-6} Ωm , the graphite resistivity (considering that the particles obtained after the comminution of the monocrystalline graphite exhibit no anisotropy) is 8.7×10^{-3} Ωm and the polymerized silicone resistivity is 2×10^8 Ωm [57, 61, 62]. When the composite sample is not placed in a magnetic field, the spatial distribution of both kinds of filling particles is random. In this case only an insignificant number of silicon steel and graphite particles are in direct contact with each other, facilitating the passage of the electric current through the composite. Therefore, the material reveals a relative high initial resistivity (see Table 3). The presence of the magnetic field determines the magnetization of the silicon steel particles and consequently, the appearance of magnetic interactions between them, followed by their displacement and arrangement in chains and then in columns [63-66], as previously described. This process involves a dislocation of the surrounding graphite particles, owing to the silicone matrix viscosity. All these result in a more ordered structure, with a higher number of connections

between the conductive particles, and the consequent decrease in the effective resistivity of the composite under the magnetic field action (see Table 3). When the magnetic field is decreased to zero, the resistivity increases much slower than it was decreasing during the magnetic field increase and, as a result, the final resistivity is smaller than the initial one (see Table 3). This means magnetoresistance hysteresis, which is the result of the residual ordered structure, whose existence is facilitated by the high viscosity of the epoxy resin [60]. The magnetoresistance values shown by this material are comparable with the giant magnetoresistance found in multilayer systems and granular structures [28, 38, 60, 67].

Table 3. Characteristic parameters of the investigated ferromagnetic composite (cylindrical shape: $\Phi=12$ mm and 20 mm in length): p_g , p_f – filling factors of graphite and silicon steel particles, respectively; ρ_{z0} , ρ_{zmin} , ρ_{zf} — initial, minimum (after the application of 1.1 T magnetic field) and final (after the field switching off) effective resistivity of the composite material, respectively.

p_g	p_f	ρ_{z0} (Ωm)	ρ_{zmin} (Ωm)	ρ_{zf} (Ωm)
0.4	0.2	92.3	11.0	61.8
	0.3	76.5	2.3	38.3
	0.4	52.1	0.27	13.7
0.5	0.2	43.9	8.8	26.4
	0.3	34.7	0.41	9.3
0.6	0.2	9.6	0.11	1.9

Unfortunately, the magnetoresistance sensitivity defined as $s=m/\Delta H$ (where m is the magnetoresistance and ΔH is the change in the magnetic field intensity determining a maximum change in resistivity), is from 140 to 176 times smaller than the maximum sensitivity obtained for other materials [60].

The experiments conducted on samples having the same composite structure, but with dimensions of 60 mm in length and 20 mm in diameter and under the influence of a magnetic

field which increases up to 8 T, give the following result on magnetoresistance: the highest magnetoresistance m reaches 37.5% for the samples with $p_f=0.4$ and $p_g=0.4$ [57]. In this case, the measured magnetoresistance values are approximately equal to half of those found in multilayer systems [28, 38]. The giant magnetoresistance of this type of composites suggests that after hysteresis reduction, they can be used for magnetic field sensors, switch-over and memory elements (in the case of properly modified hysteresis loops) [60].

Anjanappa and Wu (1996, 1997), from Department of Mechanical Engineering, Maryland University, Baltimore, developed a composite material, made of Terfenol-D particles (50 to 300 μm in diameter) inside a polymeric host matrix, to be applied as magnetostrictive particulate actuator (MPA) (Figure 3) [68, 69]. The MPA was configured as a small rectangular polymeric beam, with magnetostrictive particles dispersed uniformly and magnetically oriented in a desired direction (the particles must be magnetically oriented to maximize the performance in a desired direction). Based on the compatibility condition, a load line equation was developed to relate the free strain with the mechanical stress experienced by the magnetostrictive particles. A mathematical model, based on the magnetoelastic material properties and load line, was developed in order to depict the static macroscopic behavior of the MPA [69]. Characterization experiments were conducted to determine the orientation factor (considering that it is difficult to achieve a perfect magnetic orientation of the particles, the attainable strain in the desired direction for a given magnetic field, is reduced by a factor called “orientation factor”) and pre-stress (an ideal configuration of MPA requires a predetermined preload). It was found that the experimental results agree with the numerical ones, showing that the static performances of MPAs for an applied magnetic field depends on the volume fraction of the filling particles, orientation field, mechanical preload and stiffness of the polymeric matrix [69]. These MPAs take advantage of the remote excitation capability of the magnetostrictive particles. In general, they can be used where the structure needs to be excited with a large force and small strain, over a wide

frequency range (e.g. as micropositioners, vibration dampers, platform stabilizers, and motors) [69].

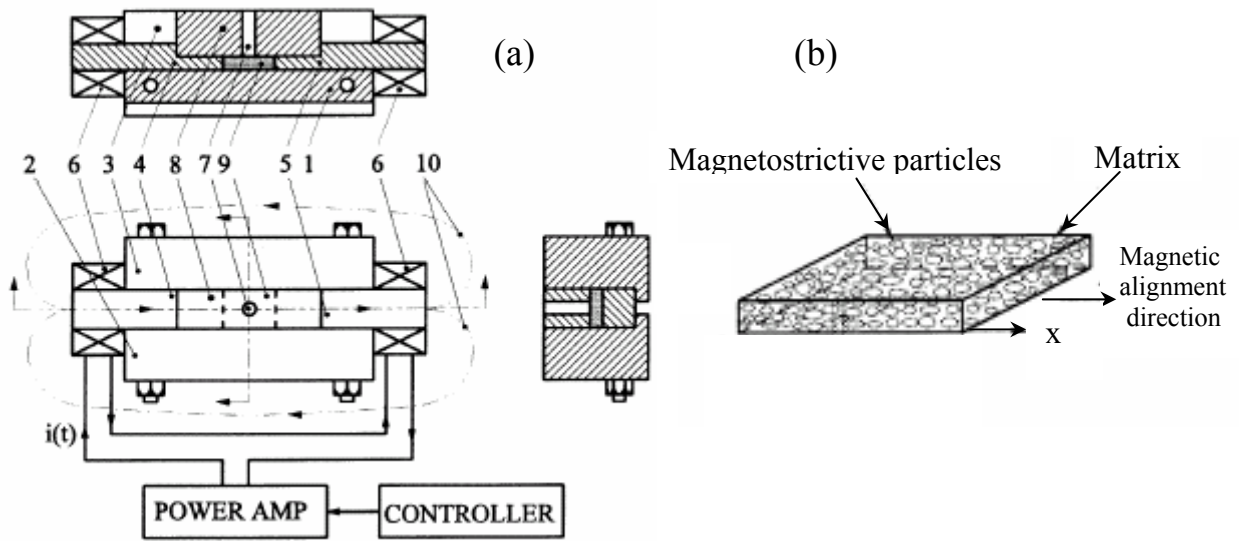


Figure 3. (a) Schematic diagram of MPA fabrication set-up: 1. bottom plate; 2. left side plate; 3. right side plate; 3. right side plate; 4. north pole plate; 5. south pole plate; 6. coil; 7. sprue; 8. top plate; MPA; 10. magnetic field. (b) Configuration of the magnetostrictive particulate actuator (MPA). Reproduced from [69].

Bednarek observed and studied also the phenomenon of magnetoresistance relaxation in ferroelast materials, explaining it by using the column-model of the particles ordering during the increasing of the external magnetic field [61]. According to this model, the process of magnetoresistance relaxation consists in a slow, spontaneous disintegration of the ordered structure when the magnetic field is switched-off. As a result, the number of connections between the conducting particles decreases, and most probably the Brownian movement of the fine graphite particles plays a significant role. The high viscosity of the silicone matrix limits the speed of this disintegration movement and prolongs the magnetoresistance relaxation process.

Bednarek found that the relaxation process of the high stresses accumulated in the elongated silicone matrix during the magnetization process has a strong influence on the observed of magnetostriction and magnetoresistance hysteresis [59, 61]. Practically, the

hysteresis is determined by a partial remaining of the ordered structure even after the end of the relaxation process.

In 1998 Bednarek investigated the thermo-magnetoelastic and thermo-electroelastic properties of the composites, made of silicon steel and graphite particles uniformly dispersed inside a silicone matrix, which exhibit a high susceptibility to elastic deformations and a low electric resistance. The samples were obtained in the shape of rod, with the diameter of 3.4 mm and 355 mm in length, by the extrusion method [62]. For the calculation of the effective magnetic permeability, effective Young's modulus and effective Poisson's ratio of this composite, Bednarek introduced specific formulas [62]. The dependence of the unit elongation, $\Delta l/l_0$, and of the relative change in magnetic permeability and resistivity on the applied stress has a linear character and does not show hysteresis when the stresses are low enough (up to 0.3 MPa) [62]. For higher values of stress, the dependence loses its linearity and shows hysteresis. The investigation of the composite thermal expansion proved that its unit elongation is directly proportional to the temperature increase in the range 20-130°C. In the same range of temperature, the effective magnetic permeability decreases with the temperature increase, due to the decrease of the filling factor p_f , and magnetic permeability of the silicon steel. The effective resistivity increases linearly with the temperature increase in the above mentioned temperature range. The relative change in resistivity reaches 70%, being much higher than the relative change in effective magnetic permeability and unit elongation, within the same range of temperature. Considering that many composite material parameters (such as length, effective magnetic permeability, effective resistivity) depend on temperature, it was investigated also the influence of a current flowing through the sample (the composite has conducting properties due to the presence of graphite particles), which causes its heating by Joule effect. It was found that in the case of a constant density current, the relative changes of appropriate magnitudes caused by the same stress become higher. For instance, the relative change in effective resistivity increases up to 800% [62]. The theoretical studies suggest that

the graphite powder can be substituted by copper or silver, in order to obtain composites with better conducting characteristics.

In 2000, Bednarek performed new investigations on the elastic and magnetic properties of conductive and non-conductive ferromagnetic composites made of iron particles (200-250 μm) and iron and graphite particles, respectively inside a silicone matrix (Figure 4) [70]. It was determined the existence of an interesting effect: the heat-shrinkability, and changes of the magnetic permeability connected with it [70].

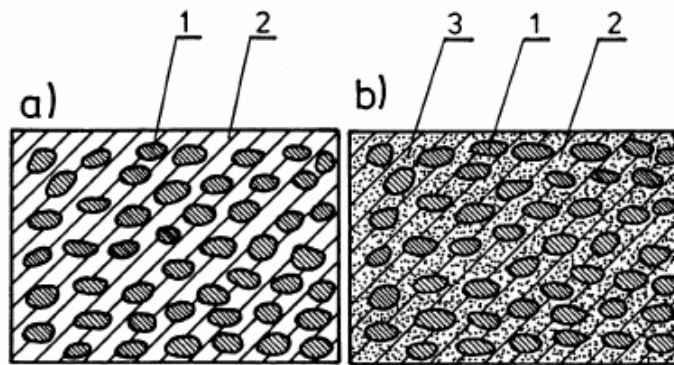


Figure 4. Structure of the heat-shrinkable non-conducting (a) and conducting (b), ferromagnetic composites: (1) pure iron particles (200-250 μm in size), (2) silicone matrix, (3) graphite particles (0.5 μm in size).

The study of both types of composites consisted in heating the extended (tensile stressed) samples, measuring then their unit elongation, ε , and estimating the relative magnetic permeability, μ_z . The tensile stress applied to the samples determines a unit elongation ranging from 5.4% (for the sample with $p_f=0.20$ and $p_g=0.50$) to 28.6% (for the sample with $p_f=0.25$) [70]. After removing the stress, ε is decreasing not to zero, but to a constant value ε_0 - initial unit elongation, as a result of the so called elastic recovery. The samples heating was realized after this elastic recovery process, by immersing the non-conductive sample in a recipient with glycerol and heating it with an electric heater, and by the electric current passing through the conductive sample. The heating causes a decrease of the initial unit elongation, ε_0 , of the samples, while the cooling to the initial temperature causes an increase in elongation up to a significantly lower value with respect to ε_0 . Therefore, it was stated that

the composites reveal a permanent heat-shrinkable effect. In the investigated range of temperature, the heat-shrinkability effect is dependent on ε_0 , p_f and p_g ; the increase of ε_0 increases the effect [70]. Bednarek discovered that the decrease in the samples elongation during the heating process is associated with an increase in the effective magnetic permeability, μ_z , which can not be explained by the increase in the relative magnetic permeability of the heated iron (which is 10-40 times smaller than the observed increase in magnetic permeability of the composite sample). In effect μ_z increase is connected with the p_f changes, determined by the composite change in volume during the heating process [70]. The obtained results suggest that the heat-shrinkable ferromagnetic composites may become a new group of materials, particularly useful for technical applications.

In 2004, Farshad and collaborators, from the Swiss Federal Laboratories for Materials Testing and Research, developed magnetoactive elastomer samples (beam-like, 60×10×4 mm, and cylindrical, 14 mm in both diameter and length), made of carbonyl iron, pure iron or nickel powders (with the size < 10 μm), uniformly dispersed inside a silicone rubber matrix, investigating their properties and exploring their potential for specific technological applications [71]. The particles volume fraction inside the composite material was 27% for all investigated samples. A constant magnetic field of 180 mT was applied (longitudinally or transversally to the main axis of the samples) during the elastomer cross-linking, determining the alignment of the ferromagnetic powders inside the elastic matrix (Figure 5) [71]. Through this alignment of the embedded particles, the tensile strength of the composite increases by 80%, the tensile modulus by 200%, and the compression modulus by more than 300% [71]. The magnetoactive composites produced by Farshad show certain actuator force properties. The magnetic-induced bending tests revealed a clear field dependent deformation. The equivalent magnetic force calculated on the basis of these experiments and the developed magneto-solid mechanics theory shows the dependence of the generated force on the ferromagnetic particles distribution in the elastomer. Compression tests on cylindrical

samples showed that the material stiffness increases in the presence of a magnetic field, due to the change in the compression modulus.

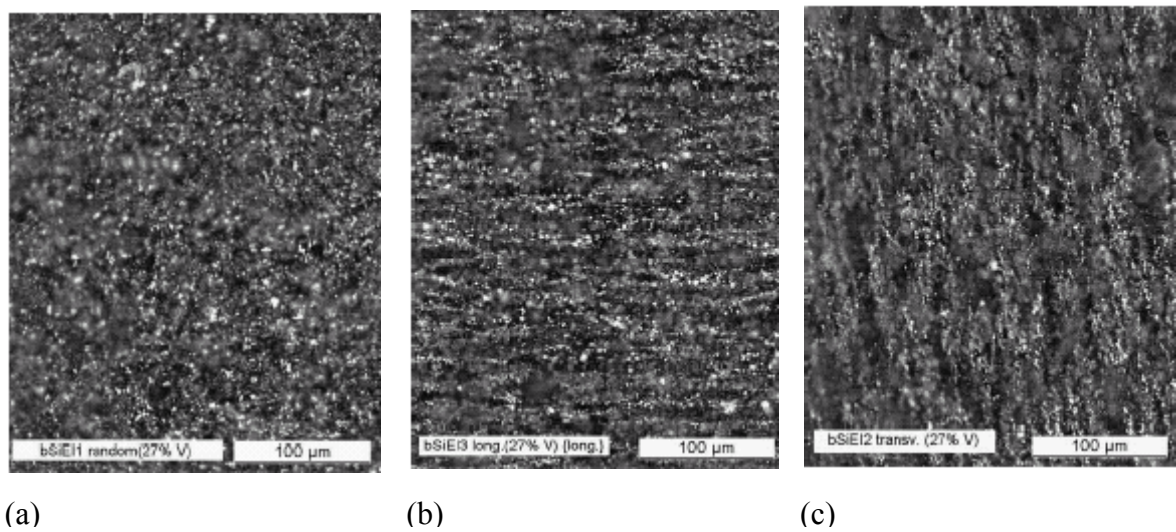


Figure 5. Microscopic picture of the silicone filled with: (a) randomly dispersed, (b) longitudinally and (c) transversally aligned carbonyl iron powder particles.

All these experiments led to useful hints regarding the use of such elastomer composites as tunable force structural elements [71]. Further investigations on the compression properties of this kind of soft magnetostrictive elastomers show clearly their potential for specific application as compressive elements with tunable stiffness or compliance, for vibration control in automobile industry, as high strain rate actuators, electro-magnetically active damping elements, muscle type actuators, etc. [72].

Nikitin and collaborators (2004) from Moscow State University developed a new magneto-controlled elastic composite material produced by dispersing ultra-fine (from 0.011 to 0.2 μm) magnetic particles of iron in a polymer matrix, based on natural or synthetic rubber [73]. The giant magneto-deformational effect, the influence of the magnetic field on the elastic properties, and the shape memory effect were investigated. The experiments were conducted on ribbon-shaped and cylindrical magnetoelastic samples. It was found that under the influence of the magnetic field, this material exhibits large elongations (of 200-300% from the initial length) - giant magneto-deformation and, when the magnetic field is removed, it

completely restores the initial shape. This effect was called pseudo-plasticity in magnetic field (or shape memory effect) [73]. It was also found that the application of a magnetic field leads to a substantial increase in the composite Young's modulus.

1.2.3. Composite materials made of soft magnetic nanocrystalline powder particles inside a polymer matrix

The range of the available soft magnetic materials has been significantly increased by the development of the nanocrystalline magnetic materials, beginning with those conceived by Yoshizawa and collaborators (1988) from Magnetic and Electronic Materials Research Laboratory, Hitachi Metals Ltd. Japan [74]. The iron and cobalt-based nanocrystalline ribbons such as FINEMET ($\text{Fe}_{73.5}\text{Cu}_1\text{Nb}_3\text{Si}_{13.5}\text{B}_9$), NANOPERM ($\text{Fe}_{83-90}\text{M}_{5-7}\text{B}_{2-6}\text{at}\%$, $\text{M}=\text{Zr},\text{Nb},\text{Hf},\text{Ta},\text{Ti},\text{V}$, etc.) and HITPERM ($\text{Fe}_{44}\text{Co}_{44}\text{M}_7\text{B}_4\text{Cu}_1\text{at}\%$, $\text{M}=\text{Nb},\text{Hf},\text{Zr}$) have been the object of extensive research all over the world in the last three decades of the XX century, due to their excellent soft magnetic properties such as high saturation induction, low coercive field, high magnetic permeability and low magnetic losses [74-81]. Generally, these soft magnetic alloys are prepared first in amorphous state, in thin ribbon shape, by rapid-quenching from the melt, and subsequently heat-treated (controlled crystallization from amorphous state) to induce the formation of nanocrystals with size of the order of 10 nm immersed into a residual amorphous matrix (with the composition different from the original one). The positive outcome of the amorphous-to-nanocrystalline transformation is the extraordinary improvement of the soft magnetic characteristic, in a unique combination of: very high initial permeability (more than 10^5), low coercivity (less than 1 A/m) and hysteresis losses, high saturation induction and almost zero magnetostriction [78, 82]. This special combination of soft magnetic properties is given by the reduced (vanishing) magnetocrystalline anisotropy, due to the ferromagnetic exchange interactions (mediated by the amorphous matrix) between the nanocrystals, in the regime $D \ll L_{\text{ex}}$ (where D is the mean

grain size and L_{ex} is the ferromagnetic exchange length) [83, 84], and by the low, almost zero magnetostriction. The peculiar characteristics of these nanocrystalline materials derive from the interdependence composition \leftrightarrow dimension of the atomic/molecular domains \leftrightarrow phasic interfaces. As consequence, the magnetic, electric, mechanic and optic performances can be easily tailored by the control of the grains dimension, composition, and grains interactions. The nanocrystalline soft magnetic materials may have a wide range of applications in magnetic cores for sensors, actuators, ground fault interrupters, inductive components for industrial electronics, telecommunications, etc. [78].

On the other hand, the nanocrystallized amorphous ribbons become very brittle, restricting their application possibilities. In addition, this limitation is complicated by the second disadvantage which is the small thickness (up to maximum 50 μm) of the nanocrystalline ribbons, determined by the specific characteristics of the rapid-quenching from the melt preparation process. Therefore, the shape of the magnetic cores based on soft magnetic nanocrystalline ribbons is generally limited to toroidal wound or stacked types [85-88]. Consequently, these materials are not the best choice for those applications in which large mass and/or volume of soft magnetic materials, or complex shaped parts are required. Therefore, in spite of their excellent magnetic properties, the large employment of the nanocrystalline soft magnetic materials in magnetic devices is much restricted.

The production of nanocrystalline metal powders by high-energy ball milling of the nanocrystalline or amorphous ribbons, or directly from elemental powders, makes possible the preparation of samples whose shape and dimension can be freely formed using various consolidation methods like sintering, hot isostatic pressing, warm compaction, explosive compaction, shock-wave compaction, etc. [89]. Apart the fact that the powders have worst soft magnetic characteristics than the nanocrystalline ribbons, their preparation methods are generally complex (due to the limiting temperature to which the powder can be exposed during the compaction process, considering the metastable state of the nanocrystals subjected

to grain growth, with the consequent drastic deterioration of the soft magnetic properties) and costly [90-92].

An alternative to the soft magnetic nanocrystalline ribbons and powders are the composite materials made of soft magnetic nanocrystalline powder particles embedded inside a polymer (silicone) matrix [93, 94]. These composites exhibit novel macroscopic magnetic properties due to the combined action of quantum-size effects, strain and surface effects, interface interactions between nanostructure and the matrix, nanostructures morphology and matrix properties. Generally, these composites have worse magnetic properties than the ferromagnetic sintered ones, but high electrical resistivity and consequently very small core losses, even smaller than those of the precursor or correspondent composite nanocrystalline ribbons. From this point of view, the soft magnetic composite materials, based on nanocrystalline ferromagnetic powders, are useful materials for high-frequency applications [95].

Many attractive properties of polymers, like noncorrosiveness, light weight, mechanical strength, and dielectric tenability can be utilized, along with the magnetic and optical properties of the nanoparticles, and the ability to be readily modeled into complex shapes, to make multifunctional materials. The polymer host matrix, in addition to provide a means of particle dispersion, mediates the magnetic interactions between the filling particles (including dipolar, exchange (isotropic and anisotropic), super-exchange and magnetoelastic interactions) [96, 97]. In this context, the inclusion of ferromagnetic or superparamagnetic nanoparticles in polymers is particularly important considering they show promise in various applications like spin-polarized devices, carriers for drug delivery, magnetic recoding media, high-frequency applications, etc [98, 99].

In 1999, Leger and collaborators prepared a composite material made of $\text{Fe}_{73.5}\text{Cu}_1\text{Nb}_3\text{Si}_{15.5}\text{B}_7$ nanocrystalline powder particles uniformly dispersed inside an epoxy resin [100]. During the polymerization process of the resin matrix, the metallic particles were

oriented under the action of a magnetic field. It was found that the particles orientation influences the magnetic permeability of the composite. The results of the investigation on the core losses, complex permeability (up to 500 MHz) and magnetic induction versus frequency (up to 200 kHz) show that such composites may ensure fair magnetic properties for middle and high-frequency (up to 1 MHz) power applications [100]. Moreover, these materials present the advantage of better magnetic behavior at high temperatures (up to 150°C for the nanocrystalline powder and at least 250°C for the resin) than ferrites, for which the working temperature is ranging between 80 and 100°C [101]. They also demonstrate better mechanical characteristics than the nanocrystalline ribbons, which enable various design possibilities for magnetic circuits, etc. In any case, there are still necessary further research in order to find a good compromise between the mechanical and magnetic properties of these composites for power electronics and telecommunication applications.

Paterson and collaborators (1999) modeled the properties of the composite soft magnetic materials made of magnetic particles (ferrite powder) in a non-magnetic, polyester resin matrix, using the effective medium theory [102]. Measurements of the high-frequency complex permeability were accomplished and the obtained results were compared with the predictions of various formalisms of the effective medium theory. The agreement between the experimental results and the predictions shows how successful is this theory in modeling the behavior of these materials over the whole range of possible compositions [102].

Dobrzanski and collaborators (2005) prepared soft magnetic composites made of nanocrystalline $\text{Co}_{68}\text{Fe}_4\text{Mo}_1\text{Si}_{13.5}\text{B}_{13.5}$ (SILAME®) powder particles inside a silicone polymer matrix (in different weight ratios), investigating their structure, magnetic and mechanical properties [103, 104]. The samples were produced in toroidal shape (inner and outer diameter of 27 mm and 35 mm, respectively and height of 5 mm) by compacting and then polymerizing the composite [104]. The microscopic examination shows a homogeneous distribution of the powder particles in the silicone matrix for high powder content, while

lower concentrations determine the agglomeration of the metallic particles (Figure 6) [104]. With respect to the $\text{Co}_{68}\text{Fe}_4\text{Mo}_1\text{Si}_{13.5}\text{B}_{13.5}$ powder, characterized by a low coercive field $H_c=36.3$ A/m and a saturation induction $B_s=0.64$ T, the composite has the following magnetic characteristics strictly dependent on the metallic powder to silicone weight ratio and particles size, for the powder to silicone weight ratio ranging from 2:1 to 6:1: H_c was ranging from 54.6 to 134.5 A/m and B_s is ranging from 0.63 to 0.72 T, respectively [104].

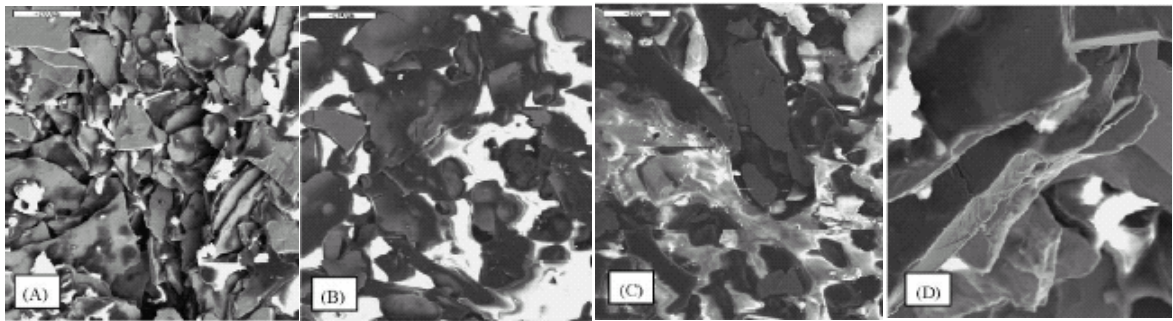


Figure 6. SEM structures of the nanocrystalline composite material based on $\text{Co}_{68}\text{Fe}_4\text{Mo}_1\text{Si}_{13.5}\text{B}_{13.5}$ powder particles inside the silicone matrix, for different weight ratios of nanocrystalline powder to silicone: (A) 6:1; (B) 4:1; (C) 3:1; (D) 2:1.

The mechanical properties of the composite revealed a significant dependence on the powder ratio, deteriorating with its decreasing. Dobrzanski stated that the rather poor mechanical properties may be determined by the excessively low silicone adhesion to the metallic powder particles, and in this respect further investigations for improvements are required [104].

Isnard and collaborators (2005) developed a soft magnetic composite made of Ni_3Fe powder inside a dielectric polymer binder, investigating its magnetic properties (initial and complex permeability, the frequency dependence of permeability and losses, in the range 1-50 kHz) and electrical resistivity [105]. The ferromagnetic powder particles (with the mean size of 17 nm) were obtained by mechanical alloying elemental Ni and Fe. The powder was mixed with the polymer and toroidal samples (inner and outer diameter of 25 mm and 35 mm, respectively) were obtained by compacting and then polymerizing the composite [105]. The obtained low core losses are the consequence of the high electrical resistivity of the samples, ($\cong 17 \Omega\text{mm}$), which is four orders of magnitude larger than the sintered material resistivity

[105]. The core losses depends on the content of dielectric binder, while the magnetic permeability depends on the samples density. Researches on the possibility to increase the compressibility of the Ni_3Fe powder are in progress. The use of these new soft magnetic composites for the production of magnetic cores for ac applications depends upon the improvement that will be achieved in the compacting density.

Nowosielski and collaborators (2005), from Institute of Engineering Materials and Biomaterials, Gliwice, Poland, reports the preparation and investigation of a nanocomposite polymer based on $\text{Fe}_{78}\text{Si}_9\text{B}_{13}$ powder particles [106]. The preparation technique of this material has the following steps [106]:

1. the amorphous $\text{Fe}_{78}\text{Si}_9\text{B}_{13}$ ribbons are milled in a high energy ball mill;
2. the obtained metallic powders are sieved to a particle mean diameter of 25-75 μm (small), 75-200 μm (medium) and 200-500 μm (large) and then annealed at 773 K for 1 h, in argon atmosphere, in order to obtain the nanocrystalline state and to reduce the stresses induced during the milling process;
3. the nanocrystalline powder particles are mixed with the silicone polymer, preparing toroidal shape samples (external and internal diameter of 34 mm and 28 mm, respectively, and height of 8 mm) having the ferromagnetic particles to silicone weight ratio of: 6:1, 5:1, 4:1, 3:1, 2:1 and 1:1;
4. the polymerization process takes place under a magnetic field $H=500$ A/m, which ensures the preferential orientation of the powder particles inside the silicone matrix.

The morphology of the milled powders was examined by scanning electron microscopy (SEM) (Figure 7). It can be observed that the larger particles (326 μm average dimension) have shape like flakes and plates, with sharp edges. The shapes of the medium size particles (127 μm average dimension) are similar, while the small size powder particles (48 μm average dimension) have very different shapes: irregular flakes, flat with round edges and perfect spherical shape, suitable to form consolidated powder cores with high density [106].

The soft magnetic properties of the obtained composite were investigated along with the possibility to control them tailoring the particles size and weight ratio. It was found that the magnetic properties can be controlled in a wide range, depending on the shape, size, mass fraction and orientation of the nanocrystalline particles. The obtained results show that the composite permeability increases with the particle size increase and the magnetic characteristics strengthen with the increasing of the metallic powder-to-silicone weight ratio. The best results ($H_c=312$ A/m, $B_s=1.06$ T, $B_r=0.084$ T and $\mu=98$ measured for a magnetic field $H=3$ kA/m, at $f=50$ Hz) were obtained for the composite filled with 85.7 wt% large size powder particles [106].

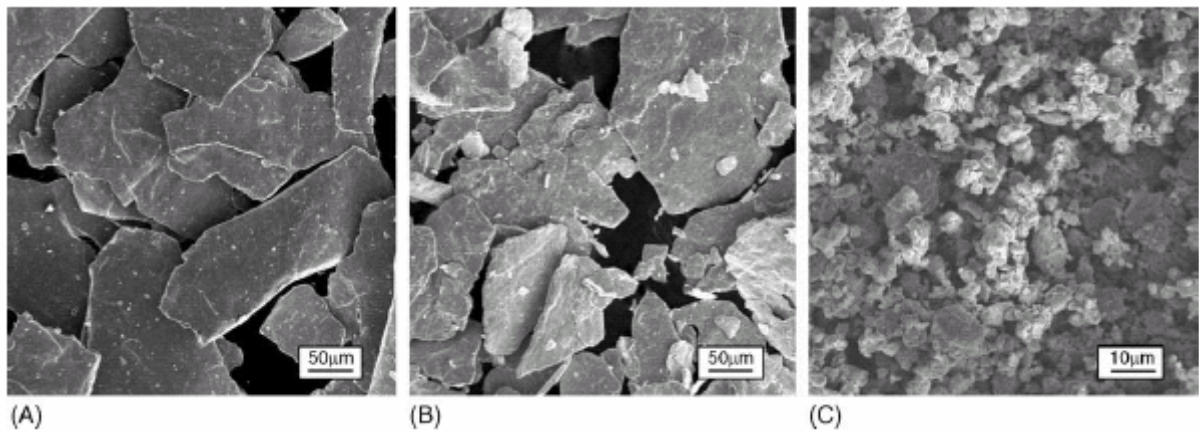


Figure 7. SEM images of the $Fe_{78}Si_9B_{13}$ powder particles with size between (A) 200-500 μm , (B) 75-200 μm , (C) 25-75 μm .

1.2.4. Magnetorheological solids (elastomers)

The solid analogous of the more familiar magnetorheological fluids are the magnetorheological elastomers, for which there is an increased interest recently [107, 108-111]. A brief presentation of the magnetorheological fluids is given in the followings, focusing on their main characteristics, performances and shortcomings, as premises for the development of the magnetorheological elastomers.

The magnetorheological fluids (MR), first reported by Rabinow in 1948 [112], are colloidal suspensions of magnetizable particles, with micrometric dimensions, which exhibit a

continuous, rapid and reversible change in the rheological properties (such as viscosity, elasticity, etc), changing their phase between liquid and solid, when subjected to an external magnetic field (Figure 8, [113]). Practically, in the absence of the magnetic field, the magnetic particles are randomly distributed inside the fluid. The action of the magnetic field determines the magnetization of the particles which interact between them with attracting forces, forming chains and columns along the field direction [114, 115].

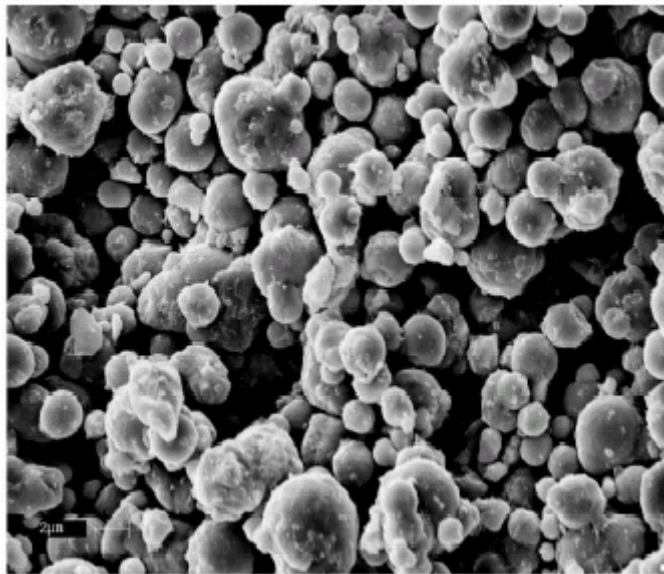


Figure 8. Reflection electron microscopy (REM) image of the ferromagnetic particles from a magnetorheological fluid.

The fibrous columns restrict the fluid flow, transforming it in a solid material [116-118]. The mechanical energy required to brake the induced columns of magnetic particles, the so called yield stress (which is the critical stress to be applied to a material in order to make it flow), is increasing with the applied magnetic field increase. When the magnetic field is removed, the material recovers its fluid state [119, 120]. Both the activation and deactivation of the MR fluids are completed within some milliseconds after the field turning on or off [107]. Generally, the magnetic fillers used for the preparation of magnetorheological fluids are ferromagnetic or paramagnetic particles, typically greater than $0.1 \mu\text{m}$ in diameter. For smaller size, the Brownian motion should prevent the formation of the chain-like structure. On the

other hand, particles larger than 10 μm make difficult the preparation of stable MR fluids against the sedimentation process [117].

The common MR fluids are suspensions of carbonyl iron, $\text{Fe}(\text{CO})$, particles [121], iron-cobalt alloy particles [122], meso-scale carbonyl iron and nickel-zinc ferrites [123]. The reason for which the preferred particles for MR fluids are based on iron is given by their high permeability and saturation magnetization, which provide high interparticle attractions and thereby, high MR effect [121]. The generally used carrier fluids are silicon oil, kerosene, synthetic oils, etc. The most important property of the matrix material, beside the rheological properties, must be a magnetic permeability as low as possible. If the matrix is magnetic, the magnetic polarization of the particles should be less effective and the MR effect smaller [107]. In any case, this is not a problem since oils and rubber materials are not normally magnetic. The third very important component of the MR fluids are the special additives, with stabilization role, used to solve the sedimentation problem, dispersion stability and re-dispersibility.

The magnetorheological properties of the MR fluids are typically dependent on the particles concentration, density, shape and size distribution, on the carrier fluid and additive properties, on the applied magnetic field and temperature, etc. The relationship between all these factors is very complex, and there is still work to develop for the optimization of the MR fluids performances. The key factor for the progress of these materials is the thorough understanding of the fundamental mechanism of the magnetorheology phenomenon.

The quick response, good reversibility and controllable performances of the MR fluids make them widely used in various devices such as dampers, clutches and brakes [124-127]. However, the MR fluids exhibit some shortcomings such as the sedimentation of the magnetic particles, due to the density mismatch of the carrier fluid and fillers, which can degrade the MR effect [118].

The solid analogous of the magnetorheological fluids are the magnetorheological solids, where the carrier fluid (oil) is replaced by a rubber material or a gel. They are expected to overcome the disadvantages of the MR fluids. The obvious advantages from using solid matrix are that the particles are not able to settle with time and there is no need to use containers to keep the MR material in its place.

The magnetorheological solids are composed of micro-sized magnetic particles of iron or iron-based alloys, such as carbonyl-iron and iron-cobalt [115, 128], dispersed in a polymer matrix. The choose of iron as basic element for the preparation of these MR materials is sustained by its high magnetic saturation (after Co, which is expensive), considering that the magnetic efficiency in changing the magnetic field dependent mechanical properties is given by a high magnetic saturation. Conventionally, the mixture is cured in the presence of a magnetic field, so that the magnetized particles are aligned, forming chainlike and columnar structures inside the elastic matrix [115, 118, 129, 130]. Whereas the MR fluids have a field-responsive yield stress, the MR solids have a field-responsive elastic modulus [131]. The maximum increase of the elastic modulus in MR elastomers has been reported to be around 0.6 MPa (which is 40% of the initial elastic modulus), when the volume concentration of iron particles is 30% [130].

The MR elastomers have attracted considerable interest especially in the recent years, being successfully brought into the market due to their potential for applications as relatively simple and quite variable stiffness devices, rapid-response interfaces between electronic controls and mechanical systems [115, 119, 132], adaptive tuned vibration absorbers, stiffness tunable mounts and suspensions and automotive bushing, etc [5, 119, 129, 133-136].

Different studies have been developed on MR solids for which the particles have been aligned in a magnetic field prior to the matrix curing [115, 129-131]. However, the conventional method to fabricate MR elastomers, with oriented particles in magnetic field (anisotropic MR elastomers), has many shortcomings which greatly limit their industrial

application. Firstly, the conventional rubber-producing equipment must be modified to provide a magnetic field during cross-linking. Secondly, the chain direction of the anisotropic samples must be considered when used in particular devices. Thirdly, thick MR elastomers can not be fabricated, because the magnetic flux density decreases sharply with the samples thickness increase.

Considering all these, in 2003, Lokander and collaborators from the Royal Institute of Technology of Stockholm, produced and investigated isotropic MR solids made of nitrile rubber (with various acrylonitrile contents), and two different types of iron particles: large, irregularly shaped iron particles and spherical carbonyl iron powders [111]. It was discovered that the MR effect in the case of irregularly shaped iron particles is larger compared to the isotropic material with carbonyl iron, and larger than first expected, considering the low value of the magnetic field (about 0.3 T) and that the particles are not aligned within the matrix. (It is well known that the interaction energy between two magnetic dipoles is inversely proportional to r^3 , where r is the distance between the particles; when they are aligned by a magnetic field, the distance between them is minimized in the field direction, resulting in a substantially larger MR effect than for isotropic materials [111]). The relatively large MR effect for the isotropic material can be explained by the quite small distances between the particles, even if they are not aligned, due to the low Critical Particle Volume Concentration of the irregular powders. Even if it is difficult to compare results from different equipments, the isotropic MR elastomers developed by Lokander and collaborators show an increase of the absolute elastic modulus of about 0.4 MPa at 10 Hz and 0.24 T in the case of large, irregular shape carbonyl iron particles, while the anisotropic rubber materials with aligned carbonyl iron (developed by other researchers) show a maximum increase of 0.7 MPa at 10 Hz and 0.85 T [115]. It is very much probable that the used adhesive causes a too high zero-field elastic modulus, and therefore also the relative MR effect (%) appears to be smaller than it is [111]. Lokander discovered that the materials with badly dispersed carbonyl iron, which

results in remaining aggregates of particles, have a similar MR effect to that of the materials with larger irregular particles [111].

Lokander continued his researches on the performances improvement of the isotropic MR rubber materials, based on irregular shape iron particles with size $< 60 \mu\text{m}$, in stronger magnetic fields, up to 0.8 T, studying the influence of the plasticisers and of applied strain on the MR effect [109]. It was found that, for an isotropic MR rubber (with 32% in volume iron), under the influence of 5.4% strain and 0.8 T magnetic field, the absolute MR effect is of about 0.8 MPa, which is twice the value obtained for the same material, but in anisotropic state [109]. It was also demonstrated that, the decrease of zero-field elastic modulus, and therefore the increase of the relative MR effect, can be obtained by the addition of plasticisers or by using a softer matrix material, such as silicone rubber [109].

In 2004, Lokander and his collaborators reported new results on the long-term stability of the MR rubber materials [110]. The high iron concentration (about 30% in volume), required to get a substantial MR effect, determines the material oxidation. It was found that the oxidative stability of the natural rubber decreases dramatically for large amounts of iron particles, due to the catalytic effect of the iron ions on the decomposition of hydroperoxides and due to the large amounts of oxygen on the surface of the iron particles. It was reported that conventional antioxidants can be used to prolong the lifetime of the MR elastomers, but in order to get acceptable lifetime, a careful selection of the antioxidant system, which should include some metal deactivator, has to be made.

Considering that many challenges have remained for the development of isotropic MR materials with high relative MR effect, in 2005, Gong and collaborators, from the University of Science and Technology of China, report their attempts to fabricate isotropic MR elastomers, with improved MR performances [118]. The sample ingredients were carbonyl iron particles (with the average diameter of $3 \mu\text{m}$), silicone oil and silicone rubber. The magnetic particles were firstly immersed in silicone oil and then mixed with the silicone

rubber. After mixing all ingredients, the resulting composite was put under vacuum to remove the air bubbles, and then cured for 24 h, at room temperature, in the absence of magnetic field. In this way, isotropic MR samples with different percentages of carbonyl iron particles, silicone oil and rubber were prepared. It was found that, due to the help of the silicone oil additive, these MR elastomers consist in a kind of self-assembled microstructure of particles. Under the magnetic field action, the particles are magnetized and move slightly, due to the lubrication action of the additive, to form a regular construction, which result in a high MR effect. The best MR effect was obtained for 60, 20 and 20% percentage of carbonyl iron particles, silicone rubber and silicone oil, respectively, the elastic modulus enhancement reaching 60%, which represent the same degree as for the anisotropic MR elastomers fabricated under a strong magnetic field [118]. Furthermore, a simple micro-assemble model, in agreement with the obtained experimental data, was proposed to explain the MR effect [118].

1.2.5. Theoretical studies

Several approaches to model the behavior of the magnetostrictive composite materials were developed. In the case of linear analytical approaches the Green's function [137] and a rule-of-mixtures to predict global properties were used [138, 139], while in the case of non-linear approaches, a constant field assumption, coupled with conventional composite models (e.g., concentric cylinders), was used to predict the internal stresses in, and around the magnetostrictive particles [140, 141]. Yin and collaborators proposed a micro-mechanical-based hyperelastic constitutive model of the magnetostrictive elastomers [142], while Hunag and collaborators developed a micromechanics approach in order to determine the effective magnetostrictive behavior of the magnetostrictive composite materials [143].

Ce-Wen Nan and Weng (1999) developed a detailed theoretical study of the effective magnetostrictive behavior of magnetostrictive composites (made of SmFe_2 and Terfenol-D

particles in an epoxy matrix) by elaborating an analytical model based on a Green's function technique, in order to investigate the influence of the microstructure (material constants, particles shape, anisotropy, orientation relative to the applied magnetic field, etc) [144, 145]. Reuss and Voigt-type approximations are also given, which yield bounds for the effective saturation magnetostriction. The numerical calculation of the effective saturation magnetostriction in SmFe₂/epoxy and Terfenol-D/epoxy composites demonstrate the strong influence of the material constants, magnetic particles volume fraction, phase connectivity, particle shape and orientation, etc [144]. The theoretical estimations were found to be in agreement with the experimental results. This theoretical model provides a general guideline for the evaluation of more composite systems, and to develop criteria for choosing the best combination of constituent materials for application in magnetostrictive actuators and sensors. The theoretical framework can also be extended to model other macroscopic properties such as strain versus H-field behavior, hysteresis, stress and thermal effect on the magnetostrictive composite materials.

A thorough theoretical study of the magneto-elastic properties of elastomer-ferromagnet composites was developed by Liliana Borcea and Bruno, from the Rice University of Huston in 2001 [146]. The macroscopic magneto-mechanical behavior of the composite materials consisting of a random, statistically homogenous distribution of ferromagnetic, rigid inclusions embedded firmly in a non-magnetic elastic matrix was investigated. Specifically, the overall magneto-elastic response of the MR material (deformations and stress-strain relation), corrected to second order in the particles volume fraction (which is the lowest order in the volume fraction expansion for which the magnetic interactions between particles are taken into account), was theoretically evaluated for given applied elastic and magnetic fields [146]. It was considered the fully coupled magneto-elastic problem in MR solids, for random microgeometries, and the overall properties in the case of small volume fraction of ferromagnetic particles were evaluated. There were calculated the

elastic and magnetic interactions between the filling particles, as well as the state of mechanical equilibrium. The displacement of the ferromagnetic particles, under the action of the magnetic field are calculated from the force and torque balance equations. The obtained solutions account for the fully coupled magneto-elastic interactions. The magnetization distribution in the composite was calculated from the basic minimum energy principle of the magneto-elasticity [146].

Davis, from Ford Research Laboratory, Michigan, used the finite element method to analyze the dependence of the effective shear modulus of the magnetorheological (MR) elastomers on the inter-particle magnetic forces [147]. Chen and collaborators investigated the relationship between the Young's modulus of the elastic matrix and the composite magnetostriction [148]. In 2000, Armstrong reported an analysis of the magnetoelastic behavior of the composites made of magnetostrictive particles [149, 150].

In 2003, Brigadnov (from the North-Western State University of ST. Petersburg, Russia) and Dorfmann (from Institute of Structural Engineering, Vienna, Austria) developed the mathematical modeling of the MR elastomer, considered as an hyperelastic, homogenized, non-polar isotropic continua [133]. The complete system of constitutive equations for the considered composite was based on the equations from the classic work of Pao [151], in which the motion equations for an isotropic non-polar continuum, in an electromagnetic field are described by Maxwell's equations and by the mechanical and thermodynamical balance laws [133]. The basic system of constitutive equations for the MR Cauchy-elastic solids was then developed, using a phenomenological approach based on the experimental data of Carlson and Jolly [108]. The resulting equations, coupled with suitable boundary and initial conditions, were used to illustrate the application of the constitutive model and of the theory, by considering the simple shearing of a MR elastomer between two parallel plates, under the action of a perpendicular magnetic field. It was found an acceptable agreement between the numerical simulation and the experimental measurements results. It was shown that the effect

of the magnetic field is to stiffen the shear response of the material. Considering the obtained results, the given mathematical framework can be used to develop more complex material laws of the MR elastomers.

Dorfmanan continued his researches in the field by:

- ▶ modeling the behavior of an isotropic magneto-sensitive composite within the framework of the electromechanical and thermomechanical theories [149]. There were discussed and incorporated in the material model, the appropriate simplifications for the constitutive laws. The theory was applied to a representative geometry for applications, in which the composite sample is confined to a circular cylindrical tube, subjected to an axial shear deformation, in the presence of a radial magnetic field. Two very specialized forms of the model were used to illustrate the experimental result: the material shear stiffness increases with the magnetic field strength [153];
- ▶ developing the governing equations for a more general form of the constitutive model and providing alternative equation forms, including a Lagrangian formulation. To verify the theory, the problem of an azimuthal shear of a circular cylindrical tube is formulated and then solved for a specific constitutive law, in the case of a magnetic field initially radial. The results show the stiffening of the azimuthal shear stress/strain response, with increasing the magnetic field strength [154].

In 2004, Kanakanala and Triantafyllidis, from Department of Aerospace Engineering, Michigan University, published an excellent review on the modeling of magnetorheological elastomers (MRE) [155]. The studied materials are rubbers filled with micron-sized ferromagnetic particles. Two different approaches to the continuum formulations for MREs, with negligible dissipative and hysteretic behavior, are presented: a direct approach, Eulerian, based on the second law of thermodynamics, plus the conservation laws method of

mechanics, and a novel energy approach, Lagrangian, based on the unconstrained minimization of a potential energy functional [155]. It is shown that both approaches yield the same governing equations and boundary conditions. Kanakanala and Triantafyllidis used a particular free energy function to illustrate the magnetoelastic coupling phenomena in a magnetorheological elastomer with cylindrical shape, subjected to traction or torsion, under the presence of external magnetic field [155].

2. ELASTOMAGNETIC COMPOSITE MATERIALS: PREPARATION

The object of this thesis is the magneto-elastic characterization and thermal stability investigation of the recently developed elastomagnetic materials made of ferromagnetic micro-particles uniformly dispersed inside a non-magnetic, elastic matrix.

From conceptual point of view, the new elastomagnetic materials [156-158] represent an interesting development of the composites previously presented in the first chapter. These materials are opening a new scenery in the field of magnetoelasticity in both fundamental investigations, for a thorough understanding of the micromagnetic interactions and intricate coupling between the elastic and magnetic processes, and engineering applications in intelligent devices.

These composites, made of ferromagnetic micro-particles uniformly dispersed inside a non-magnetic, elastomeric matrix, were called “elastomagnetic” in order to distinguish them from the usual magnetoelastic materials that are rigid magnetic materials exhibiting direct (Joule effect) and inverse (magnetomechanical effect) magnetostriction [159, 160]. An elastomagnetic composite must fulfill all the following requests: a) the magnetic particles must have a strong coupling between the magnetic moment and their body; b) the magnetic particles must be soft ferromagnetic, with a strong shape anisotropy or small permanent

magnets, with strong uniaxial magnetic anisotropy; c) the elastomeric matrix must have an elastic behavior, up to relative deformations of about 15%.

The elastomagnetic composites, object of the investigation activity developed in the frame of this thesis, are made of commercially available Sm_2Co_7 polycrystalline micro-particles (irregular shape), permanently magnetized, uniformly dispersed into a silicone matrix.

The decision to use Sm_2Co_7 (Sigma Aldrich product) as filling particles was determined by:

- ▶ their high uniaxial magnetic anisotropy [161] (which induces a high residual magnetization $\mathbf{M}_r=0.6\times 10^6$ A/m), determined by the specific crystalline structure, and strong coupling between the particles body and their magnetic moment (very important characteristic for optimum elastomagnetic performances);
- ▶ their small dimensions, with average values ranging from 2-5 μm , with respect to other commercially available powders;
- ▶ the weak dependence of the remanent magnetization and coercivity on temperature (Curie temperature, $T_C\cong 750$ °C);
- ▶ their rough surface (roughness up to 10% from the particle dimension) which ensures a good silicone adherence.

The volume percentage, V% (Appendix C), of Sm_2Co_7 particles inside the elastic matrix is a very important aspect for the material elastomagnetic performances; V% may range from 7.2%, which ensures good elastomagnetic performances and no magnetic and mechanical interactions between the particles, up to about 33%, if an increase of the elastomagnetic effect contribution is required [162]. The limit of 33% volume percentage must not be overcome in order to preserve the condition of no magnetic and mechanical interactions between the particles.

The reasons for which the commercially available silicone, Silicon 5 from Henkel, was chosen as elastic matrix for the developed composites are [163, 164]:

- ▶ exceptional ability to exhibit and retain superior mechanical characteristics (high flexibility and strength) over a broad temperature range $-50^{\circ}\text{C} \div + 150^{\circ}\text{C}$ (breaking load: 20 kg/cm^2 ; breaking deformation 550%)

Silicone can be deformed to very large strains and it springs back elastically to the original length when the applied strain is cancelled. The good elastic properties of the silicone matrix are very important to guarantee the reversibility and reproducibility of the elastomagnetic effects under small strains.

- ▶ optimum adherence to metals;
- ▶ good resistance to chemical (e.g. diluted acids and bases) and atmospheric agents, in particular to oxidants and UV radiations;
- ▶ excellent water repellency;
- ▶ excellent handability for the production of samples in complex shapes;
- ▶ outstanding thermal and electrical insulation properties;
- ▶ exceptional environmental compatibility, biocompatibility (physiologically inert, inodorous, insipid);
- ▶ cost-effective.

The used silicone is an RTV-1 type, which means: one-component, ready-to-use, room temperature cross-linking (curing). It is made of air cross-linking polydimethylsiloxanes. Silicone is commercially available in tightly closed collapsible tubes, having a gel (paste) consistency and being in a non-polymerized state. It undergoes an intrinsic polymerisation, hardening upon sufficiently long contact with the atmospheric air and forming a silicone elastomer. The curing process, which involves the reaction of silanol-terminated polydimethylsiloxanes with the oxygen from the air, starts at the surface of the applied layer of silicone, with the formation of a skin, and gradually progresses inwards. The process is

completed after about 36 h. The polymerised silicone is a very elastic solid, with Young's modulus of $E_{\text{silicone}} \cong 3.1 \times 10^4$ Pa.

The preparation process of the developed elastomagnetic composites occurs in four main steps as following:

1. demagnetization of the Sm_2Co_7 micro-particles, which have a spontaneous magnetization and consequently, the tendency to form clusters;

The demagnetization process (degaussing) was performed by applying an alternating magnetic field which decreases to zero from a value close to the saturation magnetizing field of the Sm_2Co_7 particles (about 4 T).

2. uniform mechanical dispersion of the magnetic particles inside the non-polymerized silicone;
3. the injection of the obtained mixture of Sm_2Co_7 micro-particles uniformly dispersed inside the silicone in a teflon stamp (generally having 5×5 mm² transversal cross section and 5 cm in length) in order to extrude bar shape samples; The extruded bars are left for about 36 h at room temperature for the complete polymerization of the silicone and composite forming. It was observed that the final length of the prepared samples is smaller with 4 mm than the stamp length, due to the silicone shrinkage during the curing process.

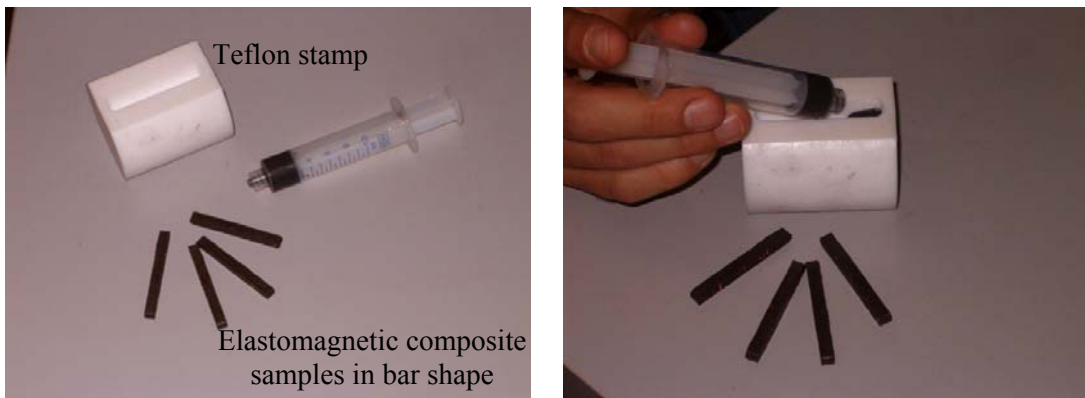


Figure 9. Injection process of the mixture of Sm_2Co_7 micro-particles inside silicone matrix in a teflon stamp. Extruded bar shape samples.

4. permanent magnetization of the elastomagnetic composite after its complete solidification.

The elastomagnetic response of the composite material depends strongly on the particles magnetic moment orientation because if it is random, any axis is equivalent for magnetization, as well as for the application of an external stress, while for particles pre-oriented with their easy magnetization axes all parallel, the magnetization along this axis is easier than along any other and the answer to an applied stress is different.

The permanent magnetization of the composite samples was induced by applying an external uniform magnetizing field of 8T, for 10 min, at room temperature, in the desired direction. A vibrating sample magnetometer (VSM), Oxford Instruments, 9T (Appendix A) was used to induce the permanent magnetization of the Sm_2Co_7 particles along a specific direction (i.e. in the most used experiments - at 45° with respect to the samples longitudinal axis, or along it). In this way, the elastomagnetic composites exhibit a remanent magnetization along the chosen direction, that is $\mathbf{M}=\mathbf{M}_r\tau V\%$ (where \mathbf{M} is the average macroscopic magnetization of the sample, \mathbf{M}_r is the remanent magnetization of the Sm_2Co_7 micro-particles and τ is the sample volume), even in the absence of an external magnetic field.

The magnetization cycles, \mathbf{M}_z versus \mathbf{H}_z , of the as-produced and permanently magnetized (with the particles remanent magnetic moment oriented at 45° with respect to the longitudinal z-axis) samples, at room temperature, up to 1 T, in the absence of strain, are reported in Figure 10 [165]. The results refer to a Sm_2Co_7 weight percentage of 4%. The effectiveness of the permanent magnetization is evident: the initial magnetization is not starting anymore from zero, but from the remanent magnetization. As can be seen, also after permanent magnetization the cycle is not squared, as for a hard magnetic material, due to the fact that the

measurements are not performed along the axis of the permanent magnetization, but along the longitudinal z-axis of the sample (Appendix A).

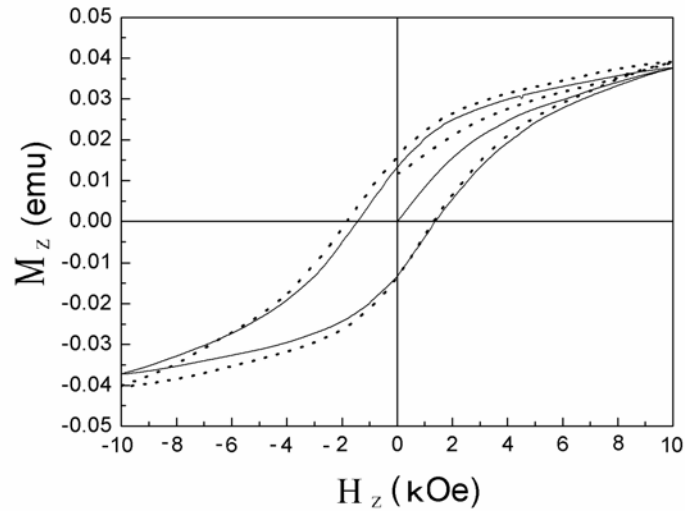


Figure 10. Magnetization cycles, M_z versus H_z , before (—) and after (-----) permanent magnetization at 45° with respect to the main axis (z) of the sample.

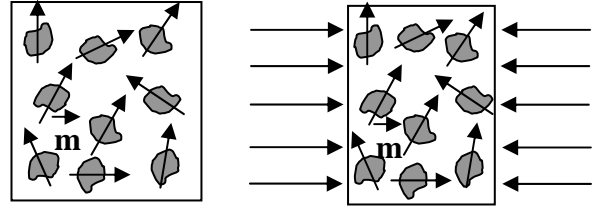
3. ELASTOMAGNETIC COMPOSITES: ELASTOMAGNETIC EFFECTS

The elastomagnetic composites, which represent the ideal system for the coupling mechanism between the elastic deformation and magnetization, exhibit elastomagnetic effects which occur by a mechanism independent on the intrinsic magnetostriction. The direct elastomagnetic effect is the sensible elastic deformation of the material, consequent to the application of an external magnetizing field. The inverse effect consists in the reversible change of magnetization determined by an elastic deformation of the composite material. These effects are as strong as the coupling between the magnetic moments of the filling particles and their body.

More specifically, in the case of a compressive strain inducing a volume deformation of the material, $\varepsilon_v = (\Delta V/V_0) < 0$ (where ΔV is the volume change and V_0 is the initial volume), magnetization changes take place through the following concurrent mechanisms:

1. particles density variation;

The average magnetization, \mathbf{M} , of the composite material is $M = \sum_i \frac{m_i}{V}$, where



V is the sample volume and \mathbf{m}_i are the magnetic moments of the ferromagnetic particles (considered as magnetic

Figure 11. The effect of a compressive stress on the ferromagnetic particles density in the elastomagnetic composite, when the sample transversal cross section is fixed.

dipoles) [166]. It is obvious that the volume modification, at fixed transversal cross section, determines a change in the average magnetization of the elastomagnetic composite (Figure 11).

2. change in the magnetic interactions between the ferromagnetic particles, due to the modification of the distances between them;

The potential energy of interaction between two ferromagnetic particles assumed as magnetic dipoles is given by [152]:

$$E = \frac{1}{4\pi\mu_0 r^3} \left[\vec{m}_1 \cdot \vec{m}_2 - \frac{3(\vec{m}_1 \cdot \vec{r})(\vec{m}_2 \cdot \vec{r})}{r^2} \right] \quad (1)$$

where \mathbf{r} is the distance between the magnetic dipoles centers and μ_0 is the vacuum permeability. From this equation it is clear that the magnetic interaction between the particles increases abruptly with the decrease of the inter-particles distance (Figure 12).



Figure 12. Change in the magnetic interaction between two ferromagnetic particles as function of the distance, r , between them.

3. change in the magnetic moments, \mathbf{m} , orientation due to the particles rotation determined by the compressive stress, σ_z (Figure 13);

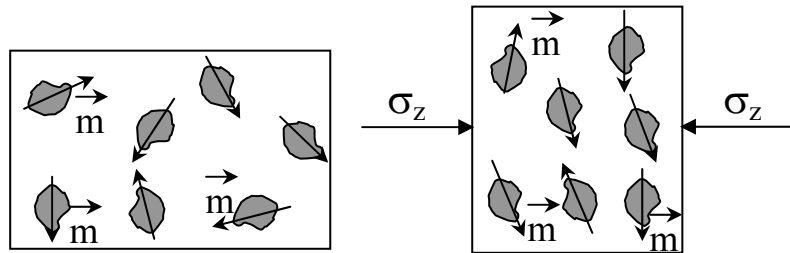


Figure 13. Change in the magnetic moments, \mathbf{m} , orientation under the action of an external stress, σ_z , due to the particles rotation.

In the case of soft ferromagnetic particles, the shape anisotropy determines the direction of the spontaneous magnetization along the main anisotropy axis, \mathbf{a} (because in this way the energy associated to the magnetic anisotropy is minimum) – see Figure 14. The coupling between the shape anisotropy and the particle magnetization is strong enough to determine in this case (of oblate particles) the rotation of the magnetic moment together with the particle rotation induced by the applied compressive stress, σ_z . In the case of hard magnetic particles with strong uniaxial magnetic anisotropy, a strong coupling between the magnetic moments and the particles body is active, determining the magnetic moment rotation simultaneously with the particle rotation under σ_z action. This magnetic moment rotation, induced by the external stress, determines a change in magnetization along the applied stress $\Delta \mathbf{M}_z = \mathbf{M}'_z - \mathbf{M}_z$: inverse elastomagnetic effect (Figure 14). In the same way, the application of a magnetizing field, \mathbf{H} , along an axis different from the easy magnetization one (which in the case of hard magnetic particles is the remanent magnetization axis) induces a rotation of the particles, due to the coupling mechanism between the particles magnetic moments and their body, in order to align the magnetic moments with the applied field; the macroscopic effect of the local rotations is the

deformation of the whole material (if it is enough elastic): direct elastomagnetic effect (Figure 15).

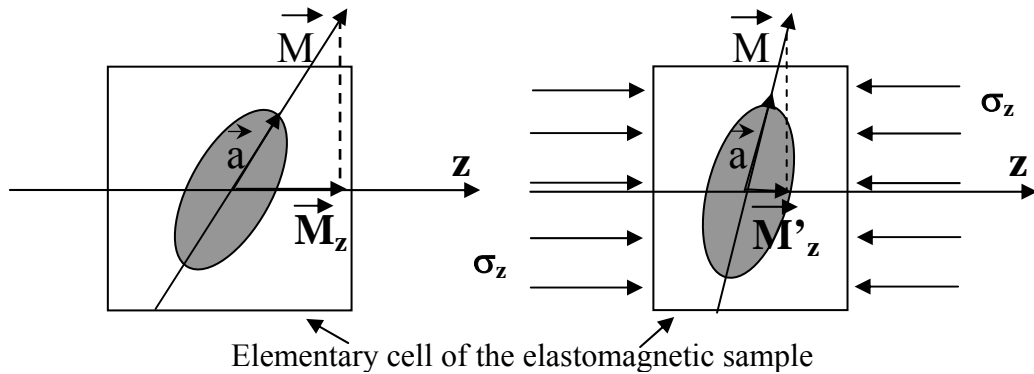


Figure 14. Inverse elastomagnetic effect: change in the longitudinal magnetization, \mathbf{M}_z , under the action of a compressive stress, σ_z , due to the coupling mechanism between the magnetic moment and particle body, for a fixed transversal cross section of the sample.

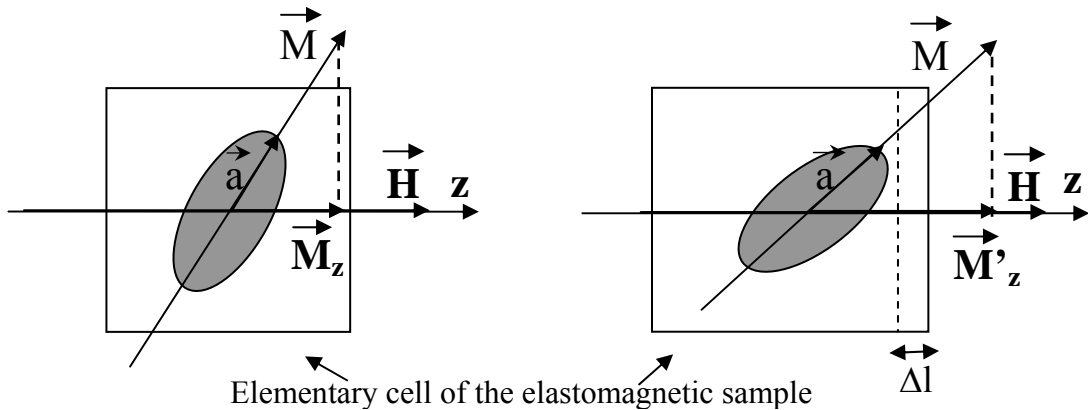


Figure 15. Direct elastomagnetic effect: change in the sample length, Δl , under the action of a magnetizing field, \mathbf{H} , due to the coupling mechanism between the magnetic moment and particle body, for a fixed transversal cross section of the sample.

The action of the magnetizing field, apart the sample elongation in the specific case, determines obviously the change in longitudinal magnetization $\Delta \mathbf{M}_z = \mathbf{M}'_z - \mathbf{M}_z$ (Figure 15).

4. magnetomechanical effect (inverse magnetostriction) due to the stress applied by the elastic matrix on the filling particles made of magnetostrictive material.

The efficiency of these four mechanisms and each one contribution to the magnetization change under the action of the external stress depend on:

1. the density of the filling particles inside the composite;

There is a threshold value of the particles concentration over which the assumption that they are not magnetically interacting in the absence of the (compressive) stress is not valid anymore [162].

2. the particles nature, shape and dimensions;

The magnetic and geometric characteristics of the filling particles determine the coupling mechanism between the particles magnetic moments and their body; at the same time, the magnetomechanical effect is possible only in the case of magnetostrictive filling particles [157].

3. the elastic properties of the non-magnetic, elastic matrix;

The elastic characteristics of the matrix determine:

- ▶ the rotation amplitude of the filling particles under the action of an external magnetic field and/or stress;
- ▶ the efficiency of the magnetomechanical effect.

4. the magnitude of the external stress;

The applied stress must be in the range for which the composite sample deformation is elastic, otherwise the effects are not reversible anymore.

5. the intensity of the magnetizing field.

It governs especially the efficiency of the coupling mechanism between the particles magnetic moment and their body; over a certain value of magnetizing field, a decoupling between the particles rotation and their magnetic moment rotation is expected.

All the above assertions are validated by the experimental results obtained during the activity of magneto-elastic characterization of the developed elastomagnetic composites and justified by the following simple model of the elastomagnetic effect.

4. THEORETICAL MODEL OF THE ELASTOMAGNETIC EFFECT

In the frame of the proposed model of the elastomagnetic effect, the following assumptions are considered:

1. the filling micro-particles are so diluted in the silicone matrix that they can be considered isolated one from the other;
2. the volume deformation of the sample, as a consequence of the external applied stress and/or magnetic field, occurs by conserving the sample transversal cross section and changing only the length along the stress/magnetic field axis;
3. in the presence of a magnetic field, each Sm_2Co_7 micro-particle behaves as a single domain, to which is associated the magnetic moment, \mathbf{m} .

In our experimental conditions, the magnetomechanical effect is negligible due to the smallness of the stress applied by silicone to the Sm_2Co_7 particles, as consequence of the small stresses transduced by silicone (e.g. for a strain of 15%, the longitudinal stress transduced by the composite matrix is $\sigma = \varepsilon_{\text{com}} E_{\text{comp}} = 15 \times 10^{-2} \times 7.5 \times 10^4 \text{ Pa} = 11.25 \times 10^3 \text{ Pa}$, where ε_{com} and E_{comp} are the strain and the Young's modulus of the composite sample, respectively), too low to induce a significant magnetomechanical effect in the Sm_2Co_7 particles ($\varepsilon_{\text{SmCo}} = \sigma / E_{\text{SmCo}} \cong 11.25 \times 10^3 / 1.3 \times 10^{11} \cong 8.6 \times 10^{-8}$) determined by the high difference between the Young's modulus of the composite elastic matrix ($E_{\text{comp}} \cong 7.5 \times 10^4 \text{ Pa}$, for $E_{\text{silicone}} \cong 3.1 \times 10^4 \text{ Pa}$) and of the Sm_2Co_7 particles ($E_{\text{SmCo}} \cong 1.3 \times 10^{11} \text{ Pa}$) [167]. At the same time, the elastomagnetic effect is significant, considering the strong coupling between the remanent magnetic moment of the Sm_2Co_7 particles and their body.

Let us consider now the elementary cell of an elastomagnetic composite sample, filled with a single irregular shape particle of Sm_2Co_7 , permanently magnetized at $\theta_1 = 45^\circ$ with respect to the main z-axis of the sample. When a magnetizing field \mathbf{H} is applied along z-axis, the magneto-mechanical moment $\mathbf{M}_m = \mathbf{m} \times \mu_0 \mathbf{H}$ produces a rotation of the magnetic moment,

\mathbf{m} , on \mathbf{H} direction (Figure 16). Due to the immersion in the elastic matrix of the silicone and strong coupling between the magnetic moment and particle body, the rotation of the magnetic moment implies a coherent rotation of the particle. The contra-reaction of the elastic matrix to the particle rotation is the elasto-mechanical moment $\mathbf{M}_e = -K\theta$, where θ is the effective particle rotation and K is the torsional elastic constant of the silicone matrix (Figure 16). Practically, the particle rotation takes place until the following equilibrium condition is fulfilled [157]:

$$m\mu_0 H \sin(\theta_i + \theta) = -K\theta \quad (2)$$

where θ_i is the initial angle between \mathbf{m} and \mathbf{H} and θ is the effective rotational angle with respect to the initial position (Figure 16). It was considered the convention: $\theta < 0$ if the rotation is clockwise.

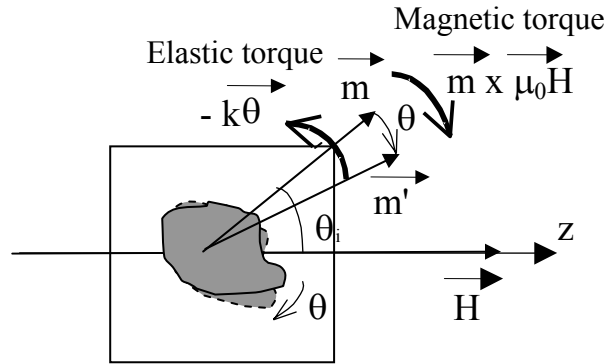


Figure 16. Equilibrium between the magneto-mechanical moment, $\mathbf{m} \times \mu_0 \mathbf{H}$, and the elasto-mechanical moment, $k\theta$, acting on the Sm_2Co_7 particle inside the elementary cell of the elastomagnetic composite under the action of an external magnetizing field, \mathbf{H} . θ_i is the initial angle between \mathbf{m} and z -axis.

Therefore, under the action of a magnetic field, the particle rotates of an angle whose value is established by the equilibrium between the magneto-mechanical moment induced by \mathbf{H} and the elasto-mechanical moment determined by the elastic reaction of the matrix. Taking into account that generally $|\theta| < 10^{-2}$ rad, Eq. (2) is equivalent to [157]:

$$m\mu_0 H \sin \theta_i \cong -K\theta \quad (3)$$

where it was considered $\sin\theta \cong 0$ and $\cos\theta \cong 1$.

In order to have the behavior of the whole elastomagnetic composite sample, the considerations for the elementary cell must be extended to the whole sample, taking into

account that the average magnetic moment of the sample is $\mathbf{M}=\mathbf{M}_r\tau V\%$ (where τ is the total sample volume). Therefore, for the macroscopic effect, Eq. (3) becomes [157]:

$$\theta \cong \frac{-M_r\tau V\% \mu_0 H \sin \theta_i}{K} \quad (4)$$

As can be seen from this equation, the particles rotation, which represents the efficiency of the direct elastomagnetic effect, increases with the magnetizing field intensity, H , particles remanent magnetization, \mathbf{M}_r , and with the decrease of K (which means increase in the silicone matrix elasticity), depending on the particles' initial magnetization orientation, θ_i .

Let us consider now the elementary cell of the elastomagnetic composite (with one filling particle) under the action of a compressive strain along z -axis, ε_z . The particle undergoes a rotation, θ_ε , due to ε_z action (Figure 17). From simple geometry, one can write:

$$\text{tg}\theta_\varepsilon \cong \theta_\varepsilon \cong \Delta d/d \text{ (considering that } |\theta_\varepsilon| < 10^{-2} \text{ rad)} \quad (5)$$

$$\sin\theta_i = \Delta d/\varepsilon_z l \Rightarrow \Delta d = \varepsilon_z l \sin\theta_i \quad (6)$$

$$\cos\theta_i = l/d \Rightarrow d = l/\cos\theta_i \quad (7)$$

Replacing Eqs. (6) and (7) in Eq. (5), θ_ε rotation determined only by strain is [157]:

$$\theta_\varepsilon = \varepsilon_z \sin\theta_i \cos\theta_i \quad (8)$$

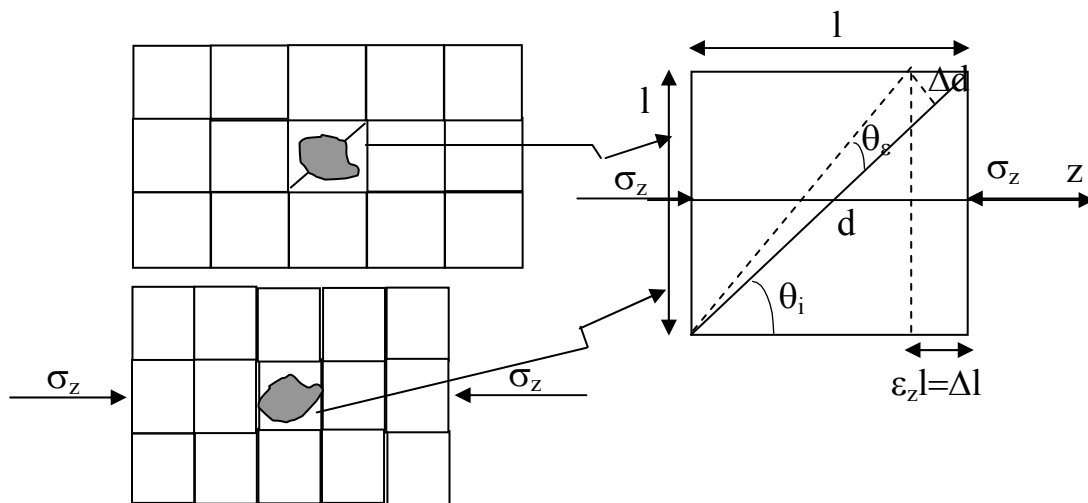


Figure 17. Particle rotation with θ_ε angle due to the sample strain, ε_z , at fixed transversal cross section of the sample.

In the presence of both ε_z and \mathbf{H} , Eq. (2) becomes:

$$m\mu_o H \sin(\theta_i + \theta) = K(\theta_\varepsilon - \theta) \quad (9)$$

where the standard convention for θ sign was applied. From Eq. (9), and considering the sample magnetization $\mathbf{M} = \mathbf{M}_r \tau V$ instead of the magnetic moment \mathbf{m} , and $|\theta| < 10^{-2}$ rad, one finds [157]:

$$\theta = \frac{-K\varepsilon_z \sin \theta_i \cos \theta_i - M_r \tau V \mu_o H \sin \theta_i}{K + M_r \tau V \mu_o H \cos \theta_i} \quad (10)$$

This is the constitutive equation of elastomagnetism, relating the average particles rotation θ to externally applied induced strain ε_z and applied magnetizing field \mathbf{H} . It takes into account the initial pre-orientation, θ_i , of the magnetic moments, and the elastic (K) and magnetic (\mathbf{M}_r) properties of the elastomagnetic composite material.

Eq. (10) can describe the effective rotation determined only by strain application, at constant field, as the difference between θ_ε values obtained at $\varepsilon \neq 0$ and $\varepsilon = 0$ [157]:

$$\theta_\varepsilon = \frac{-K\varepsilon_z \sin \theta_i \cos \theta_i}{K + M_r \tau V \mu_o H \cos \theta_i} \quad (11)$$

Note the coherence of the minus sign with the physical effect: at constant positive denominator, when the relative deformation ε is positive (elongation), the particles rotation θ_ε is negative (in the clockwise direction) and vice versa.

The inverse elastomagnetic effect is described by Eq. (11). In effect, considering the Sm_2Co_7 particle magnetization component coaxial with the applied strain and magnetic field direction by \mathbf{M}_r projection on z-axis (Figure 18), the change in this magnetization component, $\Delta \mathbf{M}_z$, determined by ε_z at constant \mathbf{H} , is given by:

$$\cos \theta_i = M_z / M \quad (12)$$

$$\cos(\theta_i + \theta_\varepsilon) = M'_z / M' \quad (13)$$

where $M=M'=M_r$, M_z and M'_z are the longitudinal component of the particle magnetization before and after particle rotation under the action of the externally induced strain. Considering $|\theta_\varepsilon| < 10^{-2}$ rad $\Rightarrow \cos\theta_\varepsilon \rightarrow 1$ and $\sin\theta_\varepsilon \cong \theta_\varepsilon$, one has the following formula for the sample longitudinal magnetization change [157]:

$$\Delta M_\varepsilon = M'_z - M_z = M^* \cos(\theta_i + \theta_\varepsilon) - M^* \cos\theta_i = -M^* \theta_\varepsilon \sin\theta_i = \frac{K\varepsilon_z M_r V \sin^2 \theta_i \cos\theta_i}{K + M_r \tau V \mu_0 H \cos\theta_i} \quad (14)$$

where M_z^* is the sample longitudinal magnetization, $M_z'^*$ is the sample longitudinal magnetization after the particles rotation under the action of the compressive strain, and M^* is the remanent magnetization of the sample.

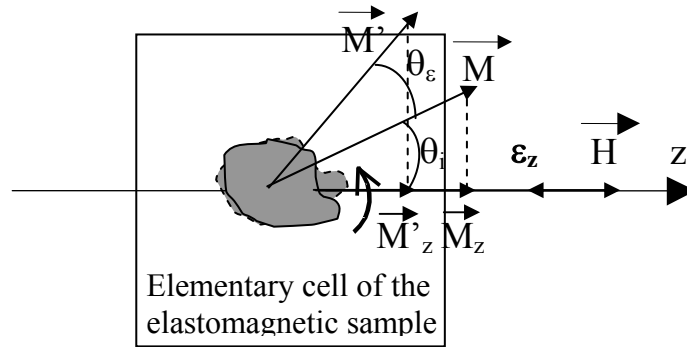


Figure 18. Magnetization moment rotation of the Sm_2Co_7 particle, θ_ε , under the action of compressive strain, ε_z , at constant \mathbf{H} and fixed transversal cross section of the sample.

From Eq. (14) it is clear that there is no contribution to the inverse elastomagnetic effect of the magnetic particles oriented at $\theta_i = \pi/2$ or 0 with respect to the direction of the applied strain and magnetic field, while there is a maximum magnetization change given by the particles oriented at θ_i ranging from $\pi/3$ and $\pi/4$. In the case of a random dispersion of the Sm_2Co_7 particles inside the elastomagnetic composite, more exactly in the absence of initial magnetization of the sample, for which $\theta_i \in [-\pi/2, \pi/2]$, the change in the macroscopic magnetization component along the applied stress and magnetic field is given by

$$\Delta M_\varepsilon = -\frac{1}{\pi} \int_{-\pi/2}^{\pi/2} \frac{K\varepsilon_z M_r V \sin^2 \theta_i \cos\theta_i}{K + M_r \tau V \mu_0 H \cos\theta_i} d\theta_i .$$

On the other hand, Eq. (10) is able to describe also the direct elastomagnetic effect, when the rotation θ is produced only by the applied magnetic field, \mathbf{H} , namely at zero strain $\varepsilon_z=0$. In this case the expression for θ is [157]:

$$\theta_H = -\frac{M_r \tau V \% \mu_0 H \sin \theta_i}{K + M_r \tau V \% \mu_0 H \cos \theta_i} \quad (15)$$

where θ_H is the macroscopic average rotation determined only by \mathbf{H} action. Also in this case the coherence of the θ_H sign with the physical effect is verified: if $\mathbf{H}>0$ (\mathbf{H} orientation coincident with z-axis) $\Rightarrow \theta_H < 0$ (clockwise rotation).

5. EXPERIMENTAL VERIFICATION OF THE DIRECT ELASTOMAGNETIC EFFECT

In order to verify the predictions of the developed elastomagnetic model, experimental investigation of the composite elastomagnetic behavior under the action of a magnetizing field was performed.

The first elastomagnetic composite studied was made of $V\%=10\%$ Sm_2Co_7 particles, permanently magnetized at 45° with respect to the sample longitudinal z-axis. The samples were produced in bar shape ($3 \times 2 \times 2 \text{ cm}^3$) [165]. When a magnetizing field \mathbf{H} is applied along z-axis of the sample, in the absence of any external stress, the Sm_2Co_7 magnetic moments rotate to align with \mathbf{H} , inducing at the same time the particles rotation (due to the strong coupling between the particles magnetic moment and their body), which can determine the sample macroscopic deformation = direct elastomagnetic effect. Using Eq. (3), which describes the equilibrium condition between the external magneto-mechanical moment induced by \mathbf{H} , $m\mu_0 H \sin \theta_i$, and the internal elasto-mechanical moment determined by the elastic contra-reaction of the matrix, $K\theta$, and considering that from experimental measurements: the torsional elastic constant is $K = 1 \text{ Nm}$, $\mu_0 M_R \cong 0.05 \text{ T}$ (M_R - remanent magnetization of the sample) and the applied magnetizing field is $\mu_0 \mathbf{H} = 0.1 \text{ T}$ (slightly lower

than the coercive field, in order to preserve the hard magnetic character of the filling particles), the particles average rotation θ can be evaluated as [165]:

$$\theta = M_R \tau \mu_0 H \sin \theta_i / K \Rightarrow \theta = 3 \times 10^{-2} \text{ rad} \quad (16)$$

In this case, the macroscopic longitudinal deformation of the sample due to θ rotation of the filling particles (Figure 19) is characterized by the longitudinal strain, ε_z , given by:

$$\sin(\theta_i - \theta) = \Delta d / \Delta l \quad (17)$$

$$\sin \theta \cong \theta = \Delta d / d \Rightarrow \Delta d = d \theta \quad (18)$$

$$\cos \theta_i = l / d \Rightarrow d = l / \cos \theta_i \quad (19)$$

Replacing Eqs. (18) and (19) in Eq. (17), one has:

$$\sin(\theta_i - \theta) = l \theta / \Delta l \cos \theta_i = \theta / \varepsilon_z \cos \theta_i \Rightarrow$$

$$\varepsilon_z \cong 6 \times 10^{-2} \text{ (considering } \cos \theta \cong 1) \quad (20)$$

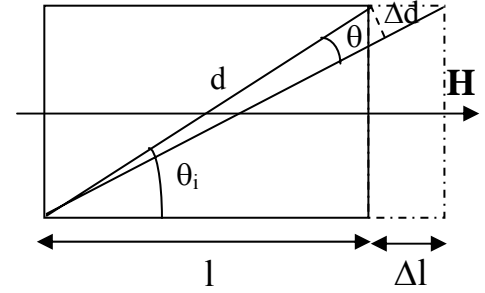


Figure 19. Macroscopic longitudinal deformation of an elastomagnetic composite sample (bar shaped) under the action of a longitudinal magnetizing field, \mathbf{H} .

The theory predicts therefore that the direct elastomagnetic effect can produce strain well higher than the best saturation magnetostriction deformation obtained so far in bulk materials.

A qualitative proof of the direct elastomagnetic effect in an elastomagnetic composite is given in the microscopy image presented in Figure 20 [165]. In this case, the investigated elastomagnetic sample has the shape of a thick ribbon (with thickness of about 0.5 mm, length of 5 mm and 2 mm wide), in order to be well observed with standard microscopy. The sample contains 4% mass percentage of Sm_2Co_7 particles (average size of 15 μm) permanently magnetized at 45° with respect to the sample longitudinal axis [165]. Figure 20(a) shows a corner region of the sample, where it is easy to individuate some ferromagnetic particles randomly dispersed in silicone. The ribbon was clamped at the opposite end to the investigated corner. In Figure 20(b) is presented the same sample region, when a uniform magnetizing field ($\mu_0 H = 0.15 \text{ T}$) is applied along the main ribbon axis. It is evident a little rotation of the particles and the deformation of the whole sample which corresponds to the

expected deformation as consequence to the direct elastomagnetic effect. As an example, in Figure 20(b) are shown the particles rotations $a \rightarrow a'$ and $b \rightarrow b'$ and the consequent equal rotation ($\mathbf{m} \rightarrow \mathbf{m}'$) of the permanent magnetic moment. In the same figure can be seen the change of the sample boundary position with respect to both marker point O ($h \rightarrow h'$) and upper side of the observation window ($d \rightarrow d'$), coherent with the expected deformation of the sample.

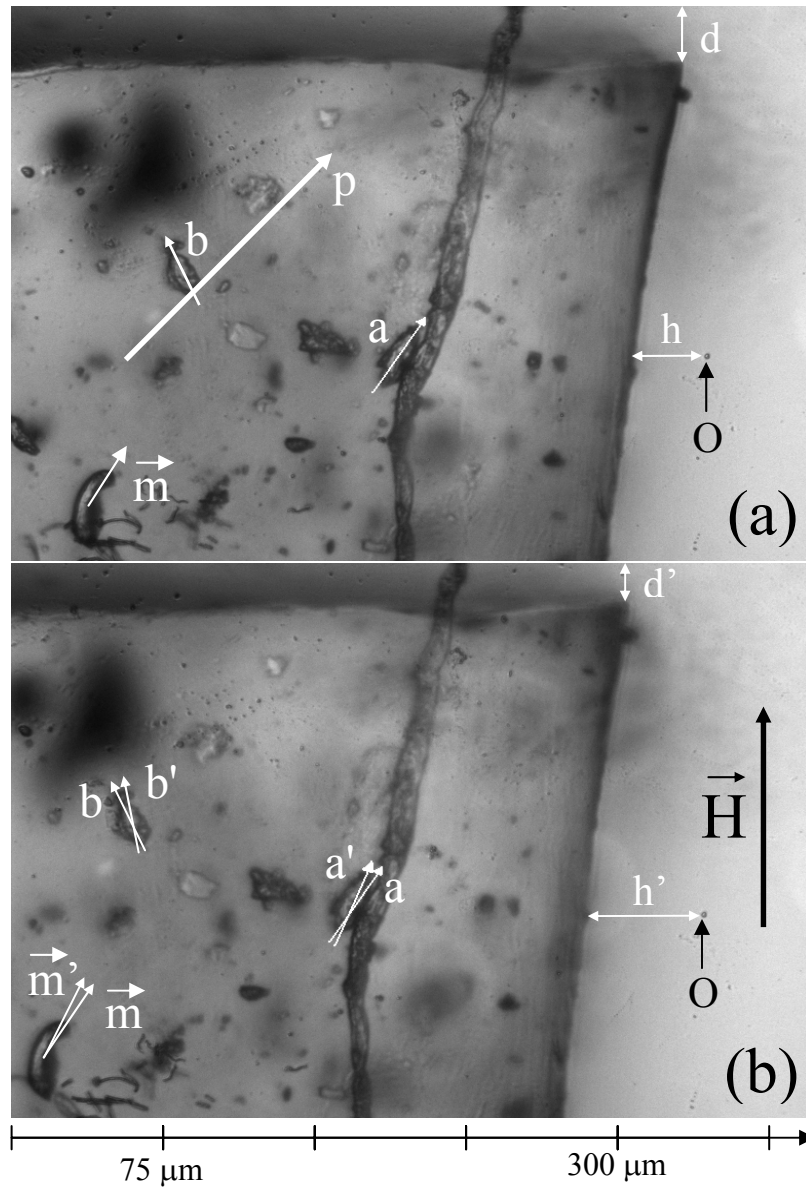


Figure 20. Microscopy images of a ribbon of Sm_2Co_7 particles (permanently magnetized along p direction) embedded in silicone matrix: a) view of a sample corner (20x magnification) in the absence of magnetizing field; b) the same sample region under the action of a uniform external magnetizing field $\mu_0 H = 0.15 \text{ T}$; $a \rightarrow a'$, $b \rightarrow b'$ and $\mathbf{m} \rightarrow \mathbf{m}'$ are examples of particles and magnetic moment rotation, respectively.

The theoretical value of the particles rotation θ can be easily evaluated using Eq. (3), and considering that from experimental measurements $\mu_0 M_R \cong 0.04$ T and $K=10^{-4}$ Nm. It was obtained $\theta \cong 1.7 \times 10^{-1}$ rad ($\cong 10^\circ$), which is almost equal to the value experimentally observed in Figure 20 [165]. It can be stated that it was possible to see by microscope the θ rotation of the particles because in the used conditions, the value of the elastic torsional constant of the composite matrix, K , is very low.

In the following, an experimental quantitative study of the direct elastomagnetic effect is presented, determining the phenomenologic equations which describe the composite elastomagnetic deformation under the action of a uniform external magnetizing field.

The investigated elastomagnetic composite is made of irregular shape Sm_2Co_7 micro-particles uniformly dispersed inside a silicone matrix in a volume percentage $V\%=33\%$ [168]. The samples were prepared in bar shape (4.5 cm in length and 5×5 mm² transversal cross section) and permanently magnetized so that all the magnetic moments, \mathbf{m} , of the micro-particles were aligned at 0° with respect to the sample main axis.

The experimental device shown in Figure 21 was conceived and developed for the study of the direct elastomagnetic effect, using a Fiber Bragg-Grating (FBG) sensor [169]. The set-up arrangement enables the micrometric displacement of two permanent magnets (a), and the adjustment of the free length (not clamped) of the sample by changing the clamping point (p). The experiments were performed for different sample lengths free to deflect, l_f .

The interrogation with the FBG sensor, tightly attached (by an appropriate glue) on the lateral side of the composite sample, assures the direct measurement of the longitudinal strain of the sample side in contact with the fiber, induced by the external magnetic field, \mathbf{H} , given by the two permanent magnets. The magnetic field uniformity in the sample place, for different magnets positions, was checked using a Hall effect probe. The field resulted uniform within a relative error of about $\pm 5\%$. The magnetic field, applied perpendicularly to the

sample main axis (coincident with the permanent magnetization direction), determines the rotation of the Sm_2Co_7 particles under the action of the induced magneto-mechanical moment $\mathbf{M}_m = \mathbf{m} \times \mu_0 \mathbf{H}$, due to the strong coupling between particles body and their magnetic moment. At macroscopic scale, and in the considered experimental configuration, this corresponds to the sample deflection as shown in Figure 21.

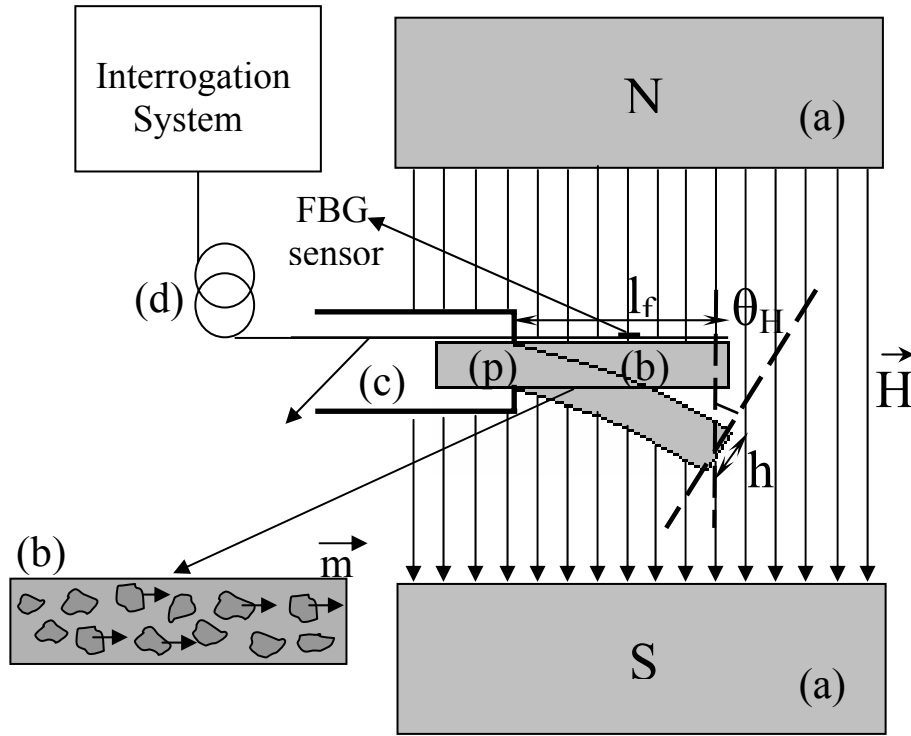


Figure 21. Schematic view of the experimental set-up used for the measurement of the elastomagnetic sample deflection by means of a FBG sensor: (a) permanent magnets, (b) sample, (c) non-magnetic clamping system, (d) transmission fiber of the FBG sensor, (p) clamping point.

The FBG sensor detects therefore the average relative elongation, $\langle \varepsilon \rangle = dl/l$, of the sample side on which is glued. The average strain of the monitored sample side as function of the applied magnetic field, $\mu_0 \mathbf{H}$, is presented in Figure 22, for different sample lengths $l_f = 2.5, 3$ and 4 cm. Three measurement cycles, obtained by plotting the average induced strain during increasing and decreasing the magnetic field strength, are reported for each investigated sample length free to deflect. The small quantitative differences between the iterated cycles are probably determined by the magnets position uncertainty, or by the possible small variations in the ambient temperature to which the FBG sensor is very sensitive.

The sample strain induced by a magnetizing field can be determined also from the theoretical model of the direct elastomagnetic effect. In our experimental case, the maximum relative deformation of the sample free end, under the action of the magnetizing field, is:

$$\varepsilon_{\max} = \Delta l_{\max} / l_f = \theta_{\max} h / 2l_f = \theta_H h / 2l_f \quad (21)$$

where h is the sample width, θ_{\max} is the maximum rotation angle of the sample free end, and $\theta_{\max} = \theta_H$ expressed in Eq. (15). Therefore, the average deformation of the monitored side of the sample can be written as:

$$\langle \varepsilon \rangle = \frac{0 + \varepsilon_{\max}}{2} \times \frac{l_f}{L} \quad (22)$$

where it was taken into consideration that the FBG sensor is measuring the deformation of the whole sample length on which the optical fiber is glued, L ($L > l_f$).

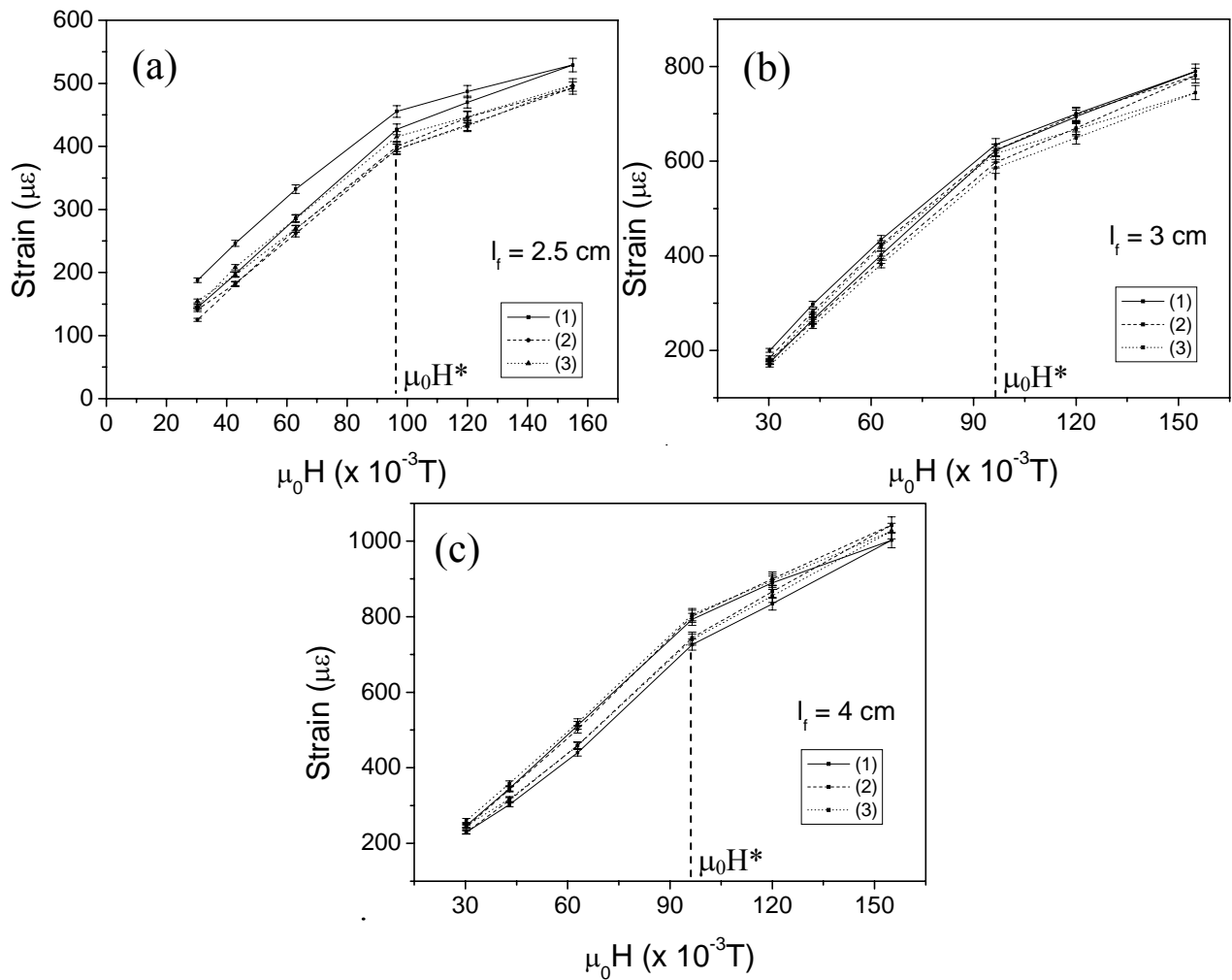


Figure 22. Strain dependence on the applied magnetic field, $\mu_0 \mathbf{H}$, for $l_f = 2.5$ cm (a), 3 cm (b) and 4 cm (c).

Replacing Eqs (15) and (21) in Eq. (22), one has the following expression for the sample average deformation [167]:

$$\langle \varepsilon \rangle = \frac{M_r S l_f V \% \mu_0 H \sin \theta_i}{2(K + M_r S l_f V \% \mu_0 H \cos \theta_i)} \times \frac{h}{2l_f} \times \frac{l_f}{L} = A l_f \mu_0 H \quad (23)$$

where S is the sample cross section and $A = \frac{M_r S h V \% \sin \theta_i}{4L(K + M_r \tau V \% \cos \theta_i)} \cong \frac{M_r S h V \%}{4LK}$ is practically a constant, considering that $M_r \tau V \% \cos \theta_i \ll K$ and $\sin \theta_i = 1$ in our experimental case.

From the phenomenologic point of view, the equations describing the behavior of the sample average deformation, $\langle \varepsilon \rangle$, with the applied magnetic field, $\mu_0 \mathbf{H}$, as reported in Figure 22, can be written as:

$$\langle \varepsilon \rangle = A l_f \mu_0 H \quad \text{for } H \leq H^* = 0.096T \quad (24)$$

and

$$\langle \varepsilon \rangle = A l_f \mu_0 H^* + C A l_f \mu_0 (H - H^*) = A l_f \mu_0 H^* (1 - C) + C A l_f \mu_0 H \quad \text{for } H \geq H^* = 0.096T \quad (25)$$

where C is a constant. \mathbf{H}^* can be interpreted as the magnetic field up to which the magnetic moment is coupled with the particle body which means that there is a linear dependence between $\langle \varepsilon \rangle$ and $\mu_0 \mathbf{H}$ for $\mathbf{H} < \mathbf{H}^*$, while for an external magnetizing field higher than $\mu_0 \mathbf{H}^*$, the magnetic moment rotates with respect to the particle body and not only together with it and consequently, the effective mechanical moment producing the particle rotation is now proportional to just a fraction of the applied magnetic field.

The magnetization cycles of the elastomagnetic composite sample, obtained by VSM measurements (Appendix A) at room temperature, for magnetic fields up to 0.3 T, are presented in Figure 23. The magnetic field was applied perpendicularly on the direction of the remanent magnetization of the sample. As can be seen from Figure 22(b), the magnetic field value up to which the sample magnetization grows linearly with the applied field is about 0.1 T. This means that $\mu_0 \mathbf{H}^* \cong 0.1$ T is the magnetizing field for which the magnetization process of the composite sample is passing from the linear (AA') to the non-linear regime (A'A'').

More exactly, \mathbf{H}^* is the magnetic field for which the coupling between the particles body and their magnetic moments is broken, and the magnetization intensity \mathbf{M} of the Sm_2Co_7 particles has a coupling coefficient with the easy magnetization axis lower than 1, decreasing with \mathbf{H} increase in the range $\mathbf{H} > \mathbf{H}^*$. This means that for $\mathbf{H} > \mathbf{H}^*$, the magnetization process requires a higher energy, being characterized by a non-linear regime.

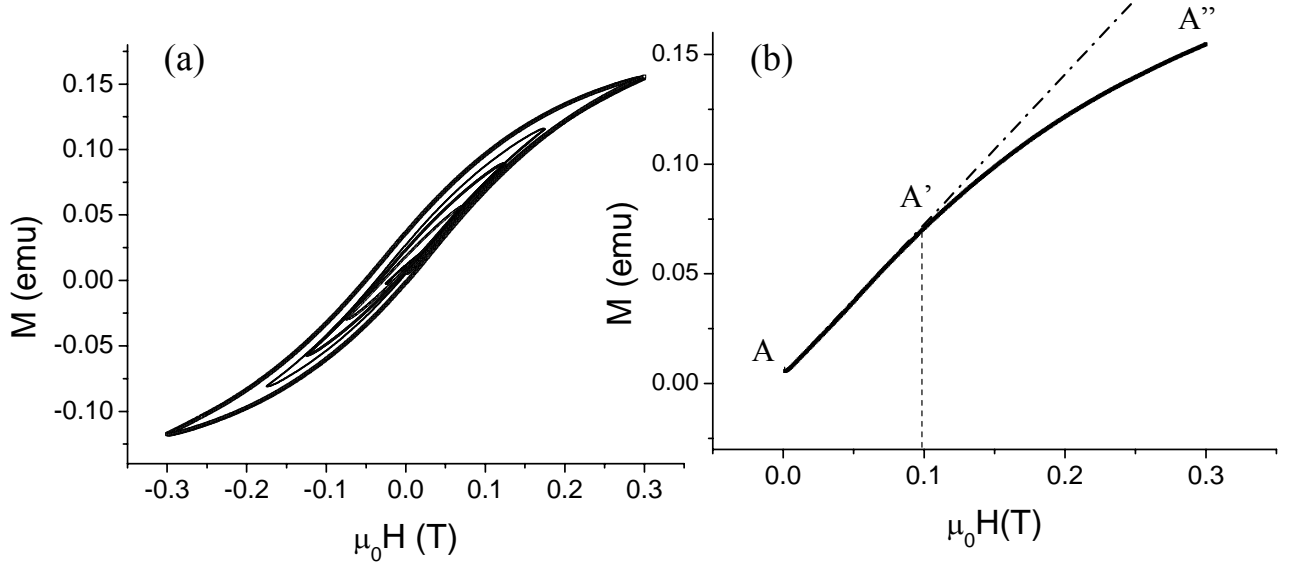


Figure 23. Magnetization cycles of the elastomagnetic composite (a); First magnetization curve of the elastomagnetic composite (b).

From Eq. 23 and considering that in our experimental condition $M_r = 0.6 \times 10^6 \text{ A/m}$, $V\% = 33\%$, $K = 0.8 \text{ Nm}$, $S = 25 \text{ mm}^2$, $h = 5 \text{ mm}$, $L = 4 \text{ cm}$, $\mu_0 H^* \approx 0.1 \text{ T}$ and $\theta_i = 90^\circ$, the theoretical value of the A constant can be determined as $A = 193 (\text{Tm})^{-1}$. The values of A and C constants determined from the experimental data presented in Figure 22 are as following: $A = 172 (\text{Tm})^{-1}$ and $C = 0.41$ for $l_f = 2.5 \text{ cm}$, $A = 211 (\text{Tm})^{-1}$ and $C = 0.43$ for $l_f = 3 \text{ cm}$, $A = 199 (\text{Tm})^{-1}$ and $C = 0.54$ for $l_f = 4 \text{ cm}$. It can be seen that the average value of the experimentally obtained A constants, $194 (\text{Tm})^{-1}$, is in good agreement with the theoretically obtained one $A = 193 (\text{Tm})^{-1}$, this proving the validity of the phenomenologic equation describing the behavior of the sample average deformation, $\langle \varepsilon \rangle$, with the applied magnetic field, $\mu_0 \mathbf{H}$, for $H < H^*$. The coherent values obtained for the C constant in the three experimental arrangements of the sample in the

external magnetizing field demonstrate that the physical phenomenon taking place for $H > H^*$ is well described by the phenomenologic equation (25).

The experimental results on the direct elastomagnetic effect evaluation, obtained by means of the FBG sensor, are consistent with the theoretical ones obtained from the developed model of the elastomagnetic effect. This agreement proves definitively the self-consistency of the theoretical model

6. EXPERIMENTAL VERIFICATION OF THE INVERSE ELASTOMAGNETIC EFFECT

Two elastomagnetic composites made of 4% and 12% mass percentage of Sm_2Co_7 particles inside the silicone matrix were prepared in bare shape ($2 \times 2 \text{ mm}^2$ square cross section and 3 mm in length). The samples were permanently magnetized at 45° with respect to the longitudinal axis (Figure 24(a)). They were accommodated into a cell equipped with a micrometric displacement cursor which can produce a controlled longitudinal compressive strain of the material (Figure 24(b)) [165].

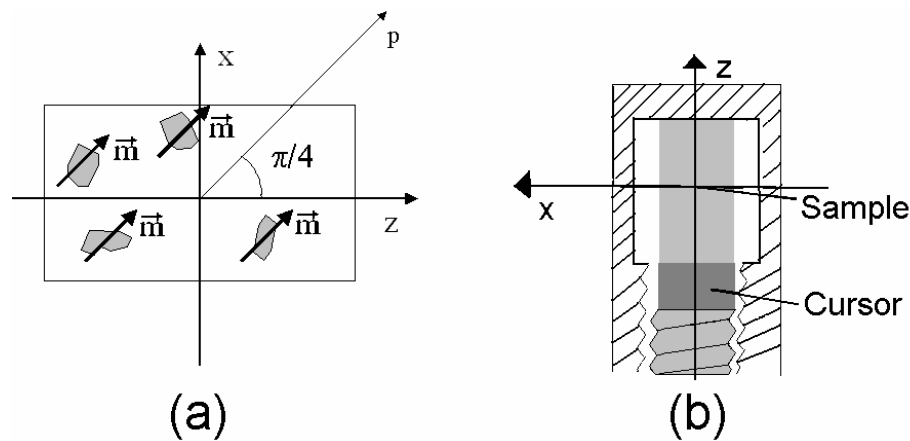


Figure 24 (a) Schematic view of the longitudinal section in the composite sample made of irregular shape Sm_2Co_7 particles uniformly distributed into the silicone matrix; p is the axis of the permanent magnetization. (b) Schematic drawing of the cell used to apply controlled longitudinal stress to the sample.

The elastomagnetic behavior of the composite samples under compressive stress was investigated by means of a vibrating sample magnetometer (VSM), Oxford Instrument, 9T (Appendix A).

When an uniaxial compressive stress σ_z is applied to the sample, by means of the micrometric displacement of the cell cursor, at zero external magnetizing field, there is a change in the sample longitudinal remanent magnetization, \mathbf{M}_z . Examining all the possible mechanisms which can influence magnetization, the \mathbf{M}_z change is determined by:

- the rotation of the magnetic moments together with the particles rotation under σ_z action, due to the strong coupling between the particles magnetic moment and their body: inverse elastomagnetic effect;
- the change in the sample volume for longitudinal strains over 20%.

For longitudinal strains lower than 20%, the particles density should not increase more than 1% because the uniaxial stress gives also a positive transversal strain which compensates the negative longitudinal one, resulting in a negligible change of the sample volume. Moreover, the exchange interactions among the particles magnetic moments are not affected by the induced strain because the particles volume percentage is very low.

The change in the sample longitudinal magnetization can not be determined by the magnetomechanical effect due to the already discussed motivations (see the second paragraph of the 3rd chapter).

In the case of external strains lower than 15%, in contrast with the weak influence of the other effects, the elastomagnetic coupling should give an important relative change of \mathbf{M}_z . In order to demonstrate this assumption, we consider that the rotation of the Sm_2Co_7 particles is coherent with the deformation of the elementary cell of the composite matrix, inducing an equal rotation of the magnetic moments due to the strong magnetic moment/particles body coupling. Therefore each magnetic moment \mathbf{m} rotates with an angle (see Figure 25) [165]:

$$\Delta\theta = \frac{|\varepsilon_z| \sqrt{2}(1+2\lambda^2)}{4\lambda^2} \quad (26)$$

where ε_z is the longitudinal strain component and λ is the strain ratio $\varepsilon_z/\varepsilon_x$. The detailed calculation of $\Delta\theta$ is given in Appendix B. This rotation produces a change in the sample magnetization component along z-axis as following (Appendix B) - see Figure 25(b) [165]:

$$|\Delta M_z| = M_r \frac{\sqrt{2}}{2} - M_r \cos\left(\frac{\pi}{4} + \Delta\theta\right) \quad (27)$$

with $M_r = M'_r = m/\tau = m'/\tau$, where \mathbf{M}_r is the remanent magnetization of the Sm_2Co_7 particles. So it is easy to calculate the relative change in the sample longitudinal magnetization as [165]:

$$\frac{|\Delta M_z|}{M_z} = 1 - \sqrt{2} \cos\left(\frac{\pi}{4} + \frac{|\varepsilon_z| \sqrt{2}(1+2\lambda^2)}{4\lambda^2}\right), \text{ considering that } M_z = M_r \cos\theta_i \quad (28)$$

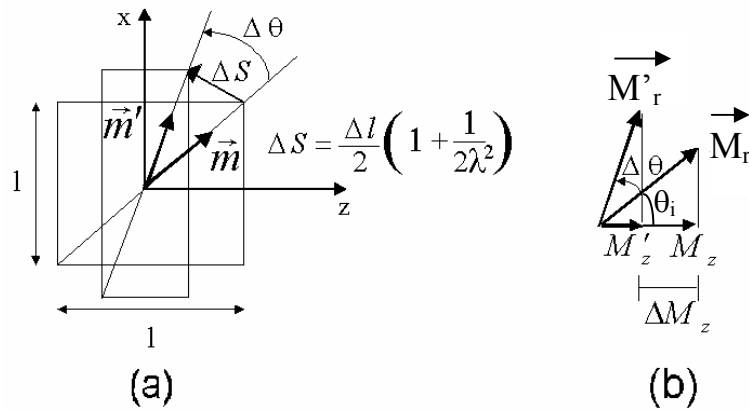


Figure 25 (a) Schematic view of the elementary sample cell deformation and the related rotation of each magnetic moment \mathbf{m} (\mathbf{m}' after deformation), (b) ΔM_z calculation.

From Eq. (28) it is possible to evaluate the theoretical behavior of the relative longitudinal magnetization variation as consequence of the inverse elastomagnetic effect in the investigated composite material. This behavior is reported in Figure 26, together with the experimentally determined behavior obtained by VSM measurements [165]. As can be seen, the simple model prediction is well confirmed by the experimental results.

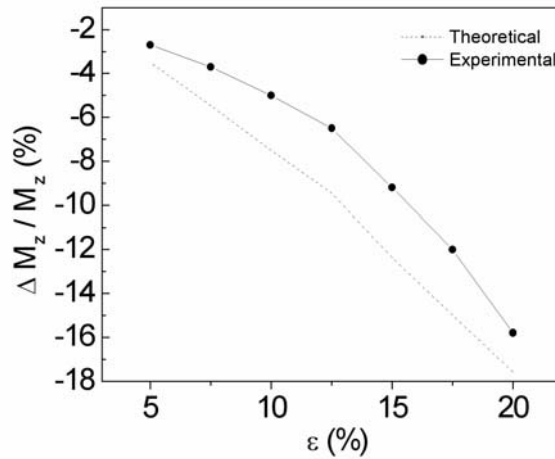


Figure 26. Relative change in the longitudinal component of magnetization $\Delta M_z/M_z$ as a function of the longitudinal strain ε_z as experimentally obtained by VSM measurements (—●—) and as predicted from the theoretical model (— — —).

Another direct demonstration of the existence of the inverse elastomagnetic effect was developed by performing the following measurements. The longitudinal remanent magnetization, \mathbf{M}_z , as function of the measurement temperature, T , for two different induced strains, in the absence of magnetizing field, for 4% and 12% mass percentage of Sm_2Co_7 filling particles is shown in Figures 27 and 28, respectively. As can be seen, at room temperature, under a longitudinal compressive strain, ε_z , of 17%, the samples longitudinal magnetization exhibits an abrupt decrease given by the prominent inverse elastomagnetic effect with respect to the other mechanism which influences magnetization. With increasing ε_z of about 100%, the longitudinal magnetization is increasing, its value being equal to that measured in the absence of strain. This can be attributed to the compensation between the inverse elastomagnetic effect, which in the given experimental conditions determines a decrease of the longitudinal magnetization, and the decrease in the sample volume, which determines the increase of the longitudinal magnetization.

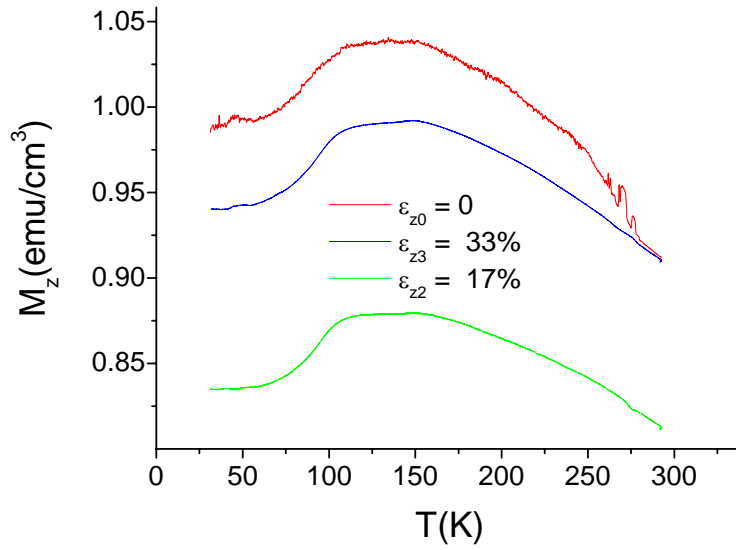


Figure 27. Longitudinal remanent magnetization, \mathbf{M}_z , as function of the measurement temperature, T , for different induced strains ($\epsilon_z=0$, 17% and 33%), in the absence of magnetizing field, for 4% mass percentage of Sm_2Co_7 filling particles.

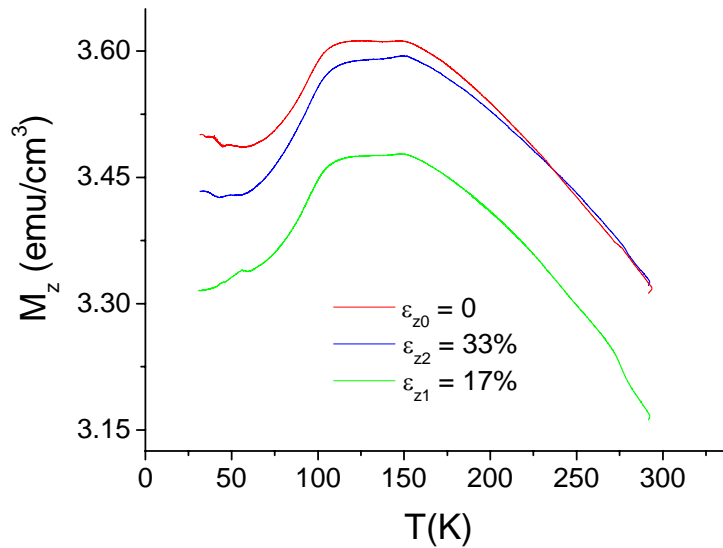


Figure 28. Longitudinal remanent magnetization, \mathbf{M}_z , as function of the measurement temperature, T , for different induced strains ($\epsilon_z=0$, 17% and 33%), in the absence of magnetizing field, for 12% mass percentage of Sm_2Co_7 filling particles.

It is well known that the silicone mechanical properties change dramatically with temperature, going from glass-like brittle behavior at low temperatures to a rubber-like behavior at high temperatures. In any case, no permanent change occurs in the physical structure of the silicone matrix after exposure to extremely low temperatures, and the original

mechanical characteristics are regained when the silicone is returned to room temperature. At low temperatures, the Sm_2Co_7 material exhibits a decrease in magnetization with respect to room temperature. For example, at 30 K the decrease is of about 15 emu/cm^3 [170]. In this context, the magnetic behavior of the elastomagnetic samples at low temperatures (that is the decrease of \mathbf{M}_z with respect to the predicted behaviour of a ferromagnetic material, as well as with respect to the value at zero strain in the case of 33% applied strain) can be explained considering the cumulative influence of Sm_2Co_7 behavior and silicone mechanical characteristics at low temperatures. Practically, at 30 K, the silicone exhibits a contraction which acts as an additional strain on the magnetic filling particles, determining an increase of the inverse elastomagnetic effect with respect to the room temperature and therefore, the decrease of the longitudinal remanent magnetization. Moreover, at low temperatures the silicone is brittle, exhibiting worst elastic characteristics due to an increased elastic modulus; therefore, it is not able anymore to oppose to the rotation of the Sm_2Co_7 particles under the strain action, this determining an additional increase of the inverse elastomagnetic effect.

7. ELASTOMAGNETIC COMPOSITES AS SENSOR AND ACTUATOR CORE MATERIALS

Based on the specific, peculiar characteristics of the elastomagnetic composites, on the developed theoretical model of their elastomagnetic effects, which was experimentally validated, one can predict that these materials have interesting performances for application as sensor and actuator cores. In order to verify thus prediction, sensor and actuator prototype devices based on elastomagnetic composite cores were designed, developed and tested.

7.1. Mechanical vibration sensor prototype based on elastomagnetic composite core

Considering the high costs of the sensors used for the structural health monitoring of the constructed civil systems, as well as their performance limits concerning especially the

vibration detection, a mechanical vibration sensor prototype, based on elastomagnetic composite core, was developed. The sensor working principle is based on the magnetization variation of the elastomagnetic core, under the action of dynamic deformation, due to the inverse elastomagnetic effect.

7.1.1. Experimental set-up and functioning

The elastomagnetic sensing core is constituted by four bars (46 mm in length and 5×5 mm² transversal cross section) of Sm₂Co₇ particles (4 μm average size), uniformly dispersed inside a silicone matrix, in a volume percentage V%=9%. The bar samples, permanently magnetized at 45° with respect to z-axis, were arranged as shown in Figure 29, so that in the adjacent samples, the magnetic moment orientation is symmetric with respect to z-axis. In this case, the macroscopic magnetization of the elastomagnetic core, \mathbf{M} , has zero transversal component and a longitudinal magnetization component $M_z = M = (\sum \mathbf{m} / \tau) \sqrt{2} / 2$, determined by the projection of each particle magnetization on z-axis [157].

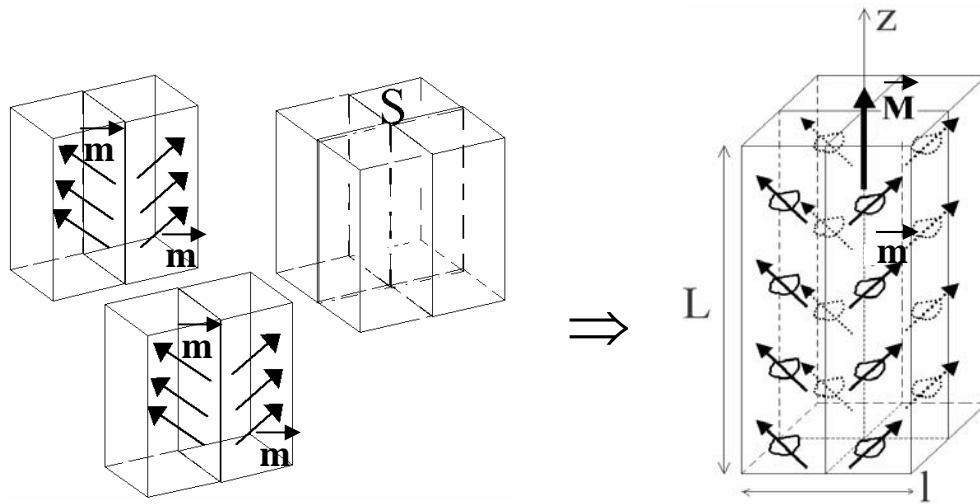


Figure 29. Schematic view of the elastomagnetic core made of 4 bar samples, with the permanent magnetic moment, \mathbf{m} , of the Sm₂Co₇ particles at 45° with respect to z-axis. \mathbf{M} = macroscopic core magnetization, $L = 46$ mm and $l = 10$ mm.

The schematic view of the experimental set-up used to test the developed sensor prototype is reported in Figure 30(a) and (c).

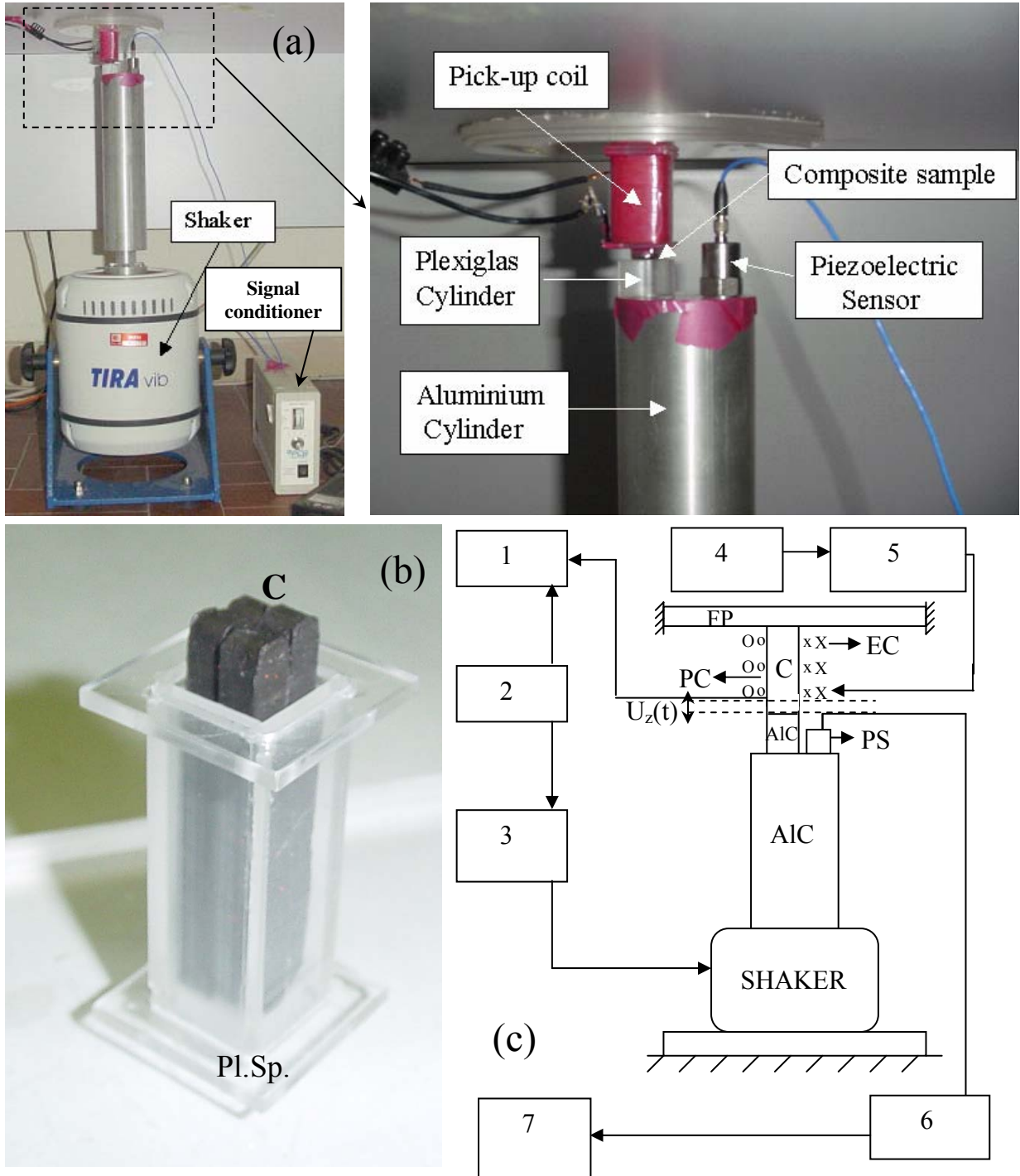


Figure 30 (a) and (c) Experimental arrangement used to study the core elastomagnetic response to dynamic mechanical deformation produced by a shaker: 1: lock-in amplifier, 2: signal generator, 3: shaker amplifier, 4: dc generator, 5: amperometer, 6: signal conditioner, 7: oscilloscope, FP = fixed plate, EC = exciting coil, PC = pick-up coil, C = elastomagnetic core, AIC = aluminum cylinder, PS = piezoelectric sensor, $U_z(t) = U_0 \sin(2\pi vt)$ = dynamic longitudinal deformation induced by the shaker vibration. (b) Elastomagnetic core (C) made of 4 bar samples inside the Plexiglas support (Pl.Sp.) for the pick-up coil.

The composite sample (C) of length $L=46$ mm is inserted inside a Plexiglas support (Pl.Sp.) with the length of 43 mm (Figure 30(b)), on which is wound the pick-up coil (PC) (Figure

30(c)). The upper part of the Plexiglas support and of the sample core at the same time are in contact with a fixed plate (FP), while the bottom end of the sample lies on an aluminum cylinder (A1C) tightly glued on another aluminum cylinder (A1C) fixed on the shaker which generates dynamic mechanical vibration (Figure 30(a) and (c)).

The elastomagnetic core transduces the dynamic deformation induced by the shaker vibration in an electrical signal, the pick-up coil detecting the elastomagnetic response (that is the change in the core magnetization under the action of the dynamic deformation, due to the inverse elastic effect) as an electromotive force.

The amplitude U_0 of the dynamic displacement $U_z(t)=U_0\sin(2\pi vt)$, generated by the shaker in the elastomagnetic core through the aluminum cylinders, is measured by a piezoelectric sensor (accelerometer), PS, fixed on A1C (Figure 30(a)and (c)).

The detailed functioning of the experimental set-up is described in Appendix A.

7.1.2. Functioning model

In the specific experimental conditions, the change in the elastomagnetic core longitudinal magnetization under the action of the shaker induced deformation is determined by:

1. the modification of the elastomagnetic core volume;
2. the rotation of the particles magnetic moment due to the indirect elastomagnetic effect.

More detailed:

1. The elastomagnetic core magnetization is $M = M_z = \frac{\sum m_z}{\tau}$, where \mathbf{m}_z is the longitudinal component of the magnetic moment of the Sm_2Co_7 particles and $\tau=SL$ is the initial volume of the elastomagnetic core ($S =$ core transversal cross section). When the core volume is changing with $\Delta\tau=S\Delta L=SL\varepsilon_z(t)$, where $\varepsilon_z(t)=U_0\sin(2\pi vt)/L$ (v -vibration frequency and

$U_0 \sin(2\pi\nu t) = \Delta L$ is the induced longitudinal strain), under the action of the shaker vibration, there is also a change in the longitudinal magnetization [171]:

$$\Delta M_{z\tau} = \frac{\sum m_z}{\tau + \Delta\tau} - \frac{\sum m_z}{\tau} \cong -M_r \varepsilon_z(t) = -M_r \varepsilon_z(t) V\% \cos \theta_i \quad (29)$$

where M_r is the remanent magnetization of the Sm_2Co_7 particles and $V\%$ is the volume percentage of Sm_2Co_7 particles.

2. From the theoretical model of the elastomagnetic effect, the change in the longitudinal magnetization component, ΔM_z , due to an applied strain ε_z , in the absence of a magnetizing field, $\mathbf{H}=0$, has the following expression (there were used Eqs. 14 and 11, for $\mathbf{H}=0$):

$$\Delta M_{z\varepsilon} = M_r V\% \varepsilon_z \sin^2 \theta_i \cos \theta_i \quad (30)$$

The total change in the core magnetization under the action of a dynamical strain, $\varepsilon_z(t)$, is [169]:

$$\Delta M_{z\text{tot}} = \Delta M_{z\tau} + \Delta M_{z\varepsilon} = -M_r \varepsilon_z(t) V\% \cos^3 \theta_i \quad (31)$$

Therefore, the electromotive force induced in the pick-up coil by the magnetic flux change in the elastomagnetic material is given by [171]:

$$V_{\text{ind}} = -\frac{d(\mu_0 \Delta M_{z\text{tot}} NS)}{dt} = \mu_0 \frac{U_0}{L} V\% NS M_r 2\pi\nu \cos^3 \theta_i \cos(2\pi\nu t) \quad (32)$$

where N is the number of the pick-up coil turns. The amplitude of this voltage is:

$$V_{0\text{ind}} = \mu_0 M_r \frac{U_0}{L} NS V\% 2\pi\nu \cos^3 \theta_i \quad (33)$$

For fixed M_r and N , S , L , θ_i parameters, Eq. (33) predicts a linear dependence between the amplitude of the output voltage, $V_{0\text{ind}}$, and: the amplitude, U_0 , and frequency, ν , of the dynamic mechanical vibration and the volume percentage, $V\%$, of Sm_2Co_7 particles inside the composite.

7.1.3. Experimental verification of the functioning model validity

The validity and the limits of the proposed functioning model of the developed sensor prototype are established the following, determining also the optimum working conditions and evidencing the advantages and the problems of the elastomagnetic composite as sensing core material.

The experimental results on the measured $V_{0\text{ind}}$ values as function of the vibration frequency, ν (at fixed $U_0=0.7$ mm) and of the vibration amplitude, U_0 (at fixed frequency $\nu = 35$ Hz), for two Sm_2Co_7 volume percentages $V\%=7.2$ and 15.5% , compared with the predicted theoretical behaviour are presented in Figures 31 and 32, respectively [171]. Each reported datum is the average value over five repeated measurements. The maximum relative error was evaluated to be lower than about 6%. The theoretical values of $V_{0\text{ind}}$ were calculated using Eq. (33) and the following values for the remanent magnetization of Sm_2Co_7 particles, permanent magnetization angle, sample cross section, initial sample length, deformation amplitude and pick-up coil turns: $M_r = 0.6 \times 10^6$ A/m, $\theta_i = 45^\circ$, $S = 10 \times 10$ mm², $L = 46$ mm, $U_0 = 0.7$ mm and $N=300$, respectively [171].

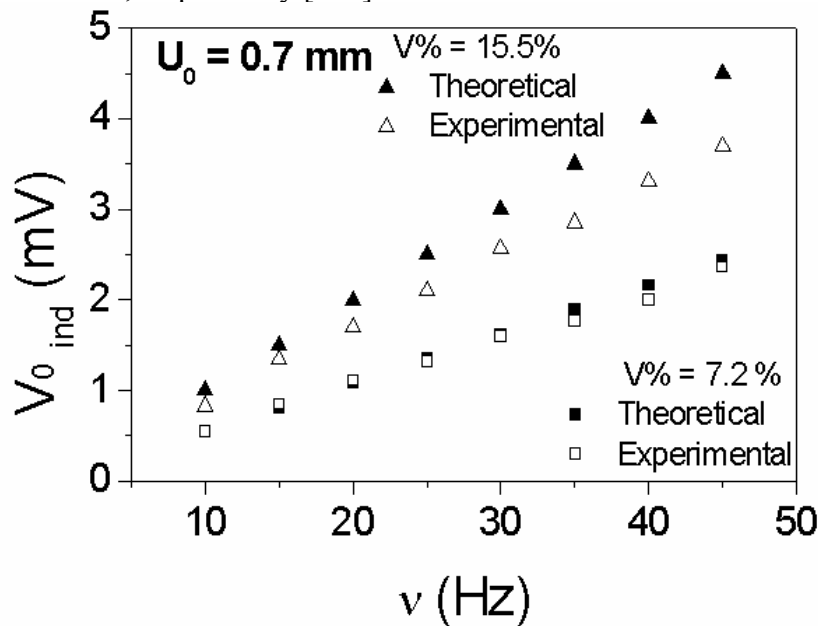


Figure 31. Dependence of the sensor output amplitude, $V_{0\text{ind}}$, on the deformation frequency, ν , as obtained from the experimental measurements (empty symbols) and as calculated from the theoretical model (full symbols), for two different Sm_2Co_7 volume percentages $V\% = 7.2\%$ and $V\%=15.5\%$, at a fixed deformation amplitude $U_0=0.7$ mm.

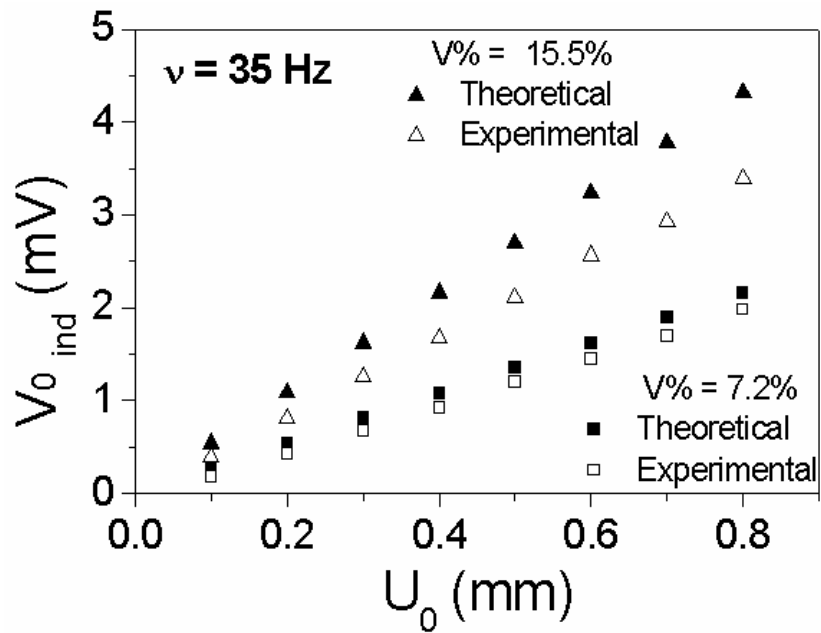


Figure 32. Dependence of the sensor output amplitude, V_{0ind} , on the deformation amplitude, U_0 , as obtained from the experimental measurement (empty symbols) and as calculated from the theoretical model (full symbols), for two different Sm_2Co_7 volume percentages $V\% = 7.2\%$ and $V\%=15.5\%$, at a fixed deformation frequency $\nu=35$ Hz.

The good reliability of the sensor response and the excellent agreement between the experimental and theoretical behaviour at low $V\%$ value (7.2%) is evident. A decrease of the experimental values as compared to the theoretical ones is evident with U_0 , ν and $V\%$ increase, while the predicted linearity of V_{0ind} with ν (at fixed U_0 and $V\%$) and U_0 (at fixed ν and $V\%$) is confirmed. For higher volume fractions, there is a high possibility that the microparticles start to exhibit mechanical and magnetic interactions which were not considered in the developed functioning model. Obviously, these interactions hinder the magnetoelastic coupling, leading to results which may not obey to the model predictions. In any case, the increment of the difference between the theoretical and experimental V_{0ind} values with $V\%$ increase from 7.2% to 15.5% may be determined by the magnetic interaction between the particles and not by the mechanical friction, since the linearity with ν is not affected by $V\%$ increase. In order to clarify this point, there were conducted experimental tests using a longitudinal biasing magnetic field, H_z , by means of a dc current passing through

an excitation coil wound around the elastomagnetic core. In the absence of the applied strain, \mathbf{H}_z determines a direct elastomagnetic effect that is the rotation of the magnetic moments from the direction of the remanent magnetization toward the biasing field direction, characterized by $\theta_H \cong \frac{-M_r \tau V \% \mu_0 H_z \sin \theta_i}{K}$, given by Eq. (4). In the case of both H_z and $\varepsilon_z(t)$ action on the

elastomagnetic core, the amplitude of the induced electromotive force, V_{0ind} , becomes [162]:

$$V_{0indH} = \mu_0 M_r \frac{U_0}{L} N S V \% 2 \pi v \cos^3(\theta_i + \theta_H) \quad (34)$$

When the sample magnetization \mathbf{M} and the applied biasing field \mathbf{H}_z have the same orientation ($\mathbf{H}_z > 0$), results $\theta_H < 0$ and V_{0ind} is increasing with H_z increasing (Eq. 31). On the other side, when \mathbf{M} and \mathbf{H}_z have opposite orientations ($\mathbf{H}_z < 0$), results $\theta_H > 0$ and V_{0ind} is decreasing with H_z increasing (Eq. 34) [162].

Considering that the theoretical model of the elastomagnetic effect was developed starting from the assumption that the magnetic particles are not interacting magnetically between them, Eq. (34) is valid only in the frame of this supposition. One expects therefore that this equation is valid only if the volume fraction of magnetic particles in the silicone matrix is lower than a threshold value, above which the magnetic interactions among the nearest particles must be taken into consideration.

In order to verify the validity limits of Eq. (34), the experimental and theoretical curves of the V_{0ind} change, $\Delta V_0 = V_{0indH \neq 0} - V_{0indH = 0}$ (produced by the application of a magnetizing field, \mathbf{H}_z , having the same or opposite orientation with respect to the sample longitudinal remanent magnetization) as function of H_z were plotted, and reported in Figure 33 [162]. For the theoretical evaluation of ΔV_0 there were used the following values $N=300$, $S=100 \text{ mm}^2$, $K \cong 0.4 \text{ Nm}$ (experimentally determined), $v=35 \text{ Hz}$, $U_0=0.7 \text{ mm}$ (experimentally determined by means of the piezoelectric sensor), $M_r=0.6 \times 10^6 \text{ A/m}$ (experimentally determined), $\theta_i=45^\circ$, $V\%= 7.2$ and 15.5% [162].

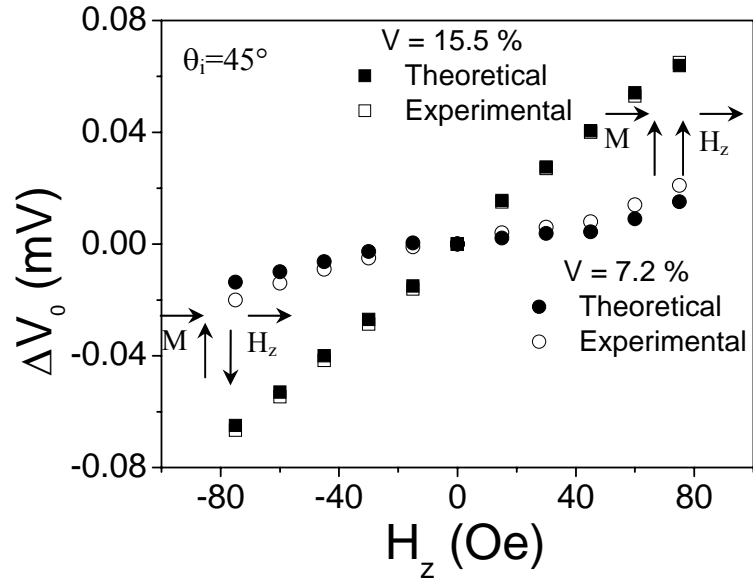


Figure 33. Experimental and theoretical $V_{0\text{ind}}$ change, $\Delta V_0 = V_{0\text{ind}H \neq 0} - V_{0\text{ind}H=0}$, as a function of the applied magnetizing field H_z , for $V\% = 7.2$ and 15.5% , when the dynamic deformation has $\nu = 35$ Hz and $U_0 = 0.7$ mm.

As can be seen, the experimental results are in agreement with the theoretical predictions in what concern the $V_{0\text{ind}}$ increase or decrease with H_z for \mathbf{M} and H_z having the same or opposite orientation, respectively. The relative symmetry between the elastomagnetic behaviors (for both $V\% = 7.2$ and 15.5%) for $H_z > 0$ and $H_z < 0$ shows that the proposed theoretical model and therefore also the hypothesis that the particles do not interact magnetically up to $V\% = 15.5\%$ (more exactly the magnetic interactions are very weak and therefore negligible) are valid.

In order to further investigate the limit of the theoretical model in what concern the magnetic interactions among the particles, an elastomagnetic core (made of one sample bar, with the length of 46 mm and transversal cross section $S = 25 \text{ mm}^2$) with a high volume percentage of Sm_2Co_7 particles, $V\% = 33\%$, and permanently magnetized at $\theta_i = 10^\circ$ with respect to the bar main axis was developed. It was used a permanent magnetization at $\theta_i = 10^\circ$ and not 45° , because by $V\%$ increasing, the action of an external biasing field should have an asymmetric effect which is well emphasized at low pre-orientation angles. In Figure 34 is reported the dependence of the output voltage amplitude, $V_{0\text{ind}}$, on the deformation amplitude, U_0 , for a fixed vibration frequency $\nu = 35$ Hz, when $H_z = 0$.

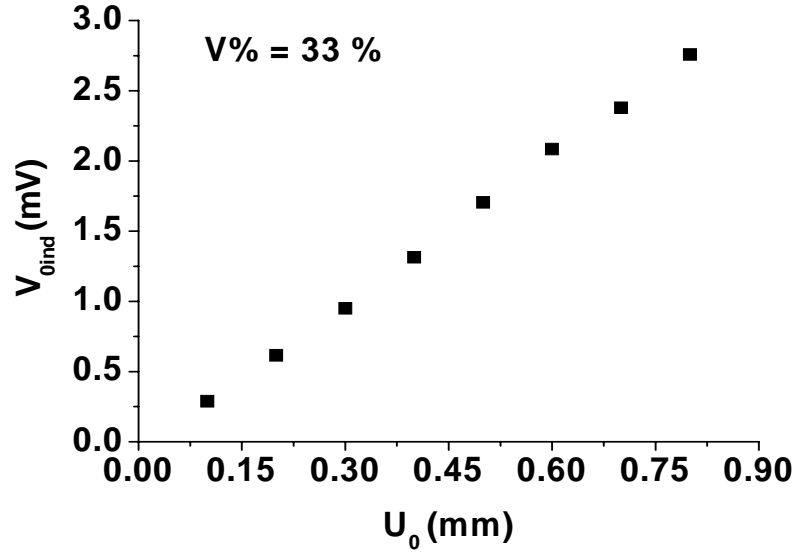


Figure 34. Output voltage amplitude, V_{0ind} , versus deformation amplitude, U_0 , for a fixed deformation frequency $\nu=35$ Hz.

As can be seen, the linear dependence between V_{0ind} and U_0 still exist at this high volume percentage.

In the case of an external biasing field $\mathbf{H}_z \neq 0$, the experimental and theoretical amplitude changes ΔV_{0ind} ($\Delta V_{0ind} = V_{0indH \neq 0} - V_{0indH=0}$) versus \mathbf{H}_z , at fixed $U_0=0.7$ mm and $\nu=35$ Hz, are shown in Figure 35 [162]. It can be seen an asymmetric response to $\mathbf{H}_z > 0$ and $\mathbf{H}_z < 0$ and a displacement of ΔV_0 experimental curve from the theoretical behavior. Similar responses are always found when $V\% > 33\%$. The explanation for this behavior is as following:

- if \mathbf{H}_z has the same orientation of \mathbf{M}_z ($\mathbf{H}_z > 0$), the magneto-mechanical moment $\mathbf{m} \times \mu_0 \mathbf{H}_z$ rotates the particles inside the silicone matrix towards the direction of the sample longitudinal remanent magnetization, \mathbf{M}_z ; in this way \mathbf{H}_z supports the magnetic interactions between the particles, this resulting in higher experimental ΔV_0 values than those expected from Eq. (34) (Figure 35);

▶ on the contrary, when \mathbf{H}_z has an opposite orientation with respect to \mathbf{M}_z ($\mathbf{H}_z < 0$), the magneto-mechanical moment $\mathbf{m} \times \mu_0 \mathbf{H}_z$ rotates the particles far from \mathbf{M}_z orientation, producing a $\Delta \mathbf{M} < 0$; therefore, the biasing field effect opposes the magnetic interactions between the Sm_2Co_7 particles and, at a threshold value of the magnetizing field ($\mathbf{H}_z \approx -90$ Oe), the magnetic interactions are broken and the experimental behavior follows the theoretical one, correspondent to the situation (Figure 35).

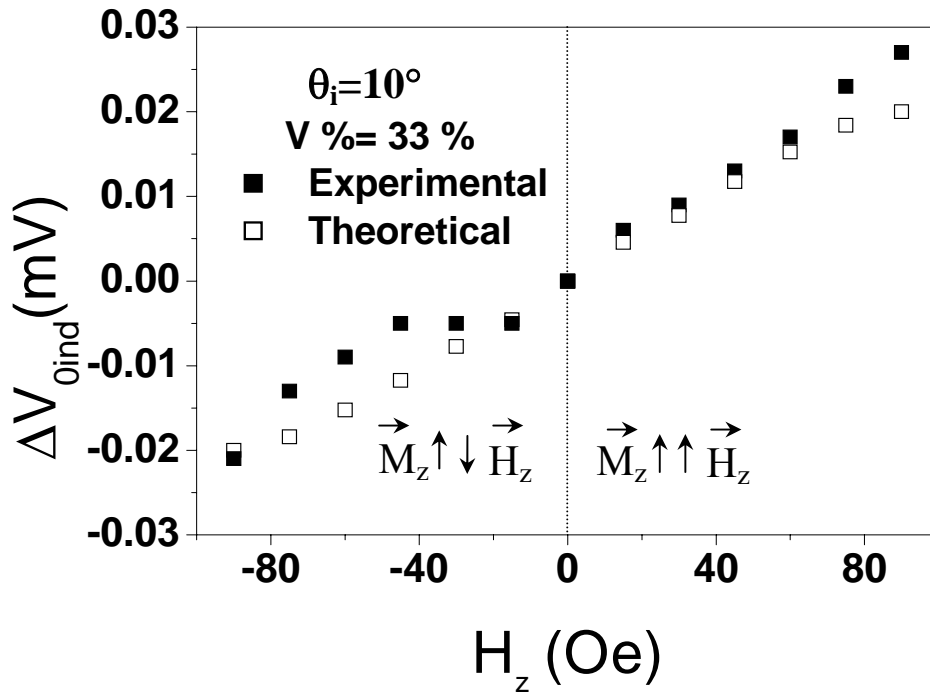


Figure 35. Experimental and theoretical V_{0ind} amplitude change, $\Delta V_{0ind} = V_{0indH \neq 0} - V_{0indH=0}$, as a function of the applied magnetic field \mathbf{H}_z , for fixed $\nu = 35$ Hz and $U_0 = 0.7$ mm.

In conclusion, the linear dependence of the sensor elastomagnetic core response (which is the amplitude of the electromotive force, V_{0ind} , induced in the pick-up coil by the magnetization change) on the frequency and amplitude of the dynamic deformation (vibration) was experimentally verified for $V\% \leq 33\%$. In the case of higher volume fractions, the effect of the interactions among the particles magnetic moments can not be neglected anymore. These magnetic interactions are active starting probably from about $V\% = 15\%$, but they do not affect the linearity of the sensor behavior with ν and U_0 .

As can be seen from Figures 33 and 34, the elastomagnetic response of the sensing core can be improved with the increment of the volume percentage of magnetic particles (at fixed magnetic pre-orientation of the filling particles), but for volume percentages higher than $V\%=33\%$ the magnetic interactions between the Sm_2Co_7 particles must be considered.

The proposed elastomagnetic sensor core appears to work well also at low frequencies (< 10 Hz), the obtained experimental data being consistent with the expected results, even if it was not possible to have an accurate indirect verification with the piezo-accelerometer response due to its poor reliability in this range of frequencies.

7.1.4. Sensor prototype performances and limits

The proposed sensor based on the elastomagnetic core can detect vibrations with amplitudes from 0.1 to 1 mm with a sensitivity of 4.5 mV/mm, in the frequency range 5-50 Hz. At higher frequencies, the internal friction mechanism probably exercises a dissipative role which deteriorates the sensor performances [171].

The optimum volume fraction of magnetic particles for a good elastomagnetic answer of the sensor, coherent with the developed functioning model, is about 15 %, higher contents leading to undesired magnetic interactions among the Sm_2Co_7 particles.

The developed elastomagnetic sensor appears to be particularly useful for the detection of low frequency vibrations, where other devices present a lack of reliability, as for example in the field of civil building monitoring. Another very interesting characteristic of the sensor elastomagnetic core is the possibility to be produced in any required complex shape.

Therefore, the use of elastomagnetic cores results particularly effective when low cost sensors are to be permanently inserted in a structure for its periodical monitoring. In the case of simple monitoring requiring high sensitivity, standard piezoelectric or piezomagnetic devices must be used. In fact, the elastomagnetic sensor sensitivity in strain measurement (for $V\%=15.5\%$) is 4.5×10^{-3} mV/ $\mu\epsilon$ (Figure 32), which is much lower than that of the standard

piezoelectric (50 mV/ $\mu\epsilon$) or magnetoelastic (1 mV/ $\mu\epsilon$) sensors [165,171]. The ratio between the elastomagnetic sensor sensitivity and piezo or magnetoelastic sensor sensitivities improves by almost four orders of magnitude for stress measurement. This is a consequence of the low value of silicone Young's modulus ($E_{sil} \cong 3.1 \times 10^4$ Pa) as compared to the Young's modulus ($E_{cer} \cong 5 \times 10^{10}$ Pa) of ceramics in piezoelectric sensors [171].

Sensors similar to the developed vibration sensor prototype can be used also for torsion or flecional deformation detection.

7.2. Actuator prototype based on elastomagnetic composite core

In order to evaluate the potential application of the elastomagnetic composites in actuator systems, it will be determined, for the beginning, the strain amount given by a bar sample under the action of a longitudinal magnetizing field, as well as the correspondent stress, if the material deformation is not free.

An elastomagnetic composite, made of Sm_2Co_7 micro-particles (average size of 3 μm), uniformly dispersed inside a silicone matrix, was produced in bar shape, with the square cross section of 5×5 mm² and 50 mm in length. The sample was permanently magnetized at $\theta_i=45^\circ$ with respect to the material longitudinal z-axis. A magnetizing field, \mathbf{H}_z , applied along the longitudinal axis of the sample, induces an average rotation of the particles, due to the direct elastomagnetic effect, with θ_H , given by Eq. (4) [167]:

$$\theta_H \cong \frac{-M_r \tau V \% \mu_0 H_z \sin \theta_i}{K} \cong -\frac{M_r \tau V \% \mu_0 H_z \sqrt{2}}{2K} \quad (35)$$

where $M_r=0.6 \times 10^6$ A/m, $K=0.4$ Nm (experimentally determined), and $\tau=125$ mm³. If the bar sample is clamped at one end, it undertakes a deflection with the average angle, θ_H (Figure 36), proportional to the volume fraction of filling magnetic particles and to the applied magnetic field, \mathbf{H}_z . When the sample deflection is hindered, being possible only longitudinal

deformations, one expects that the effect of the particles rotation under the action of \mathbf{H}_z results in a sample relative elongation (Figure 37) [167, 157]:

$$\varepsilon_{zH} = \frac{\Delta l}{l} \cong -\frac{\sqrt{2}}{2} \theta_H \quad (36)$$

If a body obstructs the free elongation of the sample, it exerts a force on the obstructing body [164, 157]:

$$F = \varepsilon_{zH} ES \cong \frac{M_r \tau V \% \mu_0 H_z ES}{2K} \quad (37)$$

where E is the Young's modulus of the composite material ($\cong 7.5 \times 10^4$ Pa) and S is the sample transversal cross section.

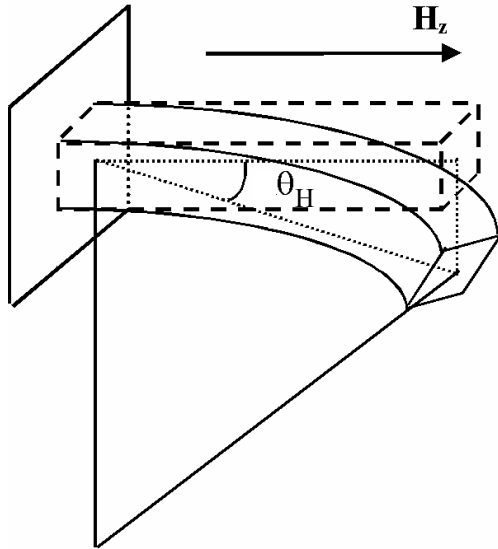


Figure 36. Deflection of the elastomagnetic bar sample, clamped at one end, under the action of a longitudinal magnetizing field \mathbf{H}_z : θ_H – average deflection angle.

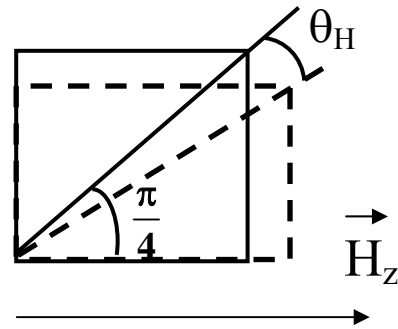


Figure 37. Longitudinal deformation of the elementary cell of the elastomagnetic composite (permanently magnetized at 45°) under the action of the longitudinal magnetizing field, \mathbf{H}_z , when the sample deflection is obstructed.

From Eqs. (35)-(37) it is easy to conclude that, in order to produce and transmit the highest force, at constant exciting field \mathbf{H}_z , it is necessary to use the highest possible volume fraction of magnetic particles, Young's modulus of the matrix material and sample transversal cross section as well as the lowest possible elastic torsion constant, K, of the composite matrix. Obviously, fixed all the above mentioned parameters, F value is proportional to \mathbf{H}_z .

The stress actuated by the elastomagnetic core material can be estimated from Eq. (37) for $V\%=9\%$ and $\mu_0 H_z=0.1$ T, as $F/S\cong 333$ Pa.

Based on this simple model, which predicts a good efficiency of the elastomagnetic composite as actuator core material, an actuator prototype was developed (Figure 38) [167, 172].

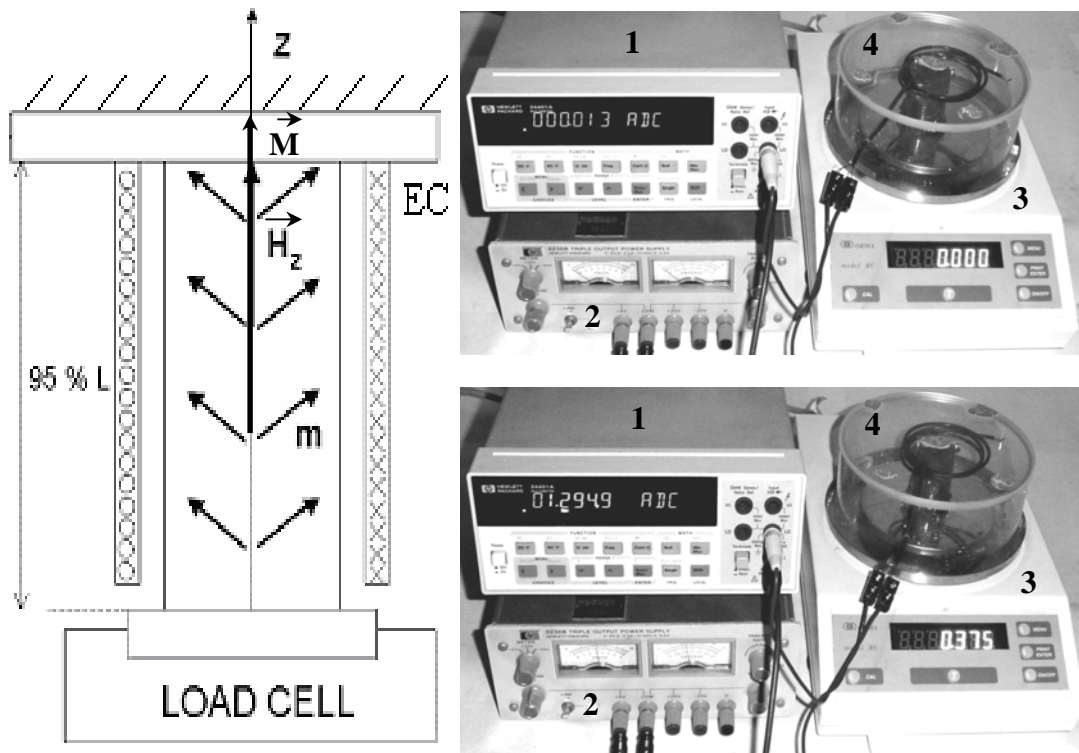


Figure 38. Experimental arrangement for the measurement of the force actuated by the elastomagnetic core under the action of a magnetizing field, \mathbf{H}_z , given by a dc current flowing in the excitation coil (EC): 1 - power supply, 2 - digital multimeter, 3 - balance, 4 – actuator prototype.

The actuator elastomagnetic core, identical to that presented in Figure 29, is inserted vertically between a fixed rigid plate and the plate of a balance, inside an excitation coil. Due to the fishbone like distribution of the particles magnetic moments, \mathbf{m} , in the adjacent bars forming the core material and due to the direct elastomagnetic effect, the sample undergoes an elongation, when the external magnetizing field, \mathbf{H}_z , is oriented in the same direction of the macroscopic magnetization \mathbf{M} , ($\mathbf{H}_z > 0$), or a contraction, when the external field, \mathbf{H}_z , is

oriented in the opposite direction with respect to the macroscopic magnetization \mathbf{M} , ($\mathbf{H}_z < 0$) As consequence to the deformation, the elastomagnetic sample can exert a force, if the deformation is not free. Initially, at $\mathbf{H}_z = 0$, the sample was pre-compressed along the longitudinal z-axis with a pre-strain of -5%, in order to have a deformation effect measurable by the balance also when $\mathbf{H}_z < 0$. Therefore, when a longitudinal magnetic field \mathbf{H}_z is applied by means of the excitation coil coaxial to the sample, the balance shows an apparent change of weight governed by Eq. (37) [164]. More exactly, for $\mathbf{H}_z > 0$ is expected an increase of the sample apparent weight, W , while a weight decrease is expected for $\mathbf{H}_z < 0$. In Figure 39 the experimental weight changes, ΔW (measured by the balance), and the theoretical F values (evaluated from Eq. (37)), with the applied magnetic field, $\mu_0 H_z$, are reported ($\Delta W = F$) [167, 172].

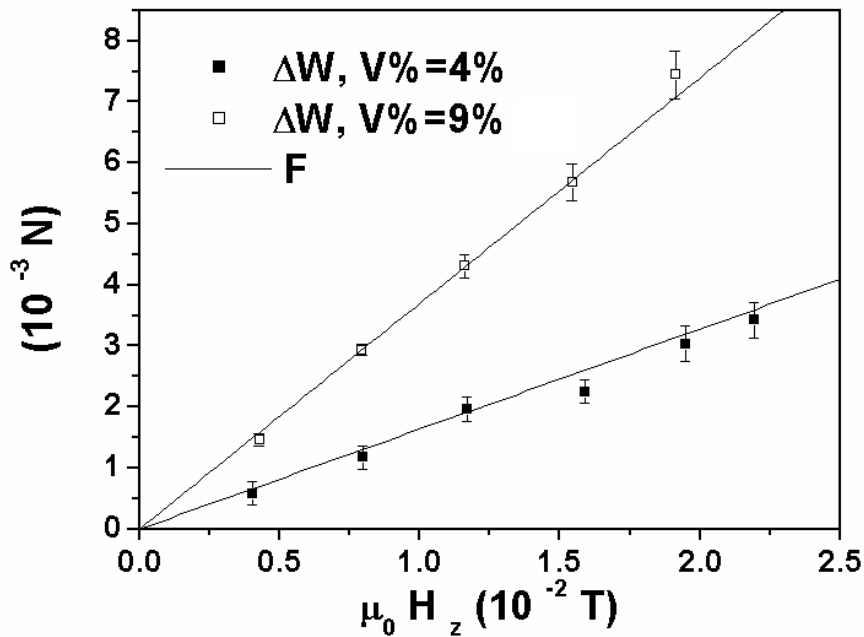


Figure 39. Dependence of the weight change ΔW , as obtained by experiment, and force F , as evaluated from Eq. (37), on the magnetizing field $\mu_0 H_z$, for two $V\%$ values.

As can be seen, the experimental results and the theoretical predictions are in good agreement, the proportionality constants between F and $\mu_0 H_z$ and ΔW and $\mu_0 H_z$ having very close values:

theoretical proportionality constants for V%=4 and 9% are 0.15 and 0.33 N/T, respectively, while the experimental proportionality constants are 0.16 and 0.36 N/T, respectively.

Extrapolating the data in Figure 39 for V% = 33%, one can predict a maximum strain of 1.4×10^{-2} and a pressure (F/S) of about 10^3 Pa, when $\mu_0 H_z \cong 10^{-1}$ T [167]. Considering that from Eq. (37) results that the force produced by this kind of actuator core is proportional to E/K ratio, an efficiency improvement can be obtained by increasing the value of this ratio. In effect, it appears not so difficult to choose a matrix elastic material so that the value of E/K parameter may increase of a factor 10.

Considering the above mentioned potential improvement and the experimentally obtained data, it is possible to make a comparison between the expected actuation performances of the elastomagnetic composite core and some standard materials used in actuators. In Table 4 are presented the actuation performances of the investigated elastomagnetic composite core (potential performances obtainable for the best production parameters) and of two standard materials (Piezoelectric and Magnetostrictive) actually used in actuators [157].

Table 4. Actuation performances of the investigated elastomagnetic composite core and of two standard materials (Piezoelectric and Magnetostrictive) actually used in actuators.

Actuator type	Max Strain (%)	Max Pressure (MPa)	Max Energy Density (J/cm ³)	Max Efficiency (%)	Relative Speed (full cycle)
Elastomagnetic Sm ₂ Co ₇ (V%≅30%) inside silcione	1.4	1×10^{-2}	7×10^{-5}	>80%	Medium
Piezoelectric Ceramic (PZT)	0.2	110	0.10	>90	Fast
Polymer (PVDF)	0.1	4.8	0.0024	90	Fast
Magnetostrictive (Terfenol-D, Etrema Products)	0.2	70	0.025	60	Fast

From the table it is evident that the energy density for the elastomagnetic core material is not so good with respect to the others, but the possible actuating strain is very high.

In conclusion, one can state that the application of the developed elastomagnetic composite as actuator core may be useful only in particular cases, as for example:

1. when a special, complex, shape of actuator is required (due to the shape forming facility);
2. in tele-operated and biomedical components (due to the remote excitation capability and silicone matrix biocompatibility, respectively);
3. when high force production is required on a very great surface.

8. STABILITY OF THE ELASTOMAGNETIC PERFORMANCES UNDER THERMAL AND MECHANICAL AGEING

The assessment of the elastomagnetic composite thermal stability and mechanical ageing is a matter of strong interest for the engineering process of this material as magnetic core for sensors and actuators.

The investigated elastomagnetic composite was made of irregular shape Sm_2Co_7 micro-particles (average size of 4 μm) uniformly dispersed inside a silicone matrix in a volume percentage of 9%. The samples were prepared in bar shape (4.6 cm in length and $5 \times 5 \text{ mm}^2$ transversal cross section), and they were permanently magnetized at room temperature so that all the magnetic moments, \mathbf{m} , of the Sm_2Co_7 particles were aligned at 45° with respect to the bar main axis [173].

The thermal stability of the samples was analyzed by differential scanning calorimetric (DSC) measurements (Appendix A). The DSC curves for Sm_2Co_7 powder, pure silicone and composite material made of Sm_2Co_7 micro-particles uniformly dispersed inside the silicone matrix are presented in Figure 40 [173].

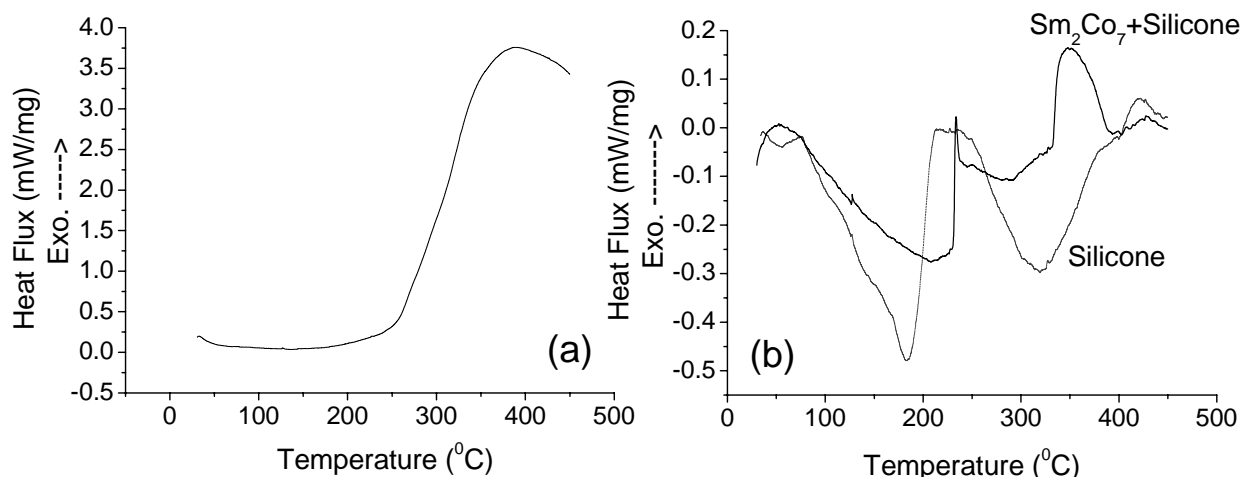


Figure 40. DSC curves for Sm_2Co_7 powder (a), pure silicone (b) and elastomagnetic composite made of Sm_2Co_7 powder ($V\%=9\%$) uniformly dispersed inside the silicone matrix (b). Heating rate: 5 K/min.

The obtained DSC curve for Sm_2Co_7 powder (Figure 40(a)) confirms the well known outstanding thermal stability of this composite, which has a maximum working temperature of 250°C . The exothermic peak centered around 380°C is likely caused by the material oxidation. The DSC curve of pure silicone shows two endothermic peaks (Figure 40(b)) which probably correspond to the partial melting of the silicone (first peak) and to the silicone decomposition (second peak). The DSC curve of the composite material exhibits three peaks (Figure 40(b)): two endothermic and one exothermic, following the superposition of the two components behaviour. The slight shift in the peaks position is probably determined by the intimate interaction between the filling particles and the silicone matrix.

In Figure 41 are presented the DSC curves for elastomagnetic composites with different volume percentages of Sm_2Co_7 particles. All the reported curves exhibit three peaks: two endothermic and one exothermic. It can be seen a good qualitative coherence between the Sm_2Co_7 volume percentages and peaks area. In effect, with $V\%$ increasing, the silicone percentage is decreasing and therefore the area of the first two endothermic peaks related to the silicone thermal behaviour is decreasing, while the area of the third peak, exothermic,

connected to the superposition between the endothermic process of silicone decomposition and the exothermic oxidation process of Sm_2Co_7 particles, is increasing.

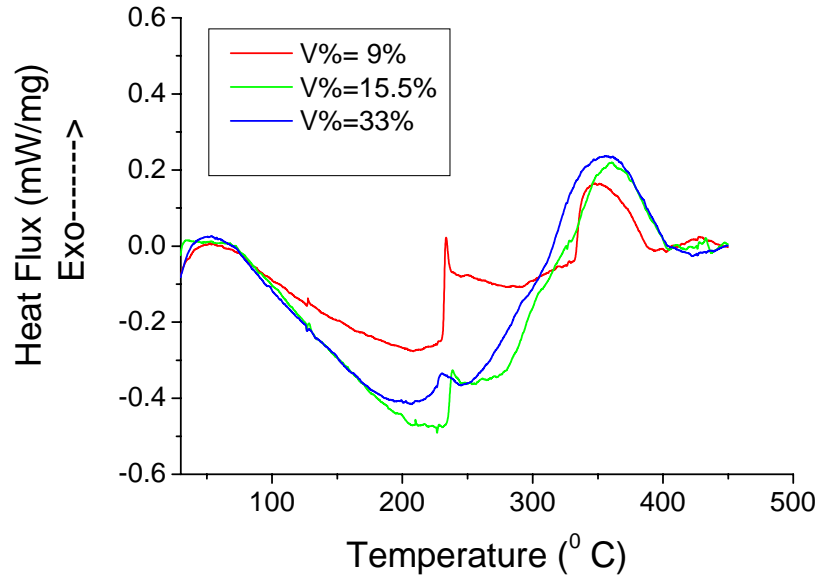


Figure 41. DSC curves for elastomagnetic composites with different volume percentages of Sm_2Co_7 particles.

The thermal treatment and mechanical ageing effects on the elastomagnetic response of the sample under the action of longitudinal dynamic deformation (of variable frequency, ν , and amplitude, D , given by a shaker) were investigated using the experimental set-up presented in Figure 30 (Appendix A). The ageing effects on the material elastomagnetic response were studied by measuring the amplitude, V_0 , of the electromotive force induced in the pick-up coil as consequence of the magnetization change due to the dynamic mechanical solicitation of the sample: inverse elastomagnetic effect.

The sample thermal treatments were performed in a furnace, in argon atmosphere, in order to avoid the material contamination. Subsequent treatments at 50, 100, 150, 200, 234, 260, 300 and 343°C, following the important temperature regions from the DSC curve, were performed in two steps program: dynamic heating from the room temperature to the required temperature (with a heating rate of 5 K/min), followed by an isothermal treatment of 2 min.

The mechanical ageing of the elastomagnetic composite was performed by exposing the sample to dynamic mechanical solicitations (at $\nu=30$ Hz and $D=0.7$ mm), carried out continuously during 48 h.

The curves of the sample elastomagnetic response, V_0 , as function of frequency, ν , and amplitude, D , of the dynamic mechanical solicitation, after different thermal treatments are presented in Figure 42 (a) and (b), respectively [173].

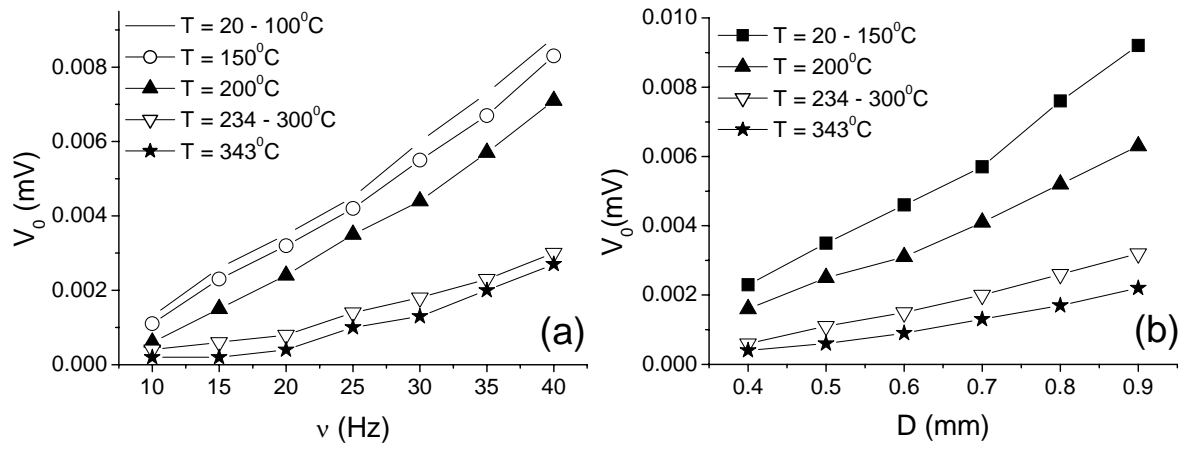


Figure 42. Elastomagnetic response, V_0 , of the sample as function of frequency, ν (at fixed $D=0.7$ mm) (a) and amplitude, D (at fixed $\nu=30$ Hz) (b) of the dynamic mechanical solicitation, after different thermal treatments. The reported V_0 data are the average values of three repeated measurements.

It can be seen that for the whole investigation range of thermal treatment temperatures, the dependence of the elastomagnetic response, V_0 , on the frequency, ν , and amplitude, D , of the externally induced deformation is linear, as predicted by Eq. (30). The amplitude of the elastomagnetic response is not changing for treatment temperatures up to 150°C . With increasing the treatment temperature, the response amplitude is decreasing, due to the joint action of the worst: silicone elastic characteristics, due to the partial melting and decomposition processes and Sm_2Co_7 magnetic properties, whose working temperature is generally limited to about 250°C , due to the oxidation (see the DSC curve in Figure 40(a)), as

well as to the possible aggregation process taking place during thermal treatments at temperatures over 200°C, correspondent to the silicone partial melting.

The dependence of the sample elastomagnetic response, V_0 , as function of frequency, ν , and amplitude, D , of the dynamic mechanical sollicitation, after different mechanical treatment times are presented in Figure 43 (a) and (b), respectively [173]. The curves V_0 versus ν and D were registered at regular 1 h intervals during the mechanical treatment, but the reported curves in Figure 43 are only those registered after 16, 32 and 48 h.

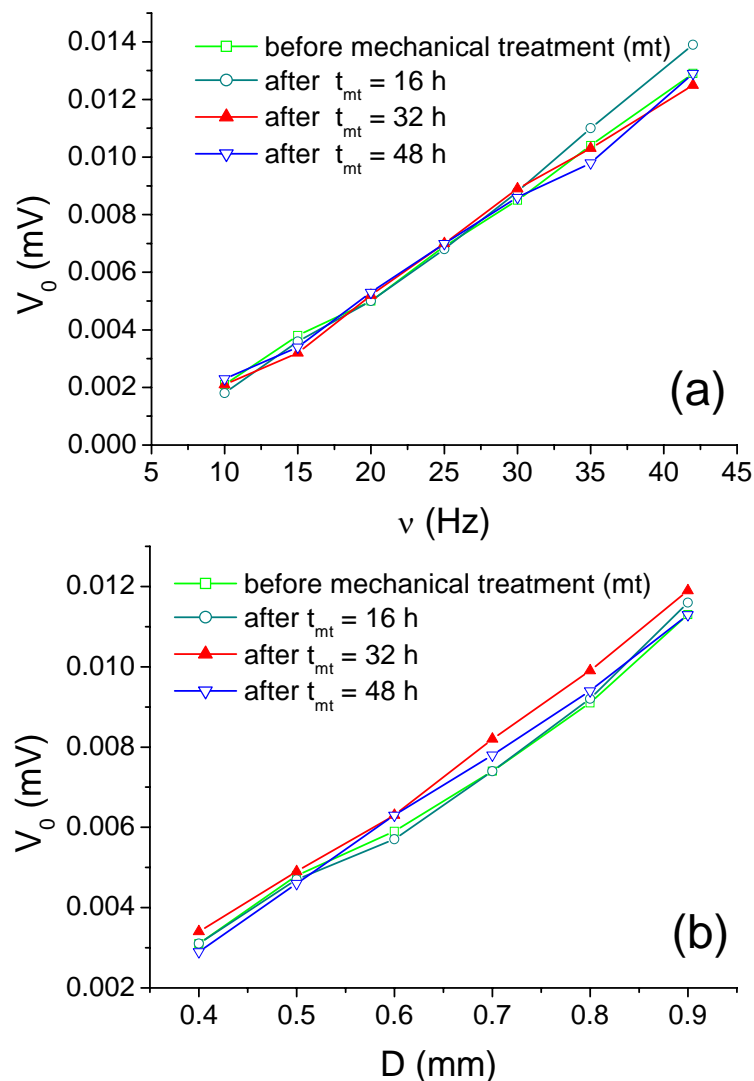


Figure 43. Elastomagnetic response, V_0 , of the sample as function of frequency, ν (at fixed $D=0.7$ mm) (a), and amplitude, D (at fixed $\nu=35$ Hz) (b), of the dynamic mechanical sollicitation, after 16, 32 and 48 h of dynamic mechanical treatment at $\nu=35$ Hz and $D=0.7$ mm. The reported V_0 data are the average values of three repeated measurements.

The analysis of the material elastomagnetic response registered after different times of mechanical treatment shows the excellent output reliability and no decrease in amplitude with the treatment time.

9. Conclusion

The progress of the magnetic materials in the 20th century has been huge and spectacular, advancing from a set of poorly differentiated hard and soft steels to a spectrum of materials exhibiting coercivity ranging from 0.1 A/m to several MA/m, extremely low, 0.1 J/cm³, or extremely large, 10⁷ J/m³, magnetocrystalline anisotropy, and saturation magnetostriction from less than 10⁻⁷ to 10⁻². Surely there is now a huge reservoir of knowledge on the production and properties of thousand of magnetic materials. The advanced magnetic materials now underpin the data storage, telecommunications, consumer electronics and appliance industries, magnetic devices for energy transfer, high power and miniature electro motors, sensors and medical applications, etc. In this context, the question is: do we really need more research on magnetic materials? Do we really need to look for more? There are several answers to this. Firstly, we do not have all the magnetic materials we desire and have a reasonable hope of acquiring. For example, there is no: true permanent magnet ($\mu_0 H_c > B_r/2$) which can be used at 400°C, a bulk ferromagnet with a polarization higher than 2.5 T, a soft ferromagnetic films combining polarization higher than 2 T with zero magnetostriction and near-zero anisotropy, a permanent magnet with an energy product of 1 MJ m⁻³, a strongly coercive magnetic powder with $B_r > 1.5$ T, etc [174]. There are clear developments possible from where we are at present in the direction of new multicomponent alloys, metastable materials, new composite and thin film structures, by the exploration of nanoscale magnetism and not only. Surprisingly, the list of different ferromagnetic materials which have found large-scale industrial application is remarkably short [174], in view of the thousands that are known. This is caused by the fact that, in order to introduce a new material

on the market, changing all the infrastructure connected with the previously produced materials, it must be really cost-effective. In this sense, the further progress in the field of magnetic materials and their application is possible if we succeed to develop materials with:

1. optimal property spectra, not only one outstanding property, where magnetic, electrical, mechanical (including processability), corrosive and thermal properties are optimized simultaneously;
2. competitive production costs (even if there is no absolute improvement in properties, the materials already in use may be processed more effectively and economically).

In this context of the research efforts for the development of new, cost-effective materials, with simultaneously improved magnetoelastic and mechanical properties, this thesis is focused on the production and characterization of new elastomagnetic composites, made of permanently magnetized Sm_2Co_7 micro-particles uniformly dispersed inside a silicone matrix, in view of their use as core materials for sensors and actuators. This kind of materials are not exactly new, but new is the composition (the use of permanently magnetized Sm_2Co_7 particles) and the idea to take advantage from the pinning mechanism of the magnetic moments of the filling particles on their own body and from the coupling between the magnetic and elastic reaction mechanical moments.

A theoretical model describing the elastomagnetic behavior of these materials, or more exactly the coupling between the magnetic state and the elastic deformation, is established, by giving a coherent description of the direct (deformation due to magnetization change) and inverse (magnetization change due to deformation) elastomagnetic effects. The developed experimental verification of the theoretical predictions validates the model through the good agreement between the experimental results and the theoretical ones, given by the established constitutive equations of elastomagnetism. From the analysis of the experimental

measurements, the model limits, related especially to the intensity of the magnetic interactions between the filling particles, were established.

Two sensor and actuator prototypes, based on elastomagnetic core, have been conceived, developed and experimentally tested, showing the potentiality of the new composites (which offers the unique possibility to use the same material to detect and actuate deformation by the inverse and direct elastomagnetic effect, respectively) as intelligent materials. The obtained results related to the elastomagnetic composite performances as dynamic deformation sensing and actuator core can be summarized as following:

1. the developed sensor prototype (in the case of $V\%=15\%$ volume percentage of Sm_2Co_7 micro-particles) is a compact and reliable device which can detect vibrations with amplitudes from 0.1 to 1 mm, with a sensitivity of 4.5 mV/mm, in the frequency range 5-50 Hz;
2. with the increase in the volume fraction of magnetic particles, the elastomagnetic response of the sensing core is improving but, for Sm_2Co_7 volume percentage higher than 33%, undesired magnetic and mechanic interactions between the particles are taking place and therefore must be considered (the threshold value $V\%=33\%$ establishes the validity limit of the elastomagnetic theoretical model);
3. the elastomagnetic dynamic strain sensors can work at low frequencies (< 5 Hz, as for example in the field of civil buildings monitoring) better than the commercially available piezoelectric accelerometers;
4. sensors similar to the developed vibration sensor prototype can be used also for torsion or flectional deformation detection;
5. in spite of the low sensitivity with respect to the standard piezoelectric (50 mV/ $\mu\epsilon$) and magnetoelastic (1 mV/ $\mu\epsilon$) sensors, the elastomagnetic composite material is a good candidate for cost-effective, very ductile, stable and reliable vibration/displacement (static or dynamic) sensor core due to: the possibility to be

produced in any required shape (the elastomagnetic composites can be easily manufactured and machined into complex shapes), the high resistance to harsh environment, long lasting performances and non-destructive (biocompatible) nature of the silicone matrix;

6. the elastomagnetic actuator core can give (in the case of optimum production parameters such as $V\%= 33\%$ and $E/K\cong 7.5\times 10^3 \text{ m}^{-3}$) a maximum strain of 1.4×10^{-2} for a low input energy, a maximum pressure of 10^{-2} MPa, and a maximum energy density of 7×10^{-5} (which is one, up to two orders of magnitude lower than the commercially available piezoelectric and magnetostrictive actuators);
7. the elastomagnetic composite core may be competitive in the field of actuators in particular cases as for example: when a special shape of actuator is required (due to its high processability), in tele-operated and biomedical components, and when high force production on extensive surface is necessary.

Considering that the assessment of the thermal stability and mechanical ageing is a matter of strong interest for the engineering process of the elastomagnetic composites as core material for sensors and actuators, their stability under dynamic mechanical sollicitation and with the temperature was investigated with good results: the elastomagnetic materials can work with optimum performances in a large range of temperatures, up to 200°C , and the elastomagnetic response after 48 h of continuous mechanical sollicitation exhibits excellent reliability and no decrease in amplitude with the time of mechanical treatment.

The obtained results encourage the assumption that the developed elastomagnetic composites are expected to be the precursors of an important class of multifunctional materials due to their peculiar, specific elastomagnetic performances and unique ability to detect and actuate deformations at the same time.

The research activity developed in the frame of this thesis is not exhausting the argument, but it represents a fundamental premise for the future development of the

elastomagnetic composites and their applications. In effect, further research is required to tailor the composition (e.g. new elastic matrices made of a more elastic material, in the case a higher elastomagnetic deformation is required, or of a less elastic material, for higher force actuated by the sample deformation), production process and structure of the elastomagnetic composites in view of performances improvement for reliable, durable and cost-effective materials for intelligent devices (e.g. the development of: elastomagnetic sensor prototypes for biomedical applications, based on the biocompatibility of the composite silicone matrix, as well as on their shape adaptability; functional elastomagnetic composites with adaptive stiffness, made of magnetic and elastic layers for application in vibration attenuation in particular).

The articles published during the three years of doctoral activity in international journals and the invited presentations (at the 4th European Magnetic Sensors and Actuators Conference held in Athens, Greece and at the 2nd International Workshop on Amorphous and Nanocomposite Magnetic Materials, Iasi, Romania) confirm the validity of the obtained scientific results, proving the international interest in the field of elastomagnetic composite materials.

List of publications related to the doctoral activity:

Journals

1. L. Lanotte, G. Ausanio, C. Hison, V. Iannotti, C. Luponio, The potentiality of composite elastic magnets as novel materials for sensors and actuators, *Sensors and Actuators A* **106** (2003) 56-60 (invited presentation at the 4th European Magnetic Sensors and Actuators Conference (EMSA), July 2002, Athens, Greece);

2. G. Ausanio, V. Iannotti, C. Hison, L. Lanotte, A. D'Agostino, R. Germano, Novel elastic magnets as actuators core, *Journal of Applied Electromagnetics and Mechanics* **19** (2004) 395-398;
3. L. Lanotte, G. Ausanio, C. Hison, V. Iannotti, C. Luponio, Elastomagnetic effect in novel elastic magnets, *J. Magn. Magn. Mater.* **272-276** (2004) 2069-2071;
4. L. Lanotte, G. Ausanio, C. Hison, V. Iannotti, C. Luponio, C. Luponio Jr, State of the art and development trends of novel nanostructured elastomagnetic composites, *Journal of Optoelectronics and Advanced Materials* **6-2** (2004) 523-532 (invited presentation at the 2nd International Workshop on Amorphous and Nanocomposite Magnetic Materials (ANMM), September 2003, Iasi, Romania);
5. L. Lanotte, G. Ausanio, C. Hison, V. Iannotti, C. Luponio, C. Luponio Jr, Particle dimension effects on magnetization and strain sensitivity for a composite of nickel particles in silicone matrix, *J. Magn. Magn. Mater.* **272-276** (2004) 1533-1535;
6. G. Ausanio, A. Barone, C. Hison, V. Iannotti, C. Luponio Jr., L. Lanotte, Mechanical vibration sensor based on elastomagnetic composite, to be published in *Sensors&Actuators A*, 2005;
7. C. Hison, G. Ausanio, V. Iannotti, L. Lanotte, G. Breglio, A. Cusano, M. Giordano, Experimental verification of the direct elastomagnetic effect, *Technical Digest of the Interdisciplinary Electromagnetic, Mechanic&Biomedical Problems, (ISEM), Bad Gastein, Austria, 12-14 September, 2005*, p. 126-127; under evaluation for the publication in the *International Journal of Applied Electromagnetics and Mechanics (IJAEM)*;
8. C. Hison, G. Ausanio, V. Iannotti, G. Lucani, C. Luponio Jr., L. Lanotte, Thermal and mechanical ageing of the elastomagnetic core material, *Technical Digest of the 3rd International Workshop on Amorphous and Nanocomposite Magnetic Materials*,

September 19-21, 2005, Iasi, Romania, p.49; under evaluation for the publication in Journal of Optoelectronics and Advanced Materials.

Books

1. G. Ausanio, C. Hison, V. Iannotti, L. Lanotte, C. Luponio, Magnetoelastic properties in amorphous ferromagnetic materials and potential applications, in *Magnetic Amorphous Alloys: Structural, Magnetic and Transport Properties*, P. Tiberto and F. Vinai (Eds.), Research Singpost, Kerala, India (ISBN:81-7736-096-5) (2003) 43-78;
2. G. Ausanio, C. Hison, V. Iannotti, C. Luponio, L. Lanotte, Magnetoelastic Stress and Strain Sensors, to be published in *Encyclopedia of Sensors*, Craig A Grimes, Elizabeth C. Dickey, Michael V. Pishko (Eds.), American Scientific Publisher (2005), 88 pages.

Appendix A: Experimental techniques

1. Vibrating Sample Magnetometer (VSM)

The permanent magnetization process, as well as the magnetic characterization of the developed elastomagnetic composites were performed by means of a vibrating sample magnetometer (VSM) from Oxford Instrument, presented in Figure 44.

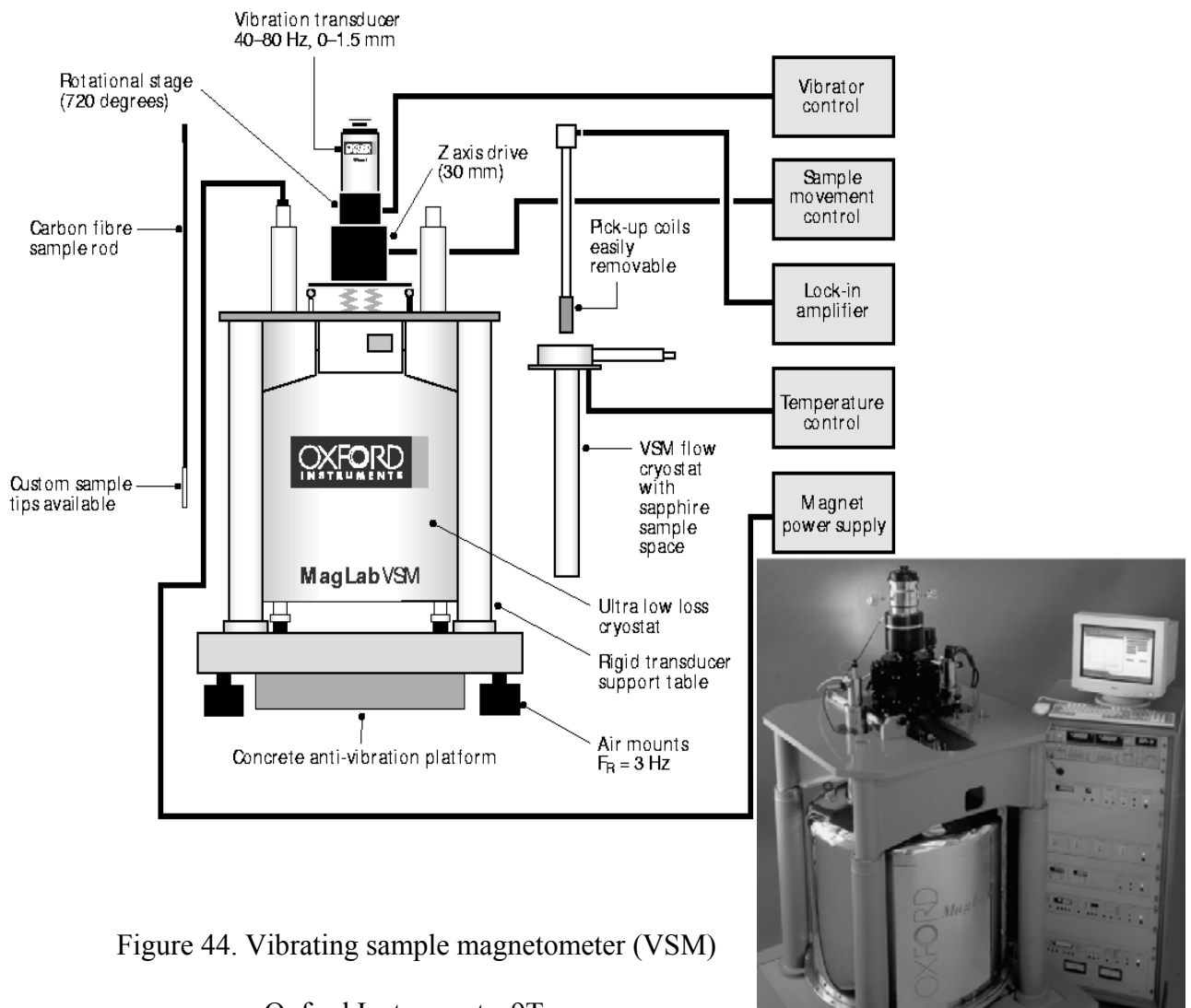


Figure 44. Vibrating sample magnetometer (VSM)

Oxford Instruments, 9T.

The magnetizing field, \mathbf{H} , used to permanently magnetize and magnetically characterize the elastomagnetic samples is generated by means of a superconducting magnet; it is vertical and it can reach up to 9T. The liquid helium utilized for the superconducting magnet is also used to perform low temperature measurements in the range 4-300 K.

During the permanent magnetization process, the sample is positioned inside the VSM device so that the magnetizing field, \mathbf{H} , has the direction of the permanent magnetization which must be imposed.

For the magnetic characterization, the sample is fixed at the inferior extremity of a rigid rod positioned between the two pick-up coils. A special positioning system is used to dispose the sample exactly in the center of the pick-up system. The rod, on which the sample is fixed, oscillates at a frequency of 55 Hz, with an amplitude of 1.5 mm. During the magnetic characterization, the sample is positioned inside the VSM device with the main axis parallel to the magnetizing field direction; the investigation is performed by measuring the sample magnetization component, \mathbf{M} , along the magnetizing field, \mathbf{H} , through the alternative electromotive force induced by the periodical displacement (oscillation) of the sample in the pick-up coil system. The amplitude of this electromotive force is proportional to the magnetic moment of the investigated sample, in agreement with the electromagnetic induction law. The vibration controller of the rod gives as reference frequency to the lock-in amplifier the rod frequency; in this way, the lock-in manages the voltage signal received from the pick-up coils by amplifying only the signal having the same frequency with the rod vibration. The applied magnetic field intensity and the temperature environment are computer controlled. The same computer ensure the data storage and management, giving the sample longitudinal magnetization as function of the applied magnetizing field, temperature and/or time. The VSM resolution is of the order of 10^{-6} emu.

2. Experimental set-up for the study of the composite sample elastomagnetic response to dynamic mechanical deformation

The schematic view of the experimental set-up used for the study of the composite sample elastomagnetic response to dynamic mechanical deformation is shown in Figure 45. The composite sample, C, is inserted inside a Plexiglas support on which are wound the excitation, EC and pick-up PC coils. The upper part of this support, and of the sample at the same time, are in contact with a fixed plate, FP, while the bottom end of the sample lies on an aluminum cylinder (AIC) tightly glued on another aluminum cylinder (AIC) fixed on the shaker which generates dynamic mechanical vibration. The role of the two aluminum cylinders is to establish a certain distance between the sensor prototype and the shaker in order to avoid noise signal in the pick-up coil, as it will be explained in the following.

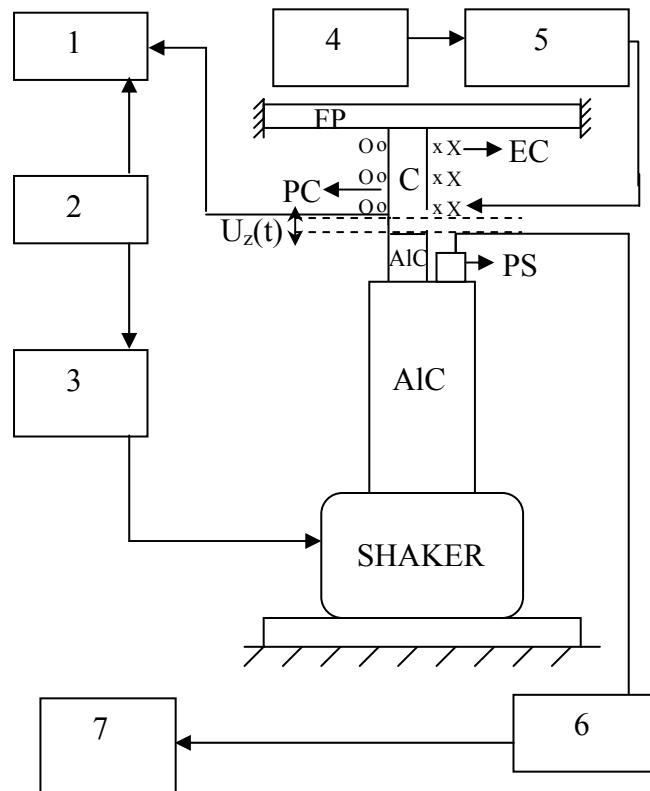


Figure 45. Experimental arrangement used to study the core elastomagnetic response to dynamic mechanical deformation produced by a shaker: 1: lock-in amplifier, 2: signal generator, 3: shaker power amplifier (BAA 120), 4: dc generator, 5: amperometer, 6: signal conditioner, 7: oscilloscope, FP = fixed plate, EC = exciting coil, PC = pick-up coil, C = elastomagnetic core, AIC = aluminum cylinder, PS = piezoelectric sensor, $U_z(t) = U_0 \sin(2\pi\nu t)$ = dynamic longitudinal deformation induced by the shaker vibration.

The elastomagnetic composite transduces the dynamic deformation induced by the shaker vibration in an electrical signal, the pick-up coil detecting the sample response as an electromotive force. The electromotive force is induced by the sample magnetization change determined by the magnetic moment rotation of the filling particles under the action of the dynamic strain (inverse elastomagnetic effect).

The used shaker is a TIRAvib S521 device from TIRA Maschinenbau GmbH. The shaker frequency range is 2 Hz – 7 kHz. It is fed with a sinusoidal or irregular signal by the signal generator. This last drives the shaker by means of a power amplifier (BAA 120), giving at the same time the reference frequency to the lock-in amplifier which manages the voltage signal received from the pick-up coil. In this way, only the component signal with the frequency equal to that of the shaker vibration is amplified by the lock-in.

The shaker is composed of a permanent Alinco-magnet producing a magnetic field which keeps the right direction of a free moving-coil, situated on the magnet frame, through which is passing an ac current. The moving-coil is connected to the expander, on which can be fixed the object to be tested (in our case this is the aluminum cylinder which has the function of separator between the shaker and the material under test). Considering the above mentioned, it is possible that the ac magnetic field generated by the moving-coil induces an electromotive force in the pick-up coil of the experimental set-up. Therefore, an unwanted over imposition of this voltage on the signal generated by the elastomagnetic response of the elastomagnetic sample is possible. A series of tests, in the absence of the elastomagnetic core deformation (i.e. in the absence of the sample elastomagnetic response), were developed in order to determine the amplitude of this “noise” signal. In Figure 46 is shown the amplitude of the voltage induced in the pick-up coil by the shaker, $V_{0shaker}$, as function of the vibration frequency, for the same distance shaker - pick-up coil as that used during the experimental study of the sample elastomagnetic response under the action of the shaker vibration.

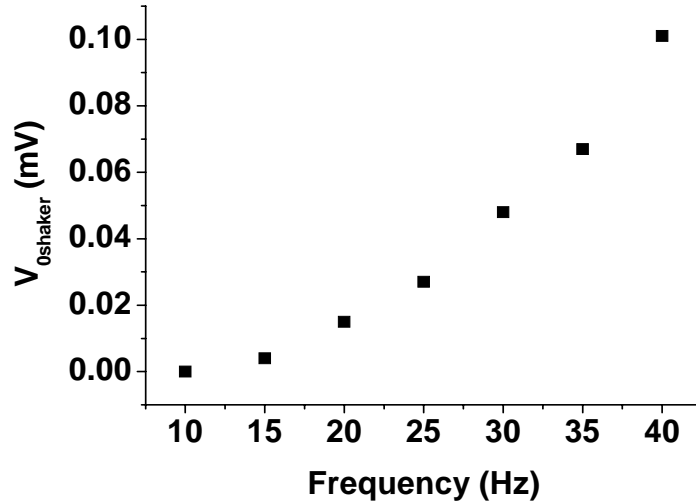


Figure 46. Dependence of the shaker induced voltage amplitude, $V_{0shaker}$, on the shaker vibration frequency, for a fixed amplitude deformation and in the absence of the elastomagnetic core deformation.

As can be seen, the values of the shaker induced voltage amplitude are about 1% from the amplitude of the signal induced by the sample elastomagnetic response (Figure 31), in the whole frequency range used for investigations. Therefore, the magnetic noise induced by the shaker in the pick-up coil can be neglected.

The amplitude U_0 of the dynamic displacement $U_z(t)=U_0\sin(2\pi vt)$ transmitted by the shaker to the sample through the aluminum cylinder is measured by a piezoelectric sensor (accelerometer), PS, fixed on AIC (Figure 30(a)). The amplitude of the sensor out-put signal given by the oscilloscope is $U_0=(a/g)\times 97$ mV. In the case of a sinusoidal shaker vibration, $(a/g)=4.026v^2D$, where v and D are the frequency and the amplitude of the shaker vibration, respectively.

The reason for which as fixed frequency v of the shaker vibration during elastomagnetic characterization was chosen $v=35$ Hz is that in the frequency range 5-20 Hz the piezoelectric sensor (which gives the signal control for the deformation amplitude) is not working in optimum conditions, while for $v>45$ Hz there is a certain instability of the

vibrating system (more exactly it is difficult to maintain a constant amplitude of the sample deformation).

3. Differential Scanning Calorimetry

The analysis of the thermal stability of the developed elastomagnetic composites was performed by means of differential scanning calorimetry (DSC), using a computer assisted NETZSCH DSC 200 instrument (Figure 47). The schematic drawing of the heating system and measuring cell is presented in Figure 48.



Figure 47. Computer assisted NETZSCH DSC 200 instrument 1: measuring part (with heating system and measuring cell), 2: controller, 3: sealing press.

The DSC investigation principle is based on dynamic heat flux differential calorimetry, where the heat flux to and from the sample is measured. More exactly, the instrument detects the heat flow difference between the sample pan and the reference pan (which is generally an empty sample pan). The pans are enclosed in a furnace, being connected by a low-resistance heat-flow metallic disc; they are designed to have a very high thermal conductivity and a very small volume, so that the thermal equilibrium inside them can be reached instantaneously. The sample weight generally ranges from 0.1 to 100 mg. The two

pans are heated or cooled uniformly (at a controlled rate) and the heat flow difference between the sample and the reference (the temperature difference between the sample and reference pans, given by the different thermal capacities of the sample pan and of the empty pan, is proportional to the heat flow between the two) is computer monitored and plotted as function of the temperature given by the furnace. When there are no thermodynamic chemical processes occurring in the sample, the heat flow difference between the sample and the reference pan varies only slightly with the temperature and shows up as a flat or very shallow base line on the plot. An exothermic or endothermic process within the sample results in a significant deviation in the difference between the two heat flows, determining a peak on the DSC curve. Generally, the differential heat flow is calculated by subtracting the sample heat flow from the reference heat flow. When following this convention, exothermic process will show up as positive peak (above the baseline), while peaks resulting from endothermic processes are negative (below the baseline).

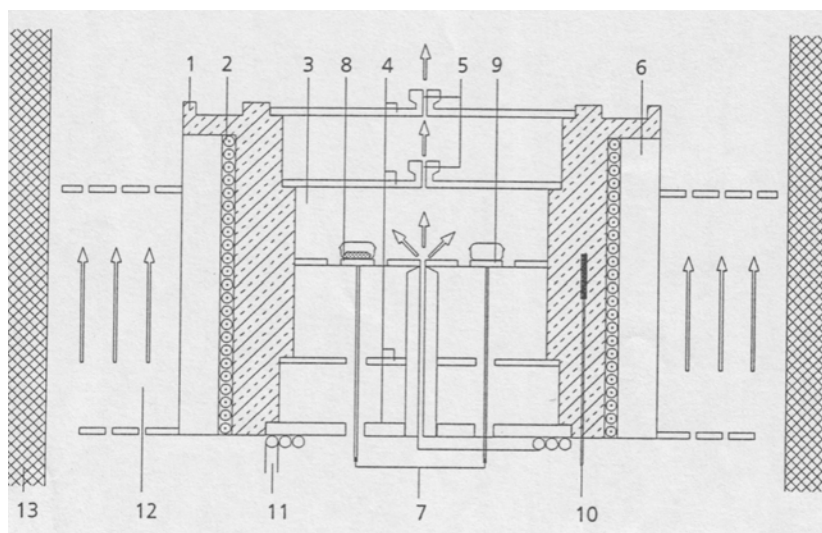


Figure 48. Schematic drawing of the DSC heating system and measuring cell. 1: cooper block, 2: jacket chamber, 3: sample chamber, 4: copper lid (gold plated), 5: gas outlet, 6: jacket for nitrogen cooling, 7: heat flux sensor and sample thermocouple, 8: sample crucible support, 9: reference crucible support, 10: control thermocouple, 11: gas inlet sample chamber, 12: jacket for air cooling, 13: insulation (outer).

The DSC measurement process takes place in the following steps:

1. Sample preparation

The sample to be investigated must be cut into a thin slice of appropriate size to the crucible dimension so that it will be distributed on all the bottom surface of the crucible.

The sample is then weighted. After this, the sample is placed inside the crucible which is hermetically sealed by means of a special sealing press (3 in Figure 47).

2. Sample chamber cleaning by acetone.

3. Insertion of the sample and reference (empty) crucibles in the measuring part of the DSC instrument, on the metal plate placed on the top of the measuring cell (Figure 49).



Figure 49. Sample and reference crucibles inside the measuring cell of the NETZSCH DSC 200 instrument.

4. Definition of the temperature program

The DSC measuring part is driven by the controller which is commanded, via a standard RS-232 interface, by the computer (there is no manual control of the instrument).

Therefore, before starting a measurement, it is necessary to define a temperature program, which contains the following instructions for the measurement to be run: starting and end temperatures; program steps (dynamic (heating, cooling) and/or isothermic treatment), heating rate, treatments time, sample mass (required for different calculations on the DSC curve).

5. Program run

6. Program execution and data collection

During the program run, the data are stored in the random access memory of the controller before transferring them to the computer.

The output of the DSC instrument provides the computer with a calibrated heat flow signal which is measured with respect to the temperature or time.

The DSC curve can be loaded in real-time during the program run.

7. Evaluation

The measuring results can be evaluated by means of a software especially developed called MITAS 3.70. The DSC evaluation contains the following features: curve scaling (analysis plot limits are defaulted to the limits of the available data; the user can change the limits to expand the region of interest), evaluation of peaks area and of partial areas, determination of the melting point, glass transition, etc.

Appendix B: Detailed calculation of Eqs. (26) and (27)

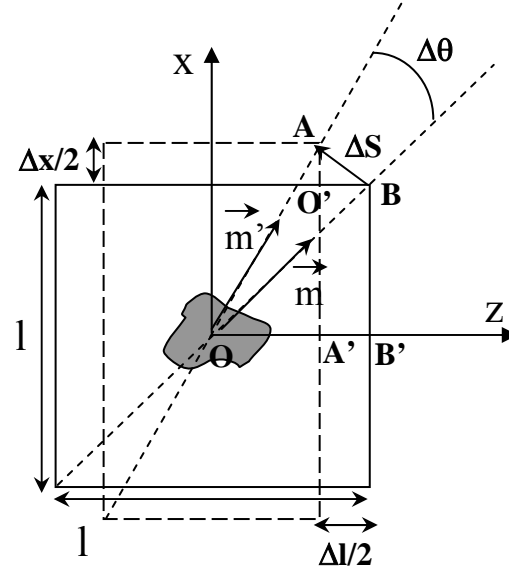


Figure 50. Deformation of the elementary cell of the elastomagnetic composite sample under the action of an external stress, and the consequent rotation, $\Delta\theta$, of the magnetic moment, \mathbf{m} , of a Sm_2Co_7 particle, permanently magnetized at 45° with respect to z-axis.

The longitudinal, ε_z , and transversal, ε_x , strains of the elementary cell of the elastomagnetic sample are:

$$\varepsilon_x = \frac{\Delta x}{l} \quad \text{and} \quad \varepsilon_z = \frac{\Delta l}{l} \Rightarrow l = \frac{\Delta l}{\varepsilon_z}$$

Let us define the $\varepsilon_z/\varepsilon_x$ ratio as:

$$\lambda = \frac{\varepsilon_z}{\varepsilon_x} = \frac{\Delta l}{\Delta x}$$

In $\triangle AO'B$ one can write:

$$AB = \Delta S = \sqrt{\left(\frac{\Delta l}{2}\right)^2 + \left(\frac{\Delta x}{2}\right)^2} = \frac{\Delta l}{2} \sqrt{1 + \frac{1}{\lambda^2}} = \frac{\Delta l}{2} \left(1 + \frac{1}{\lambda^2}\right)^{\frac{1}{2}} = \frac{\Delta l}{2} \left(1 + \frac{1}{2} \cdot \frac{1}{\lambda^2}\right)$$

$$\text{In } \triangle O'B, OB = \frac{l\sqrt{2}}{2}.$$

In $\triangle OA'A$ one can write:

$$OA = \sqrt{\left(\frac{l}{2} + \frac{\Delta x}{2}\right)^2 + \left(\frac{l}{2} - \frac{\Delta l}{2}\right)^2} = \sqrt{\frac{l^2}{2} - \frac{l\Delta l}{2}\left(1 - \frac{1}{\lambda}\right) + \frac{\Delta l^2}{4}\left(1 + \frac{1}{\lambda^2}\right)} \cong \frac{l\sqrt{2}}{2}.$$

$$\text{Therefore } OB = OA = \frac{l\sqrt{2}}{2}$$

In $\triangle OAB$ one can write:

$$\sin \frac{\Delta\theta}{2} \cong \frac{\Delta\theta}{2} = \frac{\Delta l}{2l\sqrt{2}} \left(1 + \frac{1}{2\lambda^2}\right) \Rightarrow$$

$$\Delta\theta = \frac{\varepsilon_z}{\sqrt{2}} \left(1 + \frac{1}{2\lambda^2}\right) = \frac{\varepsilon_z \sqrt{2}(1 + 2\lambda^2)}{4\lambda^2}$$

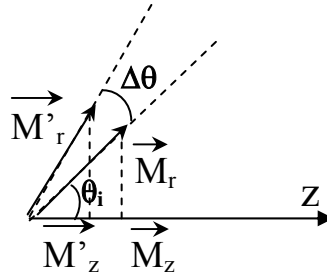
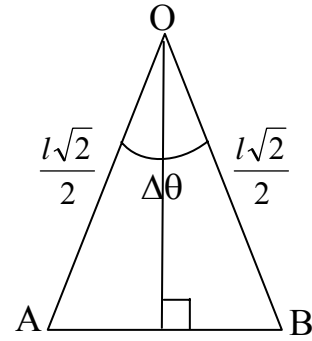


Figure 51. Change in longitudinal component magnetization, ΔM_z , due to $\Delta\theta$ particles rotation.

$$M_r = M'_r \quad \theta_i = \frac{\pi}{4}; \quad \cos(\theta_i + \Delta\theta) = \frac{M'_z}{M'_r}; \quad \cos\theta_i = \frac{M_z}{M_r} \quad \Rightarrow$$

$$\Delta M_z = M'_z - M_z = M_r \cos\left(\frac{\pi}{4} + \Delta\theta\right) - \frac{M_r \sqrt{2}}{2} \Rightarrow$$

$$|\Delta M_z| = M_r \frac{\sqrt{2}}{2} - M_r \left(\cos\frac{\pi}{4} + \Delta\theta\right)$$

Appendix C

Magnetic Units and Definition

In magnetism there are two systems of units currently in use: the MKS (meters-kilograms-seconds) system, which has been adopted as the SI units (International System of Units) and the CGS (centimeters-grams-seconds) system. The CGS system is used by many experts due to the numerical equivalence of the magnetic induction (**B**) and applied field (**H**).

When a magnetic field is applied to a magnetic material, it responds by producing a magnetic field, the magnetization (**M**). This magnetization is a measure of the magnetic moment per unit volume of material. The magnetic field applied to the material is called the applied field (**H**). Another important parameter is the magnetic induction (**B**) which is the total flux of magnetic field lines through the unit cross sectional area of the magnetic material, considering both lines of force from the applied field and from the material magnetization.

The relation between magnetic induction and magnetic field in vacuum, as well in air or any other non-magnetic environment is constant $\mathbf{B}=\mu_0\times\mathbf{H}$ The proportional factor μ_0 is called permeability constant and it has the value of $4\pi\times 10^{-7}$ H/m or 1.256×10^{-6} Vs/Am in SI units.

B, **H** and **M** are related by Eq. (1) or (1') in SI units, and by Eq. (2) in CGS units:

$$\mathbf{B}=\mu_0\times(\mathbf{H}+\mathbf{M}) \quad (1)$$

$$\mathbf{B}=\mu_0\mathbf{H}+\mathbf{M} \quad (1')$$

Both equations are giving a correct and coherent description of magnetism. In the case of Eq. (1), **B** is measured in Tesla, and **H** and **M** are measured in A/m. In the case of Eq. (1'), **B** and **M** are measured in Tesla, and **H** is measured in A/m.

$$\mathbf{B}=\mathbf{H}+4\pi\mathbf{M} \quad (2)$$

In this case **B**, **H** and **M** have the same physical dimensions and there is no need to introduce μ_0 . Even if **H** and **B** have the same physical dimension, they are measured in

different units: **H** is expressed in Oersted (Oe) and **B** in Gauss (G or Gs), while $4\pi\mathbf{M}$ is usually expressed in Gauss and **M** in emu/cm³, where emu (electro magnetic unit) is the measuring unit in CGS for the dipole magnetic moment.

In Table 5 are presented the relationships between some magnetic parameters in CGS and SI units.

Table 5. Magnetic parameters in CGS and SI, and the relationship between them.

Quantity	CGS units	SI Units	Conversion
Magnetic induction (B)	Gauss (G)	Tesla (T)	1T=10 ⁴ G
Applied magnetic field (H)	Oersted (Oe)	A/m	1A/m=4π/10 ³ Oe
Magnetization (M)	emu/cm ³	A/m	1A/m=10 ⁻³ emu/cm ³
Magnetic moment (m)	emu	Am ²	1Am ² =10 ³ emu
Vacuum permeability (μ ₀)	dimensionless	H/m	4π×10 ⁻⁷ H/m=1(cgs)

Correspondence between volume, V%, and mass, M%, percentage of Sm₂Co₇ particles inside the elastomagnetic composite

The correspondence between the volume, V%, and the mass, M%, percentage of Sm₂Co₇ particles inside the silicone matrix is given by the following formula

$$V\% = \frac{M\%m_{tot}}{\rho_{SmCo}\tau_{tot}},$$

where m_{tot} and τ_{tot} are the total sample mass and volume, respectively and

$\rho_{SmCo} \cong 8 \text{ g/cm}^3$ is the density of the Sm₂Co₇. Using this equation, the following correspondence between the volume, V%, and the mass, M%, percentages was found:

$$M\%=20\% \Leftrightarrow V\%=7.2\%; \quad M\%=40\% \Leftrightarrow V\%=9\%; \quad M\%=60\% \Leftrightarrow V\%=15.5\%;$$

$$M\%=80\% \Leftrightarrow V\%=33\%.$$

References

1. S. Bednarek, *Appl. Phys. A* 66 (1998) 643;
2. S. Jin, T.H. Tiefel, R. Wolfe, et al., *Science* 225 (1992) 446;
3. E.A. Zaltsgendler, A.V. Kolomentsev, V.I. Kordonskii, et al., *Mag. Hydr.* 4 (1985) 105;
4. J.M. Ginder, M.E. Nichols, L.D. Elie, S.M. Clark, Controllable stiffness components based on magnetorheological elastomers, in: *Smart Structures and Materials, Proceedings of SPIE*, Norman M. Weseley, 2000;
5. J.M. Ginder, W.F. Schlotter, M.E. Nichols, Magnetorheological elastomers: in tunable vibration absorbers, in: *Smart Structures and Materials, Proceedings of SPIE*, SPIE- The International Society for Optical Engineering, vol. 4331 (2001) 103-110;
6. R.M. Bozorth, *Ferromagnetism*, D.Van Nostrand Company, INC, 1968;
7. E. du Tremolet de Lacheisserie, D. Gignoux, M. Schlenker, *Magnetism*, Kluwer Academic Publisher, 2002, II-216;
8. J.P. Joule, *Sturgeons Annals of Electricity* 8 (1842) 219;
9. E. Villari, *Ann. Phys. Chem.* 126 (1865) 87;
10. BD Culity, *Introduction to magnetic Materials*, Addison-Wesley, 1972;
11. DC Jiles, *Introduction to Magnetism and Magnetic Materials*, Chapman and Hall, 1991;
12. E. du Tremolet de Lacheisserie, K. Mackay, J. Betz, J.C. Peuzin, *Journal of Alloys and Compounds* 275-276 (1998) 685;
13. A.E. Clark, Magnetostrictive Rare Earth-Fe₂ Compounds, in *Ferromagnetic Materials*, E.P. Wohlfarth (Ed.), North-Holand, Amsterdam, 1980, 531;
14. G. Ausanio, C. Hison, V. Iannotti, L. Lanotte, C. Luponio, Magnetoelastic properties in amorphous ferromagnetic materials and potential applications, in *Magnetic Amorphous Alloys: Structural, Magnetic and Transport Properties*, P. Tiberto and F. Vinai (Eds.), Research Singpost, Kerala, India (ISBN:81-7736-096-5) (2003) 43-78;
15. F. Claeysen, N. Lhermet, R. Le Letty, P. Bouchilloux, *Journal of Alloys and Compounds* 258 (1997) 61-63;
16. J.D. Verhoven, *J. Appl. Phys.* 66 (1989) 772-779;
17. A. Ludwig, E. Quandt, *J. Appl. Phys.* 87 (2000) 4691;
18. P. Marin, A. Hernando, *J. Magn. Magn. Mater.* 215-216 (2000) 729-734;
19. G. Herzer, Nanocrystalline soft magnetic alloys, in *Handbook of Magnetic Materials*, vol. 10, K.H.J. Buschow (Ed.), Elsevier Science, 1997, p. 415-462;

20. N. Hasegawa, M. Saito, N. Kataoka, H. Fujimori, *J. Magn. Soc. Jpn.*, 15 (1991), 403-406;
21. H. Warlimont, *Mater. Sci. Eng. A* 304-306 (2001) 61-67;
22. R.W. Cahn, *Background to Rapid Solidification Processing, in Rapid Solidified Alloys*, H.H. Liebermann (Ed.), Marcel Dekker, Inc., New York, 1993, 1-15;
23. N. Takahashi, Y. Suga, H. Kobayashi, *J. Magn. Mater.* 160 (1996) 98-101;
24. S. Dokupil, M.T. Bootsmann, S. Stein, M. Lohndorf, E. Quandt, 290-291 (2005) 795-799;
25. S. Mitani, H. Fujimori, K. Yahushiji, J.G. Ha, S. Takahashi, S. Maekawa, *J. Magn. Mater.* 198-199 (1999) 179-184;
26. E. du Tremolet de Lacheisserie, D. Gignoux, M. Schlenker, *Magnetism, II Materials and Applications*, Kluwer Academic Publishers (2002) 298-299;
27. R. Hunt, *IEEE Trans. Mag.* 7 (1971) 150;
28. S.S.P. Purkin, Z.G. Lie, D.J. Smith, *Appl. Phys. Lett.* 58 (1991) 2710;
29. M.N. Baibich, J.M. Broto, A. Fert, F. Nguyen Van Dau, F. Petroff, P. Etienne, G. Creuzet, A. Friederich, J. Chazelas, *Phys. Rev. Lett.* 61 (1998) 2472;
30. G. Binasch, P. Grünberg, F. Saurenbach, W. Zinn, *Phys. Rev. B* 39 (1989) 4828;
31. P. Grunberg, R. Schreiber, Y. Pang, M.B. Brodsky, H. Sowers, *Phys. Rev. Lett.* 57 (1986) 2442;
32. J. Barnas, A. Fuss, R.E. Camley, P. Grunberg, W. Zinn, *Phys. Rev. B* 42 (1990) 8110;
33. B. Dieny, V.S. Speriosu, S.S.P. Parkin, B.A. Gurney, D.R. Wilhoit, D. Mauri, *Phys. Rev. B* 43 (1991) 1297;
34. A. Barthelemy, A. Fert, F. Petroff, *Handbook of Magnetic Materials*, Vol. 12, Elsevier, Amsterdam (1999) 1-96;
35. J.Q. Xiao, J.S. Jiang, C.L. Chien, *Phys. Rev. Lett.* 68 (1992) 3749;
36. K.L. Chappara, S. Major, D.K. Pandya, *Thin Solid Films* 10 (1983) 1;
37. Bao-xin Huang, Yi-hua Liu, Jun-hua Wang, Ru-zhen Zhang, Lin Zhang, Lian-sheng Zhang, Liang-mo Mei, *J. Phys.: Condens. Matter* 15 (2003) 47-53;
38. R. Rodmacq, G. Palumbo, P. Gerard, *J. Magn. Mater.* 111 (1993) 11;
39. R.L. With, *IEEE Trans. Mag.* 39 (1994) 346;
40. M. Wun-Fogle, J.B. Restorff, *J. Appl. Phys.* 83 (1998) 7279-7281;
41. J.B. Restorff, M. Wun-Fogle, *J. Appl. Phys.* 87 (2000) 5786-5788;
42. B.A. Cook, J.L. Harringa, *J. Appl. Phys.* 87 (2000) 776-780;

43. Y.X. Li, Y.M. Hao, B.M. Wang, et al., IEEE Transaction on Magnetism 37 (2001) 2696-2698;
44. D.G.R. Jones, J.S. Abell, I.R. Harris, J. Magn. Magn. Mater. 104-107 (1992) 1468;
45. W. Mei, T. Umeda, S. Zhou, R. Wang, J. Magn. Magn. Mater. 174 (1997) 100;
46. L. Sandlund, M. Fanlander, T. Cedell, A.E. Clark, J.B. Restorff, M. Wun-Fogle, J. Appl. Phys. 75 (1994) 5656-5658;
47. L. Ruiz de Angulo, J.S. Abell, I.R. Harris, J. Magn. Magn. Mater. 157-158 (1996) 508-509;
48. L. Sandlund, T. Cedell, in Transducers for Sonics and Ultrasonics, M.D. McCollum, B.F. Hamonic, B.O. Wilson (Eds.) Technomic, Orlando (1992) 113;
49. T.A. Duenas, G.P. Carman, J. Appl. Phys. 87 (2000) 4696-4701;
50. D. Kendall, A.R. Piercy, Ferroelectrics 187 (1996) 153;
51. S.R. Kim, S.Y. Kang, J.K. Park, J.T. Nam, D. Son, S.H. Lim, J. Appl. Phys. 83 (1998) 7285;
52. T.A. Duenas, L. Hsu, G.P. Carman, Mater. Res. Soc. Symp. Proc. 459 (1996) 527;
53. J. Hudson, S.C. Busbridge, A.R. Piercy, J. Appl. Phys. 83 (1998) 7255;
54. S.H. Lim, S.R. Kim, S.Y. Kang, J.K. Park, et al., J. Magn. Magn. Mater. 191 (1999) 113-121;
55. S. Bednarek, Appl. Phys. A 68 (1999) 63-67;
56. S. Bednarek, J. Magn. Magn. Mater. 166 (1997) 91-96;
57. S. Bednarek, Materials Science and Engineering B 63 (1999) 228-233;
58. A.H. Morrish, The Physical Principles of Magnetism, Wiley, New York (1995) 301;
59. I.S. Grigoriev, E.Z. Mijlichov, Fiziceskije Vieliciny, Spravocnik (Energoatomizdat, Moska (1991) 629;
60. S. Bednarek, Materials Science and Engineering B 54 (1998) 196-201;
61. S. Bednarek, Materials Science and Engineering B 67 (1999) 113-121;
62. S. Bednarek, Materials Science and Engineering B 55 (1998) 201-209;
63. K. Raj, B. Moskowitz, R. Casciari, J. Magn. Magn. Mater. 149 (1995) 174;
64. L.B. Brasi, A.K. Buki, D. Szabo, M. Zrinyi, Progr. Colloid. Polym. Sci. 102 (1996) 57;
65. R.T. Bonnecaze, J.F. Brody, J. Rheol. 36 (1992) 73;
66. S. Bednarek, J. Magn. Magn. Mater. 202 (1999) 574;
67. J.Q. Xiao, J.S. Jang, C.L. Chien, Phys. Rev. Lett 68 (1992) 3794;
68. Y. Wu, M. Anjanappa, Proc. SPIE Smart Structures and Integrated Systems, vol 2717,

- ed I Chopra (Bellingham, WA: SPIE) pp. 517-527;
69. M. Anjanappa, Y. Wu, *Smart Mater. Struct.* 6 (1997) 393-402;
 70. S. Bednarek, *Materials Science and Engineering B* 77 (2000) 120-127;
 71. M. Farshad, A. Benine, *Polymer Testing* 23 (2004) 347-353;
 72. M. Farshad, M. Le Roux, *Polymer Testing* 24 (2005) 163-168;
 73. L.V. Nikitin, G.V. Stepanov, L.S. Mironova, A.I. Gorbunov, *J. Magn. Magn. Mater.* 272-276 (2004) 2072-2073;
 74. Y. Yoshizawa, S. Oguma, K. Yamauchi, *J. Appl. Phys.* 64 (1988) 6044;
 75. Y. Yoshizawa, K. Yamauchi, *Mater. Trans. JIM* 32 (1991) 551;
 76. A. Hernando, A. Gonzales, A. Salcedo, F.J. Palomares, J.M. Gonzalez, *J. Magn. Magn. Mater.* 221 (2000) 172-177;
 77. B. Roy, S.K. Ghatak, *J. Alloys Compd.* 326 (2001) 198-200;
 78. M.E. McHenry, M.W. Willard, D.E. Laughlin, *Prog. Mater. Sci.* 44 (1999) 291-433;
 79. J. Hu, H. Qin, S. Zhou, Y. Wang, *Mater. Sci. Eng. B* 83 (2001) 24-28;
 80. A. Zelenakova, P. Kollar, Z. Vertesy, M. Kuzminski, D. Ramin, W. Rieheman, *Scripta Mater.* 44 (2001) 613-617;
 81. K. Suzuki, N. Kataoka, A. Inoue, A. Makino, T. Masumoto, *Mater. Trans. JIM* 31 (1990) 734;
 82. G. Herzer, Nanocrystalline soft magnetic alloys, in *Handbook of Magnetic Materials*, vol. 10, Editor KHJ Buschow, Elsevier Science BV (1997) 415-462;
 83. G. Herzer, H. R. Hilzinger, *Physica Scripta* 39 (1989) 639;
 84. G. Herzer, *IEEE Trans. Magn.* 26 (1990) 1397;
 85. H. Xu, K. Y. He, Y.Q. Qiu, Z.J. Wang, X.S. Xiao, *Mater. Sci. Eng. A* 286 (2000) 197;
 86. P. Kollar, J. Kovac, J. Fuzer, P. Sovak, E. Pancurakova, *J. Magn. Magn. Mater.* 215/216 (2000) 560;
 87. M. Manivel Raja, N. Ponpandin, B. Majumdar, *Mater. Sci. Eng. A* 304-306 (2001) 1062;
 88. W. Wu, G. Jiang, R.H. Wagoner, G.S. Daehn, *Acta. Mater.* 48 (2000) 4323;
 89. S.A. Miller, Amorphous metal powder: production and consolidation, in *Amorphous Metallic Alloys*, F.E. Luborsky (Ed.), Bulterworth&Co Ltd. (1983) 506-521;
 90. D. Nuetzel, G. Rieger, J. Wecker, J. Petzold, M. Muller, *J. Magn. Magn. Mater.* 196/197 (1999) 327;
 91. M. Yagi, I. Endo, I. Otsuka, H. Yamamoto, *J. Magn. Magn. Mater.* 215/216 (2000) 284;

92. J. Xu, R.M. McMeeking, *Int. J. Mech. Sci.* 37 (1995) 883;
93. F. Mazaleyrat, L.K. Varga, *J. Magn. Magn. Mater.* 215/216 (2000) 253;
94. R. Lebourgeois, S. Berenguer, C. Ramiarinjaona, T. Waeckerl, *J. Magn. Magn. Mater.* 254/255 (2003) 191;
95. F. Alves, C. Ramiarinjaona, S. Berenguer, R. Lebourgeois, T. Waeckerle, *IEEE Transactions on Magnetics*, 38 (2002) 3135-3137;
96. B.H. Sohn, R.E. Cohen, G.C. Papaefthymiou, *J. Magn. Magn. Mater.* 182 (1998) 216;
97. A.M. Testa, S. Foglia, L. Suber, D. Fiorani, L. Casas, A. Roig, E. Molins, J.M. Greneche, J. Tejada, *J. Appl. Phys.* 90, 1534 (2001);
98. S. Sun, S. Andres, H. F. Hamann, J.U. Thiele, JEE Baglin, T. Thomson, E.E. Fullerton, CB Murray, BD Terris, *J. Am. Chem. Soc.* 124 (2002) 2884;
99. J. Chatterjee, Y. Haik, CJ Chen, *J. Magn. Magn. Mater.* 246 (2002) 382;
100. V. Leger, C. Ramiarinjaona, R. Barre, R. Lebourgeois, *J. Magn. Magn. Mater.* 191 (1999) 169-173;
101. G. Herzer, *Mater. Sci. Eng. A133* (1991) 1;
102. J.H. Paterson, R. Devine, A.D.R. Phelps, *J. Magn. Magn. Mater.* 196-197 (1999) 394-396;
103. L.A. Dobrzanski, R. Nowosielski, J. Konieczny, A. Przybyl, J. Wyslocki, *J. Magn. Magn. Mater.* 290-291 (2005) 1510-1512;
104. L.A. Dobrzanski, R. Nowosielski, A. Przybyl, J. Konieczny, *Journal of Materials Processing Technology* 162-163 (2005) 20-26;
105. I. Chicinas, O. Geoffroy, O. Isnard, V. Pop, *J. Magn. Magn. Mater.* 290-291 (2005) 1531-1534;
106. R. Nowosielski, J.J. Wyslocki, I. Wnuk, P. Sakiewicz, P. Gramatyka, *Journal of Materials Processing Technology* 162-163 (2005) 242-247;
107. B.C. Munoz, M.R. Jolly, *Composites with field responsive rheology*, in: *Performance of plastics*, W. Brostow (Ed.), Munich, Carl Hanser Verlag (2001) 553-574;
108. J.D. Carlson, M.R. Jolly, *Mechatronics* 10 (2000) 555-569;
109. M. Lokander, B. Stenberg, *Polymer Testing* 22 (2003) 677-680;
110. M. Lokander, T. Reitberger, B. Stenberg, *Polymer Degradation and Stability* 86 (2004) 467-471;
111. M. Lokander, B. Stenberg, *Polymer Testing* 22 (2003) 245-251;
112. J. Rabinow, *AIEE Trans.* 67 (1948) 1308;
113. L. Zipser, L. Richter, U. Lange, *Sensors and Actuators A* 92 (2001) 318-325;

114. J.M. Ginder, L. Davis, *Appl. Phys. Lett.* 65 (1994) 3410;
115. M.R. Jolly, J.D. Carlson, B.C. Munoz, *Smart Mater. Struct.* 5 (1996) 607-614;
116. J.M. Ginder, L. Davis, L.D. Elie, *Int. J. Mod. Phys. B* 10 (1996) 3293;
117. Jung-Bae Jun, Seong-Young Uhm, Jee-Hyun Ryu, Kyung-Do Suh, *Colloids and Surfaces A: Physicochem. Eng. Aspects* 260 (2005) 157-164;
118. X.I. Gong, X.Z. Zhang, P.Q. Zhang, *Polymer Testing* 24 (2005) 669-676;
119. J.D. Carlson, MR Jolly, *Mechatronics* 10 (2000) 555-569;
120. W.H. Li, G.Z. Yao, G. Chen, S.H. Yeo, F.F. Yap, *Smart Materials and Structures* 9 (2000) 95-102;
121. M.R. Jolly, J.W. Bender, J.D. Carlson, *Journal of Intelligent Material Systems and Structures* 10 (1999) 5-13;
122. A.J. Margida, K.D. Wiess, J.D. Carlson, *Int. J. Mod. Phys. B* 10 (1996) 3335;
123. P.P. Phule, *MRS Bull.* 23 (1998) 23;
124. B.F. Spencer, S.J. Dyke, M.K. Sain, J.D. Carlson, *Journal of Engineering Mechanics* 123 (1997) 230-238;
125. J.D. Carlson, M.J. Chrzan, F.O. James, US Patent 5,284,330, 1994;
126. J.D. Carlson, M.J. Chrzan, F.O. James, US Patent 5,277,281, 1994;
127. W.H. Li, H. Du, G. Chen, S.H. Yeo, N.Q. Guo, *Smart Materials&Structures* 11 (2002) 209-217;
128. Z. Rigbi, L. Jilken, J. Magn. *Magn. Mater.* 37 (1983) 267-276;
129. J.M. Ginder, M.E. Nichols, L.D. Elie, J.L. Tardiff, *Magnetorheological elastomers: properties and applications*, In: *Proceedings Series of SPIE Smart Structures and Materials*, vol. 3675 (1999) 131-138;
130. M.R. Jolly, J.D. Carlson, B.C. Munoz, T.A. Bullions, *J. Intel. Mater. Syst. Struct* 7 (1996) 613-622;
131. T. Shiga, A. Okada, T. Kurauchi, *Journal of Applied Polymer Science* 58 (1995) 787-792;
132. W. Kordonsky, *J. Magn. Magn. Matter.* 122 (1993) 395-398;
133. I.A. Brigadnov, A. Dorfmann, *International Journal of Solids and Structures* 40 (2003) 4659-4674;
134. W.M. Stewart, J.M. Ginder, L.D. Elie, M.E. Nichols, US Patent 5,816,587, 1998;
135. J.R. Watson, US Patent 5,609,353, 1997;
136. JM Ginder, ME Nichols, LD Elie, S.M. Clark, *Controllable-stiffness components based on magnetorheological elastomers*, In: *Proceedings Series of SPIE Smart Structures and Materials*, vol. 3985 (2000) 418-425;
137. C. Nan, *Appl. Phys. Lett.* 72 (1998) 2897;

138. M. Anjanappa, Y. Wu, *Smart Mater. Struct.* 6 (1997) 393;
139. J.F. Herbst, T.W. Capehart, F.E. Pinkerton, *Appl. Phys. Lett.* 70 (1997) 3041;
140. M. Roberts, M. Mitrovic, G.P. Carman, *Proc. SPIE* 2411 (1995) 241;
141. G.P. Carman, D.S. Cheung, D. Wang, *J. Intell. Mater. Syst. Struct.* 6 (1995) 691;
142. H.M. Yin, L.Z. Sun, J.S. Chen, *Mechanics of Materials* 34 (2002) 505;
143. J.H. Huang, C.W. Nan, Rui-Mu Li, *J. Appl. Phys.* 91 (2002) 9261;
144. Ce-Wen Nan, G.J. Weng, *Physical Review B* 60 (1999) 6723;
145. Ce-Wen Nan, *Appl. Phys. Lett.* 72 (1998) 2897;
146. L. Borcea, O. Bruno, *Journal of the Mechanics and Physics of Solids* 49 (2001) 2877-2919;
147. L.C. Davis, *J. App. Phys.* 85 (1999) 3348;
148. Y. Chen, J.E. Snyder, C. Schwichtenberg, K.W. Dennis, D.K. Falzgraf, R.W. McCallum, D.C. Jiles, *Appl. Phys. Lett.* 74 (1999) 1159;
149. W.D. Armstrong, *J. App. Phys.* 87 (2000) 3027;
150. W.D. Armstrong, *Mater. Sci. Eng. A* 285 (2000) 13;
151. Y.H. Pao, Electromagnetic forces in deformable continua, in: *Mechanics today*, Nemat-Nasser S. (Ed.), Oxford: Pergamon Press, 4 (1978) 209-306;
152. I.A. Brigadnov, A. Dorfmann,, *Int. J. Solid Struct.* 40 (2003) 4659;
153. A. Dorfmann, R.W. Ogden, *European Journal of Mechanics A/Solids* 22 (2003) 497-507;
154. A. Dorfmann, R.W. Ogden, *Acta Mechanica* 167 (2004) 13-28;
155. S.V. Kankanala, N. Triantafyllidis, *J. Mech. Phys. Solids*, 52 (2004) 2869-2908;
156. L. Lanotte, G. Ausanio, V. Iannotti, G. Pepe, G. Carotenuto, P. Netti, L. Nicolais, *Phys. Rev. B* 63 054438 (2001) 1-6;
157. L. Lanotte, G. Ausanio, C. Hison, V. Iannotti, C. Luponio, C. Luponio Jr, *Journal of Optoelectronics and Advanced Materials* 6-2 (2004) 523-532;
158. L. Lanotte, G. Ausanio, V. Iannotti, C. Luponio Jr, *Appl. Phys. A* 77 (2003) 953-958;
159. E. Olsen, *Applied Magnetism (A Study in Quantities)* Philips Technical Library, Eindhoven, The Netherlands (1996);
160. E. du Trémolet de Lacheisserie, *Magnetostriction: Theory and Applications of Magnetoelasticity*, CRC Press, Boca Raton, FL (1993);
161. A. M. van Diepen, K. H. J. Buschow, H. W. de Wijn, "On the origin of the high uniaxial magnetocrystalline anisotropy in SmCo₅",

- Proc. Third European Conf. on Hard Magnetic Materials, Amsterdam (1974) 17-19;
162. G. Ausanio, L. De Arcangelis, G. Franzeze, V. Iannotti, C. Luponio Jr, L. Lanotte, JMMM 290-291 (2005) 836-838;
163. A. Noshav, J.E. McGrath, Block Copolymers Overview and Criteria Survey, Academic, New York (1977);
164. Warrick, E.L., Pierce, O.R., Polmanteer, K.E. and Saam, J.C., Rubber Chem. Technol., 52 (1979) 437;
165. L. Lanotte, G. Ausanio, C. Hison, V. Iannotti, C. Luponio, Sensors and Actuators A 106 (2003) 56-60;
166. S. Chikazumi, Physics of Ferromagnetism, Oxford Science, New York (1997) 7;
167. G. Ausanio, V. Iannotti, C. Hison, L. Lanotte, A. D'Agostino, R. Germano, Novel elastic magnets as actuators core, Journal of Applied Electromagnetics and Mechanics 19 (2004) 395-398;
168. C. Hison, G. Ausanio, V. Iannotti, L. Lanotte, G. Breglio, A. Cusano, M. Giordano, Technical Digest of the Interdisciplinary Electromagnetic, Mechanic & Biomedical Problems, (ISEM), Bad Gastein, Austria, 12-14 September, 2005, p. 126-127;
169. A. Cusano, G. Breglio, M. Giordano, L. Nicolais, A. Tutolo, IEEE-ASME Transactions on Mechatronics 9 (2004) 40-49;
170. K.J. Strnat, D. Li, H. Mildrum, High and low temperature properties of sintered Nd-Fe-B magnets, paper no VIII-8, Technical Digest of the 8th International Workshop on Rare Earth Magnets and Their Applications, Dayton, OH, 6-8 May, 1985;
171. G. Ausanio, A. Barone, C. Hison, V. Iannotti, C. Luponio Jr., L. Lanotte, to be published in Sensors&Actuators A, 2005;
172. L. Lanotte, G. Ausanio, C. Hison, V. Iannotti, C. Luponio, J. Magn. Magn. Mater. 272-276 (2004) 2069-2071;
173. C. Hison, G. Ausanio, V. Iannotti, G. Lucani, C. Luponio Jr., L. Lanotte, Technical Digest of the 3rd International Workshop on Amorphous and Nanocomposite Magnetic Materials, September 19-21, 2005, Iasi, p.49;
174. J.M.D. Coey, Journal of Alloys and Compounds 326 (2001) 2-6.

TABLE OF CONTENTS

1. Composite materials made of magnetic particles inside a non-magnetic, elastic matrix...	5
1.1. Introduction.....	5
1.1.1. Magnetostriction.....	7
1.1.2. Magnetoresistance.....	11
1.2. State-of-the-art.....	12
1.2.1. Composite materials based on Terfenol-D.....	12
1.2.2. Composite materials made of silicon steel(+graphite)/ iron(+graphite) particles inside a silicone matrix.....	17
1.2.3. Composite materials made of soft magnetic nanocrystalline powder particles inside a polymer matrix.....	28
1.2.4. Magnetorheological solids (elastomers).....	34
1.2.5. Theoretical studies.....	40
2. Elastomagnetic composite materials: Preparation	44
3. Elastomagnetic composites: Elastomagnetic Effects.....	49
4. Theoretical model of the elastomagnetic effect.....	54
5. Experimental verification of the direct elastomagnetic effect.....	59
6. Experimental verification of the inverse elastomagnetic effect.....	67
7. Elastomagnetic composites as sensor and actuator core materials.....	72
7.1. Mechanical vibration sensor prototype based on elastomagnetic composite core.....	72
7.1.1. Experimental set-up and functioning.....	73
7.1.2. Functioning model.....	75
7.1.3. Experimental verification of the functioning model validity.....	77
7.1.4. Sensor prototype performances and limits.....	83
7.2. Actuator prototype based on elastomagnetic composite core.....	84
8. Stability of the elastomagnetic performances under thermal and mechanical ageing ...	89
9. Conclusion.....	94
10. Appendix A: Experimental techniques.....	95
11. Appendix B: Detailed calculation of some equations.....	104
12. Appendix C: Magnetic units and definition; Correspondence between volume and mass percentage of Sm_2Co_7 particles inside the elastomagnetic composite.....	106
13. References.....	108